Republic of Iraq
Ministry of Higher Education and Scientific Research
Babylon University
College of Engineering
Civil Engineering Department

Flexural Behavior of Cold-Formed I-Steel Beams with Hollow Flanges

A Thesis

Submitted to the College of Engineering / University of Babylon in Partial Fulfillment of the Requirements for the Degree of Master in Engineering/ Civil Engineering /Structures.

By

Alyaa Salah Falah Mishaal

(B.Sc. Civil Engineering, 2009)

Supervised By

Asst.Prof.Dr . Najla'a Hameed Abbas AL-Shareef

1445 A.H **2023 A.D**

بِسْمِ اللَّــهِ الرَّحْمَـٰنِ الرَّحِيمِ

(وَمَنْ يَتَوَكَّلْ عَلَى اللّهِ فَهوَ حَسْبه إِنّ اللَّه

بَالِغ أَمْرِهِ قَدْ جَعَلَ الله لِكلِّ شَيْءٍ قَدْرًا)

صَدَقَ اللهُ العَلِيُّ العَظيم

الآية (٣) سورة الطلاق

Certificate

I certify that supervisor's this thesis entitled " **Flexural Behavior of Cold-Formed I-Steel Beams with Hollow Flanges**", was prepared by " **Alyaa Salah Falah Mishaal** ", under my supervision at the Department of Civil Engineering at the University of Babylon in partial fulfillment of the requirements for the degree of Master of science in Structural Engineering.

Signature:

Name: **Asst.Prof.Dr . Najla'a Hameed Abbas AL-Shareef**

Data: / /

ACKNOWLEDGEMENTS

First of all, thanks be to God, Lord of the worlds, who helps me to complete this study, uses me to advance this great knowledge, and enables me to work for it.

I would like to take this opportunity to express my sincere thanks to my college (the College of Engineering/Civil Department) and my supervisor; Asst.Prof.Dr. Najla'a Hameed AL-Shareef for reviewing my research and guiding me throughout the course of the project. I had the honor of being under her guidance and supervision. Her precious advices and constructive suggestions are highly distinct throughout this work.

To the heart that beats with love and mercy, to my beloved mother, may God prolong her life, to straighten my back, my beloved father, may God prolong his life.

To the lamp of my path, my life partner, and my second half, my beloved husband, may God bless his life. To the candles with which I see my way to my children (Ali, Haider, and Mohammed), may God protect them and make them good offspring and a source of our pride.

To all those whom I am indebted to and whose names cannot be mentioned. Great Thanks for All.

Alyaa Salah Falah Mishaal

2023

ABSTRACT

Cold-formed steel is commonly used in products like steel sheets, strip plates, and flat strips, which are shaped at temperatures close to room temperature through processes like bending, press-brake, and machine press operations. These products have various thicknesses ranging from 0.25mm to 12mm. They find applications in bridges, towers, construction, as well as in automobiles, railways, airplanes, ships, agricultural machinery, electrical equipment, and more.

This study involves both experimental and numerical analyses of the flexural behavior of twelve cold-formed steel sections with hollow rectangular flanges. These sections were studied with and without strengthening, resulting in two groups.

For both groups, the clear span length of each section was 1500mm, beam depth was 300mm, and flange width was 150mm. The connection between the flanges and the web was achieved using bolts with a diameter of 10mm, spaced at a distance equal to one-sixth of the clear span length.

In the first group, the controlling factor was the flange depth. Four sections were created with flange depths of 30mm, 60mm, 90mm, and 120mm. The section with a flange depth of 60mm exhibited the lowest load-carrying capacity and was selected for creating eight sections in the second group. In the second group, the type of strengthening material used for the hollow rectangular flanges was the controlling factor. Two types of concrete, normal and lightweight, were used to strengthen two sections. Additionally, the same concrete mixture was used, but certain aggregates were replaced with alternative materials such as recycled concrete, sawdust, fine and coarse rubber, iron filling, and broken glass. These alternative materials were used to strength six more sections.

After conducting all the necessary tests on the sections from both groups, as well as conducting tensile and compressive tests on the concrete, and calculating the results, it was found that in the first group, after the depth of the flange increases beyond 60 mm, the flexural behavior improves. This led to higher load-carrying capacity, reduced deformation, and deflection. When comparing the results to the section with a flange depth of 60mm, improvements in load-carrying capacity ranged from 11% to 18%.

Regarding the second group, when compared to the section with a flange depth of 60mm, there was an decrease in load-carrying capacity ranging from (13% to 26%) and a decrease in deflection ranging from 65% to 86%. It was observed that the increase in load-carrying capacity was directly proportional to the compressive strength of the concrete used for strengthening.

In the numerical aspect, non-linear analysis using the finite element method was employed, and numerical models were analyzed using the **ABAQUS** software (**ABAQUS/standard/explicit 2017**). The results from the software were compared and calibrated with experimental results in terms of load-deflection curves, failure mode, showed good agreement between theoretical and practical results. The difference in load-carrying capacity between numerical and experimental results ranged from -1% to 15%.

List of Contents

List of Tables

List of Figures

List of Plates

Notation

Most commonly used symbols are listed below, these and others are defined where they appear in the research;

Symbol	Description	Units
d_h	Hole Diameter	mm
h_w	Web depth	mm
b_f	Width of flange	mm
H	Depth of cross section	mm
h_f	Depth of flange	mm
h_w	Depth of web	mm
Es	Modulus of elasticity	MPa
F_y	Yield stress of steel profile	MPa
Fu	Ultimate tensile strength of Steel	MPa
L	Total length of cold formed steel beam	mm
Pu	Ultimate load	kN
t	Thickness of plate	mm
t_f	Flange thickness of steel profile	mm
t_w	thickness of web	mm
X	The ratio between depth of beam and depth of flange	mm
fc'	Compressive strength of concrete	MPa
f_{st}	Splitting tensile strength of concrete	MPa

f_r	Flexural strength	MPa
Δs	Deflection at service load	mm
Δu	Deflection at ultimate load	mm
K'	stiffness parameter	KN/mm

ABBREVIATIONS

Abbreviations	Descriptions
AISI	American Iron And Steel Intuition
ASTM	American Society for Testing and Materials
AS	Australia Standards
AS4100	AS4100-1990 steel structures. Standards Australia
AS4600	Standards Association Australia
AS/NZS4600	Standards Australia/Standards New Zealand (SA) (2005)
BD	Distortional Buckling
Cb	Moment gradient
CFPFBs	Concrete-Filled Pentagonal Flange Beams
CFS	Cold Formed Steel
CFTFs	Concrete-Filled Tubular Flanges
CW	Corrugated Web
DSM	Direct Strength Method
EC3	EUROCODE 3: Design of Steel Structures
Exp	Experimental
FE	Finite Element
FEA	Finite Element Analysis
HFB	Hollow Flange Beam
HFBs	Hollow Flange Beam steel
HFSPG	Hollow Flange Steel Plate Girder
HRS	Hot-Rolled Steel
HS-CFTFB	High-Strength Concrete-Filled Tubular Flange Beam
HTFGS	Tubular Flange Girders with Hollow Tubes
HTFPG	Hollow Tubular Flange Plate Girders

LB	Lateral Buckling
LD	Lateral distortional
LRFD	Load Resistance Factor Design
LSB	Lite Steel Beam
LTB	Lateral Torsional Buckling
Max	Maximum
Min	Minimum
No	Number
Num	Numerical
NZS	New Zealand Standards
RHFCB	Rectangular Hollow Flange Channel Beam
RHFCFSB	Rectangular Hollow Flange Cold-Formed Steel I-Beam
RHFB	Rectangular Hollow Flange Beam
SP-C	I-girder with trapezoidal corrugated web with stiffeners
SP-N	I-girder with trapezoidal corrugated web without stiffeners

CHAPTER ONE

INTRODUCTION

CHAPTER ONE

INTRODUCTION

1.1 Overview

Nowadays, by employing less resources in their projects, several construction industries aimed for a more sustainable development. The most recycled commodity in the world is steel, which is used to create lighter, more fuel-efficient cars and higher, safer buildings. While competing materials concentrate their sustainability claims on certain product application stages, steel member's excellent sustainability performance lowers environmental effect when assessed throughout the course of the product's complete life cycle. The process used to manufacture steel is crucial because it distinguishes the qualities of steel and reduces disparities in their strength, structural performance, and mode of failure [1].

In steel construction, the two most common varieties of structural steel members are hot-rolled and cold-formed. Hot-rolled steel is formed in blast furnaces or electric arc furnaces at temperatures up to 1400 °C, then rolled through a mill into the desired shape and cooled. Since the steel can shrink during cooling, there is little control over the final size and form.

The building industry uses thin sheet steel for purlins, roof sheeting, and floor decking. These are usually prefabricated frames or panels or basic construction components that may be constructed on-site. Cold-forming thin steel pieces involves using uniformly thick steel sheets to manufacture them without heat. These are "***Cold-Formed Steel Sections***" generally. They are also called "***Cold Rolled Steel Sections***" or "***Light Gauge Steel Sections***". Bending, press-brake and machine press are shaping methods. Cold-formed steel (CFS) sheets are usually 0.5 to 6mm thick. Up to 8mm thick material can be made if pre-galvanized is not needed. These commodities differ from

hot-rolled steel sections due to their manufacture process. Typically, the yield strength of steel sheets employed in CFS is no less than (280N/mm^2), but greater strengths and sometimes (350 N/mm^2) are employed, [2]. Hot-rolled steel members were once the most common type of steel, but high-strength CFS structural members have become increasingly popular, [3].

CFS construction materials have grown in use since 1946, when standards were established. The construction industry uses thin gauge sheet steel for structural and non-structural components. Studs, beams, joists, built-up sections, and others are structural components., as shown in Plates(1-1) and (1-2). [4]

Plate (1-1): CFS Building. [4]

Plate (1-2): CFS Building. [7]

1.2 Advantages and Disadvantages of CFS

The following are some of the primary advantages of CFS [4] :

- Light weight.
- Extremely rigid and strong.
- Simplicity of mass production and prefabrication.
- Quick and simple installation.
- Substantial reduction of weather-related delays.
- Accurate detailing.
- Non-shrinking and non-creeping at surrounding temperatures.
- No requirement for formwork.
- Resistant to rot and termites.
- Consistent quality.
- Economy of handling and transportation.
- A recyclable substance.
- Enclosed cells for conduits can be provided by panels and decks.

Also there are some disadvantages for cold-formed steel(CFS) as following[5]**:**

- More expensive.

- There are fewer forms available for cold-formed objects (sheets, box section shapes: CHS, SHS, RHS).
- If the steel is not stress alleviated before cutting, grinding, or welding, additional treatments may result in internal tension in the metal, which might lead to unexpected warping.
- Low fire resistance.
- Not easy to connect the parts.
- It is exposed to all kinds of buckling (local, lateral and distortional) and web crippling due to its thinness.

The advantages of cold-formed steel over other materials like timber and concrete are [7]:

- High strength.
- Lightness.
- Quick installation.
- Recycle products.
- A pleasing look.
- Easy to maintain.

1.3 Structure Made of Cold-Formed Steel

CFS constructions are structural elements created using cold-bending flat sheets of steel into a variety of shapes that can be applied to satisfy both functional and structural needs. A broad classification that includes individual structural frame components, panels, and decks can be applied to the cold-formed shapes utilized in the building industry.

In terms of generic configurations, many structurally useful cold-formed forms approximate hot-rolled structural sections. Roll forming allows for the creation of channels, angles, and zees from a single piece of material in a single step. I sections are often created by joining two channels together or

by joining two angles to a channel using welding [4],as shown in Plate(1-3) and Figure(1-1)

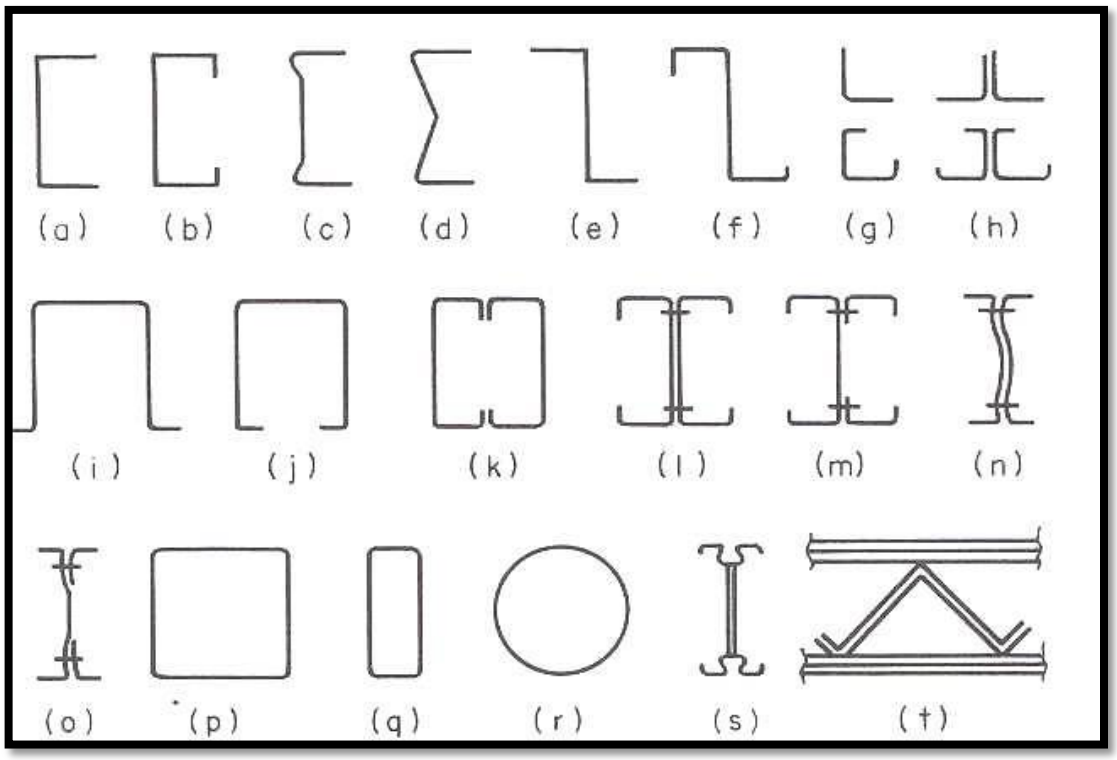

Figure (1-1): Common Sectional Forms of CFS, [3].

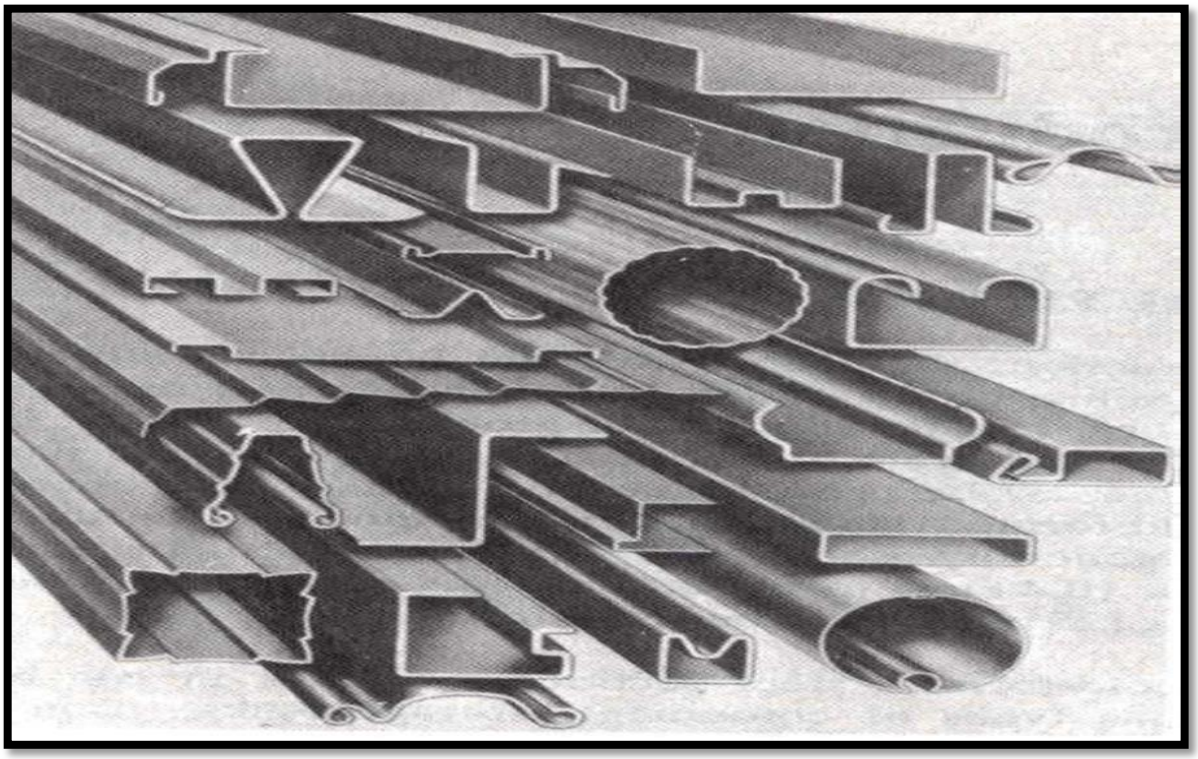

Plate (1-3): Different Shapes of CFS Sections [3].

The following are some of the most used applications and favored sections:

- Steel racks to hold storage pallets.
- Roof and wall systems for commercial, industrial, and agricultural buildings.
- Supporting components for space and plane trusses.
- No frame was used, stressed skin structures: Small buildings with a clear span of up to (30 feet) and no interior framework use corrugated sheets or sheeting profiles with reinforced edges. [4].

1.4 Hollow Flange Cold-Formed Steel Beams HFB

The inception of HFB may be traced back to 1965, when O'Connor et al. conducted a study demonstrating the enhanced buckling performance of I-section beams through the addition of closed cells, as depicted in Figure (1-2). Increasing torsional rigidity improved buckling behavior. The researchers focused on CFS sections with robust torsional flanges to delay or resolve structural instability issues. HFB beams are CFS sections with robust torsional flanges.

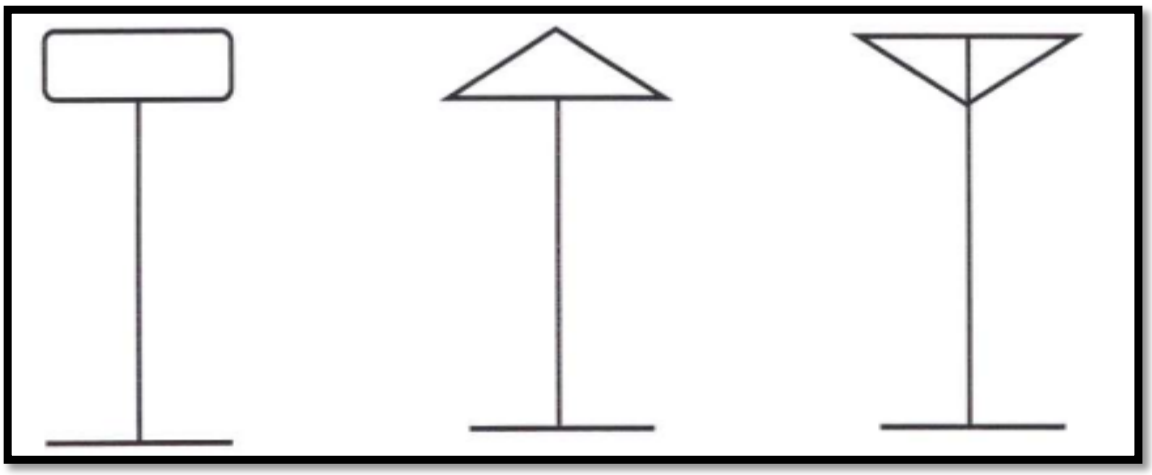

Figure (1-2): Types of Closed-Cell Sections, [3].

According to the data presented in Figure (1-3), Palmer Tube Mills engaged within the large-scale production of cold-formed, sections of high-strength steel beam throughout earlier 1990s. These beam sections were characterized

by two closed hollow triangular flanges. This structurally strong steel section was produced using an automated cold-forming and electric resistance welding technique, which effectively transformed only one strip of high-strength steel. Palmer Tube Mills used an acceptable electric resistance welding technique; however, it adds considerable complexity and expense to the manufacturing process. This was one among the factors that led to the triangular HFB manufacture stopping in 1997. Additionally, it could only make one group of HFB with triangular flanges that were 90 mm wide. Other flange widths (60 mm to 250 mm) and forms (rectangular, square, or other geometries) might significantly increase the effectiveness of structural for HFBs while removing or postponing many problematic buckling modes. [3].

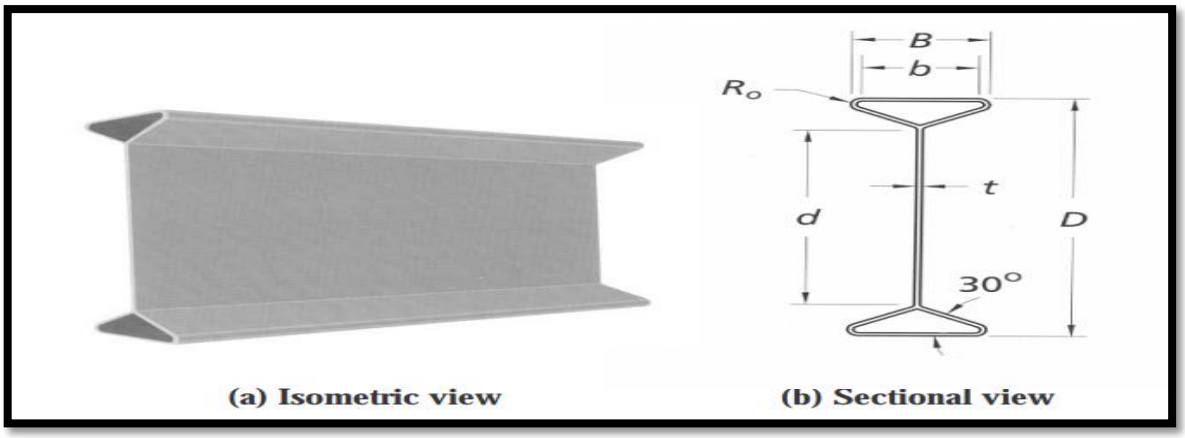

Figure (1-3): Geometric Form and Sectional Parameters for HFB [3].

1.5 Connection Types

The connection mechanically fastens structural components and is where the fastening occurs. Thus, the link is necessary for structural stability, load and moment transmission from structural components to support parts. Within the field of the construction industry, various types of joints are commonly employed in Cold-Formed Steel (CFS) applications. These include bolts, blind rivets, powder-actuated pins, self-tapping screws, welding of spot, welding of puddle, nailing, and clinching, [6], as shown in Figure (1-4).

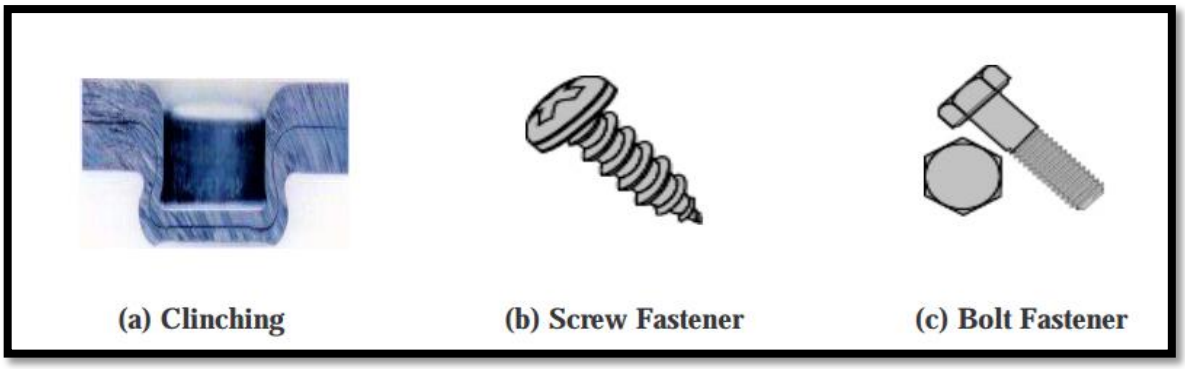

Figure (1-4): Generally used Cold-Formed Steel Fasteners, [3].

A recently found connection type with several benefits over other traditional techniques used in CFS connections is the self-piercing riveting, which HENROB commercialized, see Figure (1-5) due to the material's relatively thin thickness, connecting technology is crucial in creation of structures made of CFS members. Despite being accessible and utilized in CFS constructions, the aforementioned standard techniques of connections are less acceptable in terms of cost, quality, and construction efficacy for thin-walled member connections [11]. The choice of connection type is crucial in the CFS industry because it influences the entire project's cost, quality, and construction efficiency, [3].

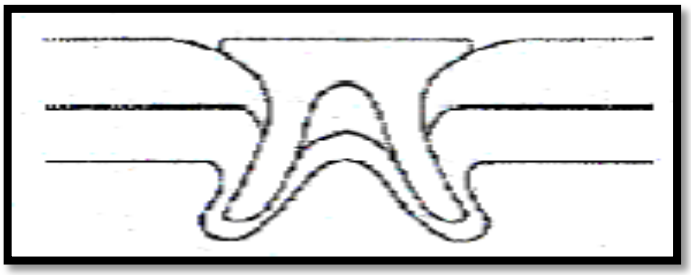

Figure (1-5): Self-penetrating Rivet Cross Section, [3].

Arc welds and **resistance welds** are two different types of welds that are used in building construction. **Arc welding** is an electric process used to join metal to metal and converting it into thermal energy to create enough heat to melt the edges of the metal to be welded. **Resistance welding** is one of the welding techniques that utilizes heat and pressure. Heat is generated by the passage of a high-intensity, low-voltage electric current through the weld

joint for a brief period of time and the welding process takes place at the point or place whose temperature has risen by pressure by polarity. [8]

Bolts serve the purpose of connecting thicker cold-formed sections, these connections are easy to install on site, bolted ties come in a variety of shapes and sizes. The use of bolts to connect CFS components is similar to that of hot-rolled construction; however, due to the thinness of the material and the small size of the components, the primary design considerations are typically ending distance and bearing capacity. [9]

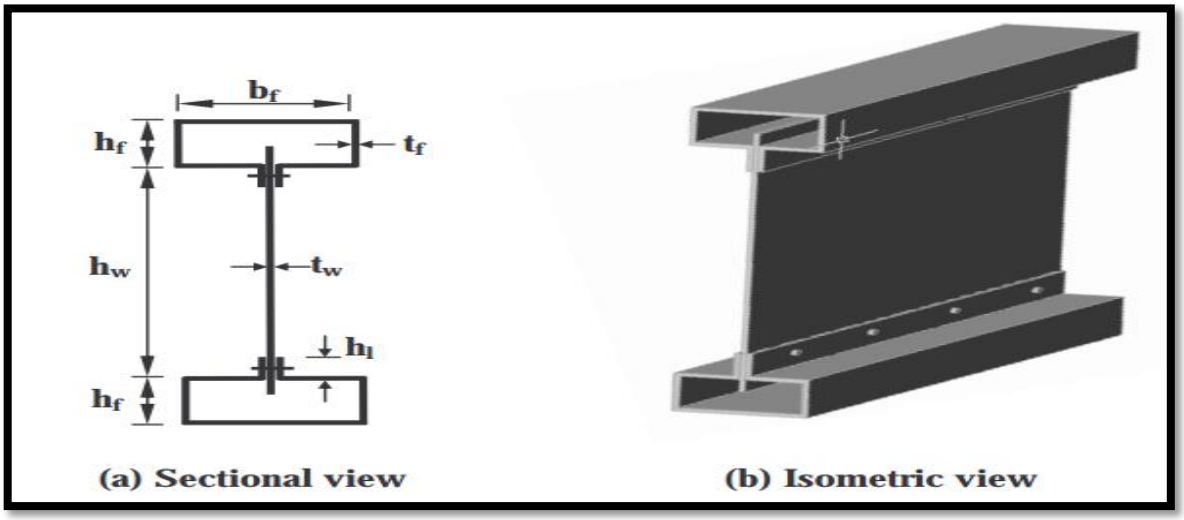

Figure (1-6): Geometry of a Typical RHFB, [3].

Some of the advantages and disadvantages of bolts as following, [13]:

-Advantages of Bolts:

- Quick bolt-on installation process.
- The process of installing the bolts is done quietly and does not make noise, unlike the rivet connections, which make a lot of noise during installation.
- Bolt connections are stronger than rivet connections, especially if high strength bolts are used, and therefore the number of bolts will be less than the number of rivets.
- The installation of bolt connections is done on cold and not like welding connections that are fused, so we will not be exposed to the risk of fire.

- The bolts can be removed and replaced with other bolts if a breakage or damage occurs in one of the bolts, unlike welding joints and rivet joints that cannot be disassembled later.

-Disadvantages of Bolts:

- Bolt joints reduce the free area of the profile and this greatly affects the element design.
- The strength of the bolt joint decreases if it is subjected to dynamic loads.
- The shape of bolt connections is not architecturally preferred.

1.6 Strengthening of Hollow Flange

Various filler materials were suggested for the hollow flanges of the cold-formed steel (CFS) I-beam with the aim of enhancing its resistance to buckling and capacity for strength. After conducting a comprehensive evaluation of several criteria, such as cost-effectiveness, lightweight properties, and exceptional strength. Various types of wood waste, lightweight concrete, normal concrete, polymer-mortar, and other materials are employed as strengthening materials. The improvement of the beams' strength is contingent upon the strength of the filler material, [11].

1.7 Applications of CFS Structural Elements within Engineering Structures

Web cleats connect CFS secondary members to HRS (hot-rolled steel) primary structural members as moment or pinned connections, depending on the configuration, while HRS sections support claddings in external building envelopes. In recent years, CFS sections have become the primary structural elements found in low- to medium-rise residential buildings, commercial structures with multiple stories and portal frameworks with moderate spans. Plates (1-4) and (1-5) show its application in building transmission towers,

bridges, storage and drainage facilities, bins and tall buildings' minor structural components. [6]

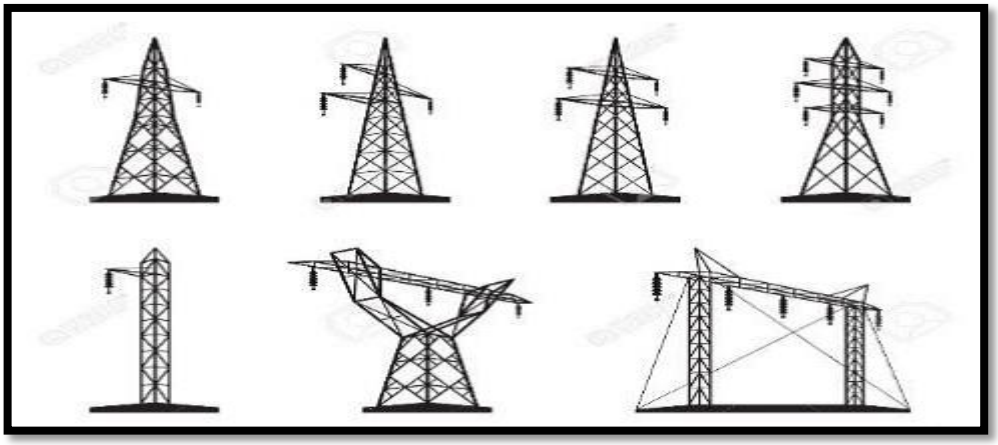

Plate(1-4): Some of CFS Applications, [9].

Plate (1-5): Some of CFS Applications, [6]

1.8 Flexural Behavior of Hollow Flange Steel Beam

The behaviour of flexural members is governed by various factors, including as geometric shape, section characteristics, loading configuration, material qualities, and support circumstances. The primary factor influencing the structural behaviour of cold-formed steel (CFS) sections, specifically hollow flange beams (HFBs), is the presence of thinner regions that exhibit high strength, in contrast to hot-rolled heavy steel sections. The consideration of stiffness and moment resistance holds substantial importance in the design process of flexural components constructed from cold-formed steel (CFS).

Various types of buckling, including as local, lateral distortional, and flexural-torsional buckling, significantly influence the moment resistance of flexural members, particularly those with thin sections, [3].

1.9 Research Objectives

The purpose of the research is to investigate, (experimentally and numerically) the flexural behavior of CFS built-up members with hollow flange steel beams on failure modes and load carrying capacity. This study's key targets can be outlined as following:

1- Execute experimental on four specimens with different depth of hollow flange CFS beam to investigating influence of flange depth on flexural behavior under two points load condition.

2- Execute Experimental on eight specimens with one depth of the flange that were filled with different strengthen materials to investigate the effect of these materials on the flexural behavior.

3- In this study, the **ABAQUS Standard/Explicit 2017** programmer was employed to assess the reliability and accuracy of finite element analysis (FEA) in simulating the failure of CFS (cold-formed steel) beams with non-linear behavior.

1.10 Research Layout

Chapter One: This chapter introduces cold-formed steel beams in general.

Chapter Two: Includes a review of related literature, such as studies on cold-formed steel beams that used experimental results and finite element analysis.

Chapter Three: explains the process of setting up an experiment and gives a description of the specimens, materials, molds, and tools.

Chapter Four: This chapter shows the experimental results and its comparison.

Chapter Five: The ABAQUS computer program was used to perform a finite element analysis for tested CFS beams in this chapter, and the findings of the analysis were compared to those of the experiments.

Chapter Six: Finally, the major conclusions and recommendations are included in this chapter.

CHAPTER TWO

LITERATURE REVIEW

CHAPTER TWO

REVIEW OF LITERATURE

2.1 Introduction

The academic realm has witnessed a growing interest for Cold-Formed Steel (CFS) structural elements, prompting an emergence of a multitude of studies on this subject. Despite this surge in research output, there has been a noticeable scarcity in the publication of works pertaining to hollow flange beams (HFBs). These beams, introduced in the early 1990s, have not received ample attention until recent years, resulting in their relatively limited exploration in the academic discourse. This chapter is dedicated to provide a concise overview of prior research endeavors centered around cold-formed steel beams, with a specific focus on delving into the analysis of hollow flange beams (HFBs).

2.2 Cold-Formed Steel Sections

(Luis L. et al, 2014), [12] examined how CFS beams with sigma-shaped sections behaved flexural in fire and environmental settings. Two different kinds of sections were subjected to four-point bending tests, including single sigma (B.AT.S) and built-up I-sections made of two sigma sections(B.AT.2S), as shown in Figure (2-1). Their study took into account three iterations of one component. Their samples had a (3 meter) span length. Two of the sigma parts were joined together using self-drilling screws.

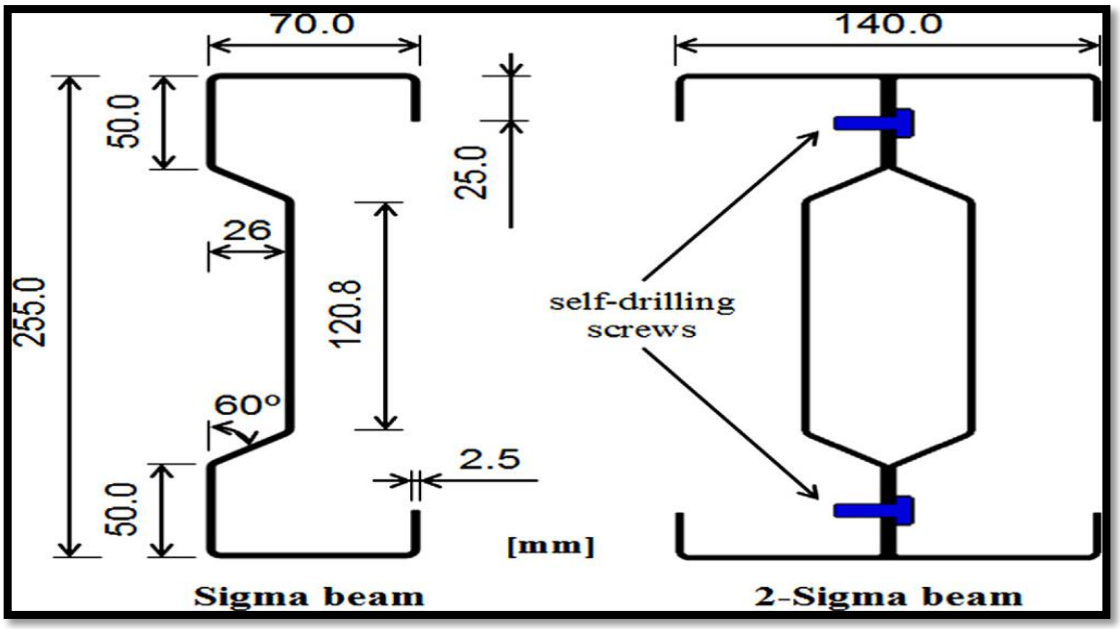

Figure (2-1): Cross sections of sigma and 2-sigma.

Their findings demonstrate that the form of the section had an impact on the beam's load capacity, considering a built-up I-section ultimate load of two sigma sections being 2.9 times larger than that of the single sigma section. It implies that the two-sigma symmetry portion performed better than the one sigma asymmetry section. For the built-up I-section with two sigma, local, distortional, and lateral torsional bucking were discovered. The load-displacement curves were shown in Figure (2-2).

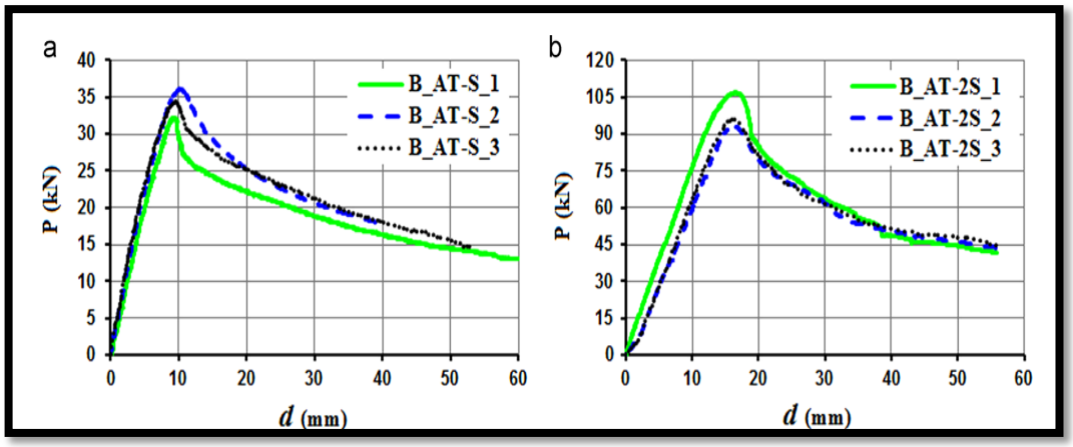

Figure(2-2): Curves of Load-displacement for
(a) a sigma and (b) 2-sigma beams at ambient temperature.

(Ali A. et al, 2015), [13] developed CFS-timber composite compression members for roof constructions resistant to termites. The strength and stiffness of the composite portions were significantly higher than those of the non-composite parts. Wood sheets, each (15 mm) thick, were screwed to the web of CFS pieces to construct them. Flexural-torsional buckling and local buckling were two of the failure modes.

(Liping W. et al, 2017), [14] carried out an investigation to assess the impact of web holes with varying diameters on the structural performance of thin CFS built-up sections. The study involved comparing the moment capacities of these beams with predictions derived from the Direct Strength Method (DSM) equation, utilizing both computational simulations and experimental data. The construction process encompassed the assembly of I-shaped open segments as well as closed sections configured in a box-like manner, these elements were fashioned by positioning two fundamental channels in a configuration face to face. The specimens were characterized by a range of hole diameter-to-web depth (d_h/h_w) ratios spanning from 0 to 0.80. The presence of web openings within the constructed open and closed section beams resulted in a decrease in their moment capacities, consequently leading to localized failures. Specifically, as the dh/hw ratio progressed from 0 to 0.5, the ultimate moments of the built-up open section beams exhibited a reduction of 7%, while the closed section beams experienced a reduction of 11%. Notably, altering the d_h/h_w ratio from 0 to 0.8 resulted in a more substantial reduction in moment capacities, with built-up open section beams and closed section beams experiencing reductions of 18% and 25%, respectively. The findings underscored that the influence of web openings on the structural integrity of closed-section beams was more pronounced compared to open-section beams. This investigation highlights the significant impact of varying web hole diameters on the attitude of thin

CFS built-up sections, contributing valuable insights to the understanding of their structural performance.

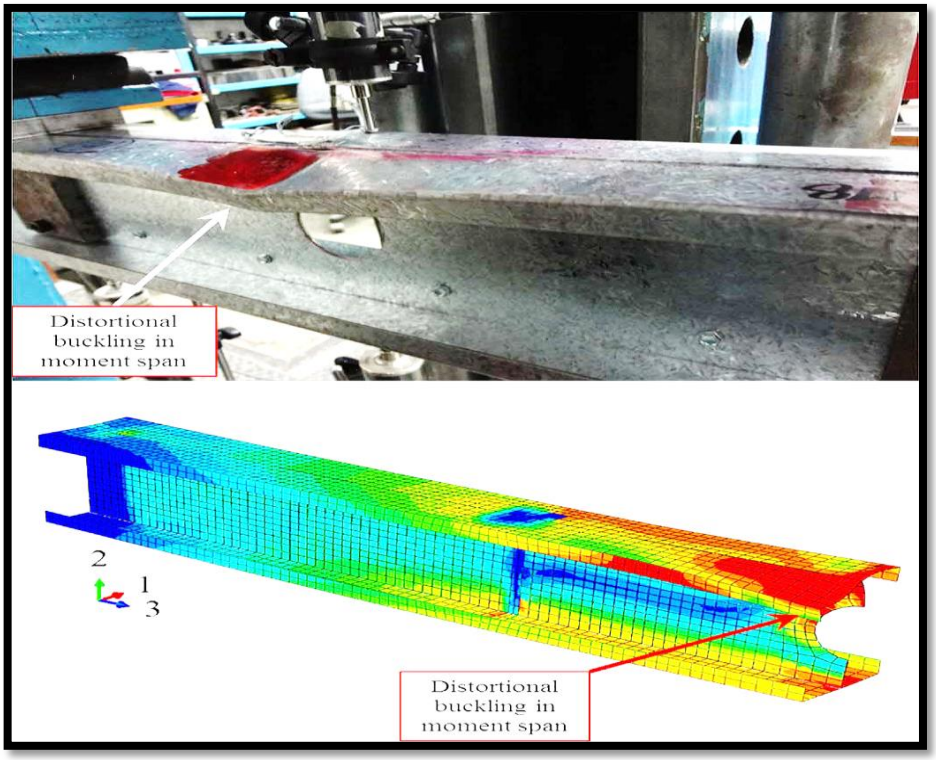

Plate(2-1): Distortional Buckling in Test.

(Jenitha G. et al, 2016), [15] examined channel and built-up CFS beams. Two cold-formed steel channel beams, two CFS (C back-to-back) beams, and one hot-rolled steel I-beam were tested to find the maximum load and deflection at maximum load. To compare with the results of the tests, the beams were also modeled using the ANSYS 14 program. The maximum load of a CFS beam (C back-to-back) was higher than that of an ordinary beam. The advantages of CFS beams over hot-rolled steel beams included low weight, cost savings, ease of molding, and thermal insulation.

(Kimcheng K. et al, 2017), [7] investigated a flexural characteristic of CFS beams arranged in a back-to-back configuration under four-point loading conditions. To achieve this, two C-section beams were connected using bolts. A total of twelve specimens were examined, each possessing three distinct cross-sectional dimensions: C10012, C10015, and C15015, with

depths of 100mm, 150mm, and thickness of 1.5mm. The spacing between each of these connected beam segments was set at L/2, L/3, L/4, and L/6, where L represented the length of the beam, specifically measured at 4 meters. The thickness and spacing of the C back-to-back beams were found to influence the experimental results. Notably, all specimens underwent failure due to lateral-torsional buckling and distortional buckling. In this study, the beam specimens were subjected to nonlinear finite element analysis to simulate their behavior. The FEA results were subsequently compared with the practical findings. The observed failure modes in the experimental tests were consistent with the failure modes predicted by Finite Element Analysis. Moreover, when comparing the ultimate load values between the experimental results and the numerical predictions, the disparity was found to be within the range of 21% to 36% for all the examined sections. This convergence between practical and numerical outcomes adds credibility to the specificity of the FEA in predicting the behavior of CFS beams in a back-to-back configuration.

(Krishanu R. et al, 2020), [16]. examined the strength of flexural for built-up CFS channel sections with gaps between them under four-point bending circumstances, using experimental and numerical methods. An extensive analysis of 72 finite element analytical simulations and 18 laboratory tests evaluated the flexural capacity of these sections. The study built plain channels, channels with one web stiffener, and channels with two web stiffeners. The beam spans were (1000 and 2000) mm in experimental tests. An extensive parametric investigation using a validated finite element model examined how web stiffeners and link-channel spacing affect gapped built-up beam flexural capacity. The investigation found that AS/NZS (2018) and AISI (2016) design provisions were more conservative, resulting in a 27% overestimate. Built-up CFS channel sections with gaps between them and

two web stiffeners increased beam flexural capacity by 10% compared to beams made of back-to-back channel sections and plain channel sections.

(Ji-Hua Z. et al, 2021), [17]. employed non-linear Finite Element Analysis to comprehensively investigate the structural behavior of twelve distinct beam models, which were subjected to four-point bending. The newly developed numerical model underwent validation, after which a parametric analysis was executed to explore the response of structural for hollow section beams across the broader spectrum of cross-sectional sizes. This extensive research endeavor encompassed the examination of 36 numerical data points. Additionally, the study entailed an evaluation of five contemporary design methodologies employed for CFS structural elements. These methodologies included [Euro Code 3 (EC3), North American Specification, Australian/New Zealand Standards, direct strength method & continuous strength method]. The assessment was conducted based on empirical observations as well as computational data. The findings of this research reveal a consistent trend across all three design standards, indicating that they tend to provide conservative estimations. Notably, both direct strength technique and continuous strength method exhibited a higher level of reliability in their predictive capabilities based on the empirical and computational data.

2.3 Hollow Flange Cold-Formed Steel Beams

(Avery P. et al, 2000), [18] analyzed the flexural behavior of beams with hollow flange (HFBs) by FEA model. This model employed non-linear analysis techniques to simulate the response of flexural members. Notably, the model considered a range of influential factors that have the potential to impact the strength of structural members. These factors included inelasticity of material, local buckling, instability of member, distortion of web, stresses residual, and imperfections of geometric. The efficacy of the proposed FEA

model was demonstrated through its ability to accurately predict critical points, such as the onset of LTB and the load-bearing capacities of HFB elements. This capability facilitated the construction of design curves and the advancement of design methodologies. These analytical capacity curves provide a means to directly determine the flexural section capacity of HFB members and their response to uniform bending moments. The study placed particular emphasis on the comparison of design approaches for HFB flexural members, focusing on the methodologies outlined in AS4100 and AS4600. Among these approaches, it was determined that the most accurate prediction of member capacity can be achieved by adopting the coefficients, analytical section capacities, and member capacity equations proposed by Trahair[19]. This research introduces a comprehensive approach to understanding and predicting the behavior of hollow flange beams under flexural loading, contributing to the enhancement of design practices in this field.

(Somadasa W., 2005), [3] constructed a CFS beam using two torsion-ally rigid rectangular hollow flanges and a skinny web, interconnected through intermittent fastening of screw in an effort to improve strength of flexural with minimizing production costs. This innovation led to the development of the Rectangular Hollow Flange Beam (RHFB). The RHFB was subjected to flexural testing with variations in steel grades, thicknesses, section dimensions and screw spacing. A total of 30 specimens were used for testing, focusing on lateral buckling behavior and section moment capacity. The study encompassed the characterization of the moment capacity testing and various failure modes including local buckling, lateral distortional buckling, and lateral-torsional buckling of RHFB. The research compared the experimental results to predictions derived from design standards and methodologies. Finite element software was employed to accurately represent the conditions of physical observed during LB and moment

capacity tests for section. The FE models progress was capable to effectively replicate the behavior of buckling and ultimate failure of RHFB, as validated by the experimental and finite element analysis results. The parametric analysis was employed, this analysis led to the formulation of new design equations for RHFBs that encounter phenomena related to local, LD, and LDB. In summary, this research contributes to the advancement of design practices in CFS beams by introducing the innovative Rectangular Hollow Flange Beam, exploring its behavior through experimentation and finite element analysis, and formulating improved design equations to account for various buckling phenomena.

(Jun D. et al, 2008), [20] examined how cross section distortion affects HTFGS's lateral-torsional buckling flexural strength using finite element model. A transverse web stiffener arrangement was discovered to minimize cross section distortion's effect on LTB strength. FE models were evaluated for nonlinear load-displacement to determine HTFG flexural capacity. Residual stresses were significant in parametric analysis. The LTB was used as a limit state in design flexural strength estimates compared to FE results. The AASHTO LRFD Bridge Design Specifications calculations overstate HTFG LTB strength. While Sause and Kim's [21],[22] design flexural strength calculations can predict HTFGs' LTB flexural strength.

(Hassaneein M.F. et al, 2013), [23] employed an elastic Finite Element model of three-dimensional that focused exclusively on geometric nonlinearity to investigate the resistance of buckling of hollow tubular flange plate girders (HTFPGs). This model was designed to capture various modes of buckling, including local, interaction, and LTB, by specifying the types and quantities of components present in the system. In contrast to traditional beams that possess solid webs, the girder shape and slenderness uniquely affect the moment-gradient component C_b in finite element analysis. Consequently, an equation for calculating the C_b factor was introduced

specifically for HTFPGs with thin stiffened webs. The non-linear strengths of flexural of these girders were subjected to examination and compared against estimates provided by the American Institute of Steel Construction (AISC). The earliest AISC predictions incorporated both the currently planned C_b value and the code-recommended C_b value, both of which demonstrated conservatism. The recommended AISC strength (C_b = 1.35) was identified as the most accurate value but exhibited a discontinuity in the relationship between flexural strength and un-braced length. To address this, a linear representation was commonly used to approximate the relationship's central tendency. The proposed AISC methodology introduced in this research offers the potential to estimate the strength of flexural of HTFPGs within narrow stiffened webs by Finite Element data.

(Pologanathan K. et al, 2014), [24] noted an experimental study of the Lite Steel Beam (LSB), a CFS hollow flange channel beam, under coupled bending and shear. The latest AS/NZS4600 and AS4100 design standards compared 18 specimens. Based on experiment results, two lower bound design equations were proposed. These equations make building LSBs for coupled bending and shear motions more confident and cost-effective. Three-point loading was used throughout 18 tests. The study's observations revealed a notable decline in shear capacity when the applied bending forces reached 65% of the section's moment capacity. Furthermore, the ability to withstand bending loads was compromised when shear stresses surpassed 65% of the shear capacity. In cases where the failure mode of LSBs was primarily due to shear, distinct features were observed, including the formation of web yield zones and the progression of diagonal post-buckling tension field mechanisms. On the other hand, instances where failure occurred primarily during the initial bending process were characterized by buckling phenomena and yielding of the compression flange located in proximity to the point of loading.

(Ropalin S. et al., 2016), [25] documented the moment capacities of sections belonging to a rectangular hollow flange channel beam (RHFCB) that were joined using rivets, consisting of two rectangular hollow flanges and a web. Mono-symmetrical RHFCBs have more capacity than other cold-formed sections because they have no open edges. A low-cost intermittent self-pierced rivet holds two hollow flanges to a web by RHFCB manufacture. Moment capabilities of section of RHFCBs fastened with rivet were assessed to delay narrow web element buckling. 15-section moment capacity testing encompassed RHFCB flexural parts. Intermittent web-flange junction riveting lowered section moment. The latest [AS 4100, AS/NZS 4600 & AISI S100] steel design standards were compared to testing ultimate moment capacities. Tests compare maximum moment capacity to cold-formed and hot-rolled steel design specifications and typical bending moment-vertical deflection curves. Reduced rivet spacing lowers section moment, expect cautious AS 4100. AS/NZS 4600 predictions agree reasonably well with test moment capacities of RHFCBs rivet fastened at (50 and 100) mm spacing, but were un-conservative for 200mm rivet spacing. Current DSM predicts the moment capacities of RHFCBs with smaller rivet spacing (50 and 100) mm reasonably well. The comparisons for 50 mm spacing were similar to those for welded hollow flange channel beams.

(Nilakshi P. et al, 2017), [26] measured section moment capabilities of 12 HFSPGs with compact, non-compact and thin sections under four-point load with span length of 1800mm. Local plate element compression buckling in uniform moment region failed all HFSPG specimens. Ultimate HFSPG failure moments pointed out the link between bending moment and mid-span vertical deflection. Comparing HFSPG and UB section moments. HFSPGs could replace industrial WBs and UBs. The test findings were compared to steel design standard design equations. The comparison highlighted that all

steel design standards exhibited conservative estimations, with the accuracy varying based on the type of section considered.

(Mohammad A.D. et al, 2019), [27] presented cutting-edge packing material research on rectangular hollow compression flanged sections. Using four-point flexural testing, the CFS composite beam specimens' flexural capacity, failure modes, and deformed morphologies were evaluated. The comparative analysis of the design strengths of the experimental specimen was conducted by evaluating its compliance with both [North American Specifications & Indian Standard] to CFS constructions. Unique rectangular compression flanged CFS composite beams with innovative packing materials have good strength and stiffness. Strong cardboard and wood packing, especially in the flange, raised the section's capacity. The packing materials' CFS interaction improved these parts' bendability, thus, this inquiry met its objectives.

(Balaji S. et al, 2021), [28] used the four-point loading system to study built-up section flexural behavior, strength, and failure modes. Figure (2-3) provides a visual representation of the arrangement of built-up I-beams. These I-beams are made by linking stiffened or unstiffened channels back-to-back at the web. I-beams have hollow tubular rectangular flanges at the top and bottom. Experimental tests built and validated non-linear finite element models. The built-up I-beam behavior was precisely predicted by the FE models. Using validated FE models, a parametric investigation on CFS up beam sections was conducted on thickness, depth, and yield stress. According to [American Iron & Steel Institute AISI] guidelines for CFS structural members, the beams' flexural strength was calculated using the direct strength method and compared to experimental results and FE model failure loads. The experimental data fit the FE model failure mode forecast completely.

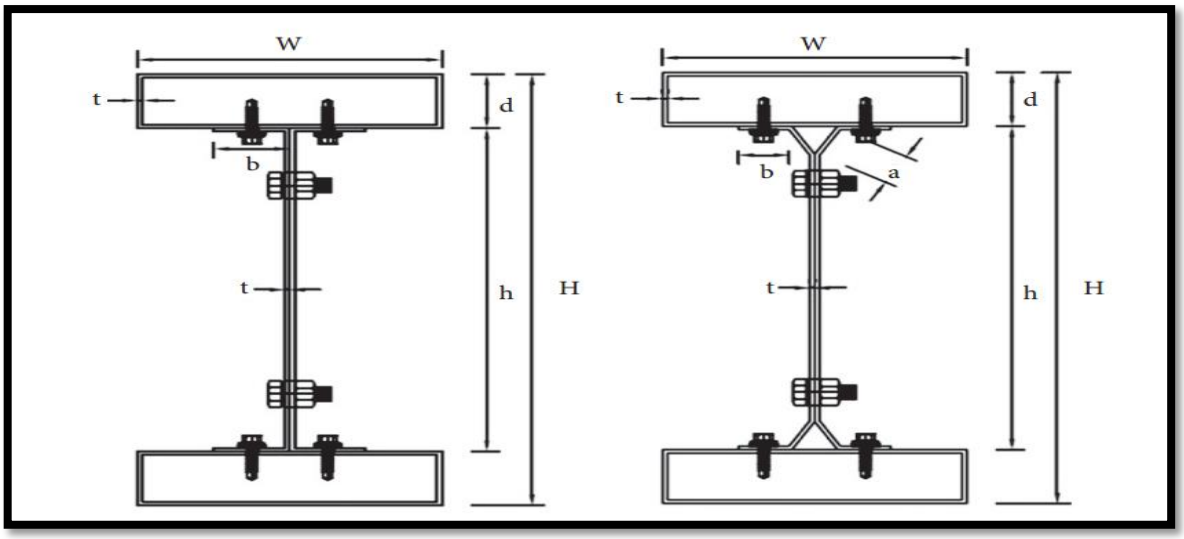

Figure (2-3): Section geometries**.**

2.4 Strengthening Hollow Flange CFS Beams

(Gao F. et al, 2014), [29] explored the characteristics of flexural for simply supported pentagonal concrete-filled flange beams (CFPFBs) when subjected to midpoint-span loading, utilizing a combination of experimental and computational approaches. Two CFPFB specimens tested to failure under static load conditions. One test specimen had a transverse stiffener around its midsection, while the other had no stiffener. The material and geometry of both test specimens were identical. Experimental data showed that the stiffener increased flexural capacity by 10%. The failure pattern showed how a transverse stiffener improved final flexural strength and prevented beam web distortion. The four-node shell and eight-node solid elements simulated steel and concrete. The CFPFBs' maximum capacity with and without stiffeners indicates good FE model simulation. The maximum load and test specimens' flexural behavior differed by less than 10%. In the experimental phase of the study, the structural response of two simply supported beams, referred to as BWTS and BWS. The observed failure modes in the BWTS beam included LDB and LB of the web, while the BWS beam exhibited a failure mechanism primarily characterized by lateral-

torsional buckling. The FE analysis showed that the specimens' ultimate capacity and a FE models agreed within 10%. Experimental and FE research showed that the transverse stiffener was essential to preventing web local buckling and distortion failure. Improved CFPFB member ductility and capability were also critical. CFPFBs in-filled concrete improve flange strength, stiffness, and stability over HPFB versions.

(Yongbo S. et al, 2016), [30] involved a new design for an I-girder configuration characterized by a corrugated web and a concrete-filled rectangular tubular flange. This innovative I-girder design employs the concrete-filled tubular flange to enhance its resistance against global buckling by significantly improving its torsional and flexural rigidity. In comparison to the alternative of using a flat web with either transverse or longitudinal stiffeners, the corrugated web not only provides superior local buckling resistance but also maintains a lighter weight due to its light thickness, and resist the shear force due to its improved bending stiffness in out-of-plane. This investigation examined two specimens. The first I-girder's static failure mechanism was evaluated using a classical I-girder with flat-plate flanges and web. Both specimens were subjected to a concentrated load at mid-span. The new I-girder SP-N has a trapezoidal corrugated web, flat-plate flange, and concrete-filled rectangular tube flange. The typical I-girder SP-C follows, a flat-plate web, two flanges, and five transverse stiffeners characterize an I-girder (SP-C). Test results show that the classic I-girder buckles globally due to its open section's weak torsion resistance. The new I-girder fails at mid-span flexural yielding despite greater torsional rigidity from a closed tubular flange. Even though the corrugated web is smaller, its out-of-plane bending stiffness resists shear stress. The accordion-effect corrugated web of the redesigned I-girder bends less.

(Hassanein M.F. et al, 2017), [31] performed experiments on square, thin-walled steel flexural members filled with cementations' material. The

restricted concrete, used as a filler material in the hollow areas, served to increase the flexural resistance of these sections by preventing the plate components from buckling.

(Wang Y.M. et al, 2019), [32] focused on a three-point shear loads on W-girders using Concrete-Filled Tubular Flanges (CFTFs) and Corrugated Webs (CW). The study used FE simulations and theoretical studies. The key findings of the study are as follows:

- The flange component played a predominant role in determining the strength of flexural for W-girders with (CFTFs and CW). Additionally, the cross-sectional configuration of (CW) led to a consistent shear stress distribution.
- Properly designed CW sections may cause flange flexural yielding in composite I-girders with CFTFs and CW during shear strain. The CW's inadequate resistance to tension or compression forces may cause the flanges to buckle before shear-based buckling. The composite girder can support greater loads due to this feature.
- The strength of flexural estimation for an I-girder incorporating CFTFs and CW can be achieved by assessing the limit of yielding for the tensile steel tube situated in the bottom flange.
- Consider CFTFs and CW when determining shear strength. CFTFs sustain more than 10% of shear force, hence they cannot be ignored.

(Ashraf A.R. et al,2020), [10] examined the behavior of flexural of improved hollow tube flanged CFS I-beams. Four-point loading in bending tests was performed on Nineteen specimens. Two groups of specimens were made: one without strengthening and the other with various strengthening agents. These materials included particleboard, sawdust combined with cement mortar, epoxy, and polyester. Lightweight concrete and polymer mortar were also used to strengthen. In the experimental evaluation, all specimens failed in two modes at constant bending moment. However, the

control specimen failed exclusively due to into-there local buckling of the compression flange at the midpoint-span. Despite filler materials, strengthened specimens showed compression flange local buckling under external load. This demonstrated that filler materials did not significantly affect failure modes in improved specimens. The experimentally observed failure modes reveal the structural response of these strengthened elements under bending stresses.

- Adding wood waste materials to the flange at compression of test specimens increased the capacity of ultimate load by (26.19% to 42%) compared to the control specimen. Polymer-mortar material increased ultimate load by (61.1%) above the control specimen. Lightweight concrete increased ultimate load capacity by (40.3%) over the control specimen. The specimens that strengthening with different materials had higher toughness and stiffness than the control specimen, demonstrating the positive impacts of strengthening on structural performance.
- Increasing the strength of compressive of the material improved the ultimate load on strengthened specimens during testing directly.
- Shear connections strengthened the connection between steel compression flanges and strengthening components. The capacity of ultimate load increased (1.7% to 3.8%) with these connectors compared to specimens without connectors.

(Fei.Gao et al, 2021), [33] focused on the theoretical, numerical, and experimental aspects of designing and testing a novel high-strength concrete-filled tubular flange beam (HS-CFTFB). The research encompassed several key components:

- Theoretical and Numerical Models: The study involved the development of theoretical models to assess the elastic strength of LTB and plastic strength of HS-CFTFB. The models aimed to predict inelastic local

buckling strength, and the buckling factor for the inelastic model was generated through (FE) models.

- Experimental Verification: The models of FE were verified versus experimental data, demonstrating good agreement between the two. This verification process ensured that the numerical simulations accurately represented the behavior of the physical HS-CFTFB.
- Parametric Analysis: The research employed parametric analysis to explore the elastic LTB characteristics of simply supported HS-CFTFBs when exposure to a concentrated load at the midpoint of the span. Eleven parameters, such as span length, flange and web dimensions, material properties, and the presence of stiffeners, were varied to investigate their effects on the behavior of the beams.
- Flexural Behavior and Design Curve: Many of the FE models exhibited similar flexural behavior, leading to the creation of a design curve that correlates non-dimensional slenderness and the buckling factor. However, it was noted that this curve does not fully account for the shear failure, flange local buckling, and web distortion present in HS-CFTFBs.
- Structural Influences: The presence of in-filled concrete within the tubular flanges contributed to a reduction in localized buckling. Transverse stiffeners positioned at the midpoint of the span played a critical role in controlling web deformation. Moreover, the ratio of web slenderness helped mitigate the risk of shear failure.

(Fei. Gao et al, 2020), [34] studied the primary objective of behavior of LTB in HS-CFTFBs. This examination was conducted through a combination of experimental and computational methods. A total of six specimens were subjected to a simple support configuration, where an unrestrained lateral concentrated load was applied for testing purposes. The other examples exhibit LTB failure control, with two specimens demonstrating flexural yielding (F_y) failure control. Upon constructing FE

models, empirical findings indicate that these models possess the capability to effectively predict HS-CFTFB failure processes, load-displacement relationships, and ultimate capabilities. The research in question aims to explore the impacts of changing depth of flange, properties of concrete material and characteristics of steel on a variety of span lengths. To achieve this, validated finite element models are employed as computational tools for analysis and prediction. The moment capacity of steel beams, particularly those made of high-strength steel, exhibits a notable drop as the span length increases. Increasing the flange depth enhances LTB strength. The utilization of in-filled concrete enhances the ability of the flange to withstand deformation and ultimately raises its overall capacity. The influence of concrete strength on ultimate capacity is infrequently observed. When the span length is short, increasing the yield strength (F_y) may enhance the capability of LTB, however, the advantages diminish as the span length increases. When the elastic limit of a long thin beam (LTB) is exceeded, it is possible to enhance the post-buckling stiffness and ductility by raising the yield strength (F_y).

(Mohamed S.et al, 2021), [35] evaluated the flexural performance of light-weight normal and high-strength concrete-in-filled hollow flange CFS (CF-HFCFS) beams. A numerical study was followed by a simpler design technique to estimate CF-HFCFS' maximal moment capacities. Non-linear FE models were created to study the behavior of structural for (HFCFS) beams. These models were designed to analyze the response of the beams under different loading conditions and configurations, including scenarios with and without the inclusion of lightweight concrete infill within the steel members. Summarize the research conclusion:

- The maximum moment capacity of CF-HFCFS beams is greatly enhanced by the presence of concrete filling within the hollow flange, which has a notable impact on failure modes and load distribution.

- The finite element (FE) modeling methodologies employed in the study exhibited a high degree of agreement with empirical data, as evidenced by an average value and coefficient of variation (COV) of (1.03 and 1.4%), respectively.
- The increase in capacity was somewhat influenced by the grade of concrete. The addition of concrete filling in CF-HFCFS beams resulted in an enhanced composite action, successfully reducing the occurrence of early local buckling.
- The confinement factor and top flange slenderness were used to estimate maximum capacity using the capacity enhancement factor technique. Since an average value and COV are 1.00 and 3.6%, respectively.

2.5 Summary

Extensive research had been conducted on the behavior of flexural of built-up structures from Cold-Formed Steel (CFS), which had included both experimental studies and finite element analyses (FEA). Various influencing factors, such as hollow flanges, steel yield strength, section depth, thickness, beam span, geometries, stiffeners arrangements, screw configurations, and comparisons between single and built-up sections, as well as closed and open section beams, were investigated in these studies. The objective of this study was to evaluate the performance of flexural of a composite Cold-Formed Steel (CFS) beam with a hollow flange. The experimental and numerical analyzes of the flexural behavior of the sections with hollow flanges were performed. In addition, the study investigated sections with hollow flanges that had been strengthened with a variety of materials. The primary objective of this study was to evaluate the effect of these strengthening techniques on the structural performance of beams as a whole. Through a comprehensive analysis of experimental and numerical results, this study seeked to contribute to a better understanding of the behavior of flexural of hollow

flanges cold-formed steel beams and their response to various strengthening techniques.

CHAPTER THREE

EXPERIMENTAL WORK

CHAPTER THREE

EXPERIMENTAL WORK

3.1 Introduction

The object of this research is to study the effect of rectangular hollow flange cold-formed steel I-beam(RHFCFSB) on the flexural strength of specimens. The University of Babylon's Laboratory prepared and evaluated all cold-formed steel (CFS) beam specimens under two concentrated loads conditions in order to achieve this goal. This chapter also includes a discussion of the testing instruments and specimens, the experimental work, and the test procedure after going over the tested preparations, geometry, dimensions, specimen properties, forming and cutting processes. The steps for designing steel beams were listed in the appendix A.

3.2 Properties of Steel Sections

3.2.1 Tensile Test of Steel

Tensile testing was performed on specimens taken from the steel sheets used to build the flange and web in accordance with ASTM Standard test method **(A370- 05)**[36]. The dimensions of the tensile testing specimen are depicted in Fig.(3-1) and the thickness of the specimen was 4mm. This test was conducted in the Mechanical Engineering Laboratory at the University of Babylon. A testing device holding a tensile specimen and tested coupons are shown in Plate (3-1). Table (3-1) displays the yield and ultimate stress for flanges and webs based on their tension their coupons from the steel plate. Figure (3-2) shows the load-deformation curve for steel coupons. The Poisson's ratio and modulus of elasticity were considered to be 0.3 and 200 GPa , respectively.

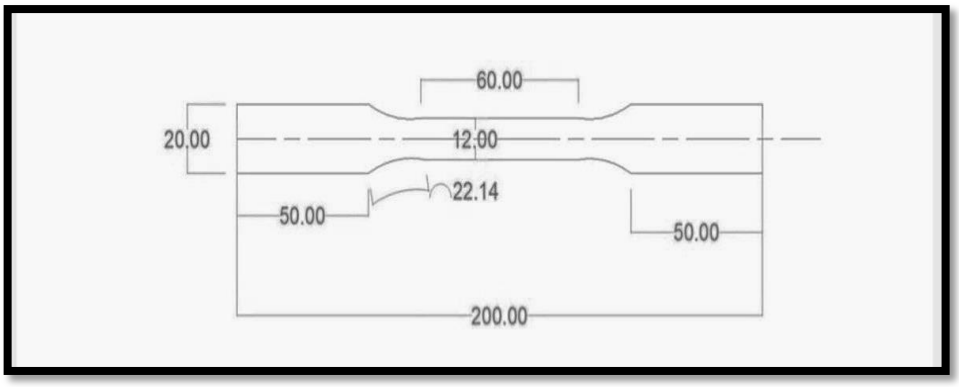

Figure (3-1): Specimen for tensile testing, [36].

Plate (3-1): Machine for Tensile Testing and Tested Coupons**.**

Table (3-1): Yield stress and ultimate tensile strength**.**

Tested coupons	Yield stress (MPa)	Ultimate tensile strength (MPa)
1	**265**	**375**
2	**265**	**370**
3	**270**	**380**
Average value	**266.7**	**375**

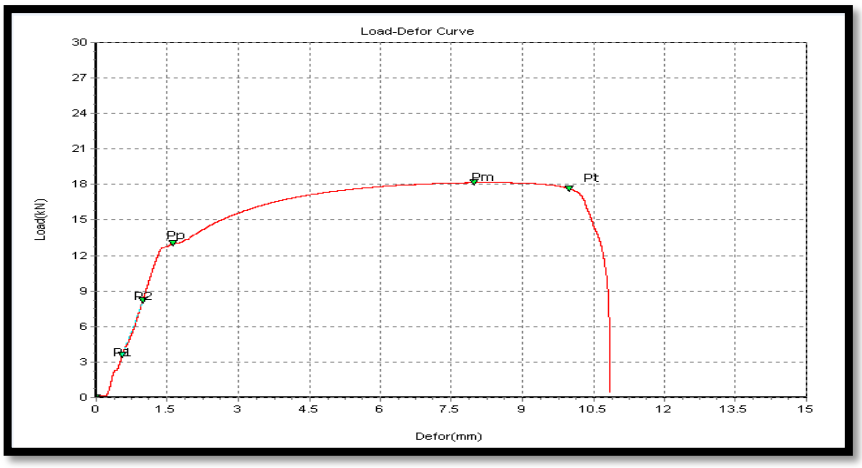

Figure(3-2): Load-Deformation Curve for Steel Coupons.

3.2.2 Properties of Bolts

Bolt connections with a 10 mm diameter, a 55 mm overall length, a 17 mm ahead diameter, and a 5 mm height were used in each test specimen to join two hollow flanges with web and prevent shear at the interface between the two components as well as horizontal separation between them. Three randomly selected specimens were tested under direct tension to show the mechanical characteristics of the bolt connectors. The results of the test, which were completed in Al-Musayyab Technical Institute's mechanical laboratory using a universal testing device, are displayed in plate (3-2). Table(3-2) provides the tensile test results.

Plate(3-2): Universal Testing Machine.

Table(3-2): Bolt Properties.

Nominal diameter, mm	Actual diameter, mm	Area, mm^2	Yield stress, MPa	Ultimate tensile strength, MPa	Modules of elasticity(*), GPa
10	**9.9**	**78.53**	**255.5**	**306.6**	**200**

(*) assumed.

3.3 Description of Specimens

This section will give a detailed description of the steel section fabrication method, the research hypothesis, and the shape of the tested specimens.

3.3.1 Geometry of Specimens

Twelve specimens of ST37 carbon steel sheet of thickness (4mm) were tested under four point loading scenarios to evaluate the ultimate load capacities and failure modes of built-up section beams with similar span lengths (1500mm).

3.3.2 Specimen's Dimensions

A CFS Built up rectangular hollow flange beam with dimensions (H=300mm, b_f=150mm, t_f =4 mm and t_w =4 mm) was used for all sections of specimens. All tested beams consist of two rectangular flanges and web connected with each other by carbon steel bolts with diameter (10mm). Tested specimens are shown in Figures((3-3) and (3-4)).

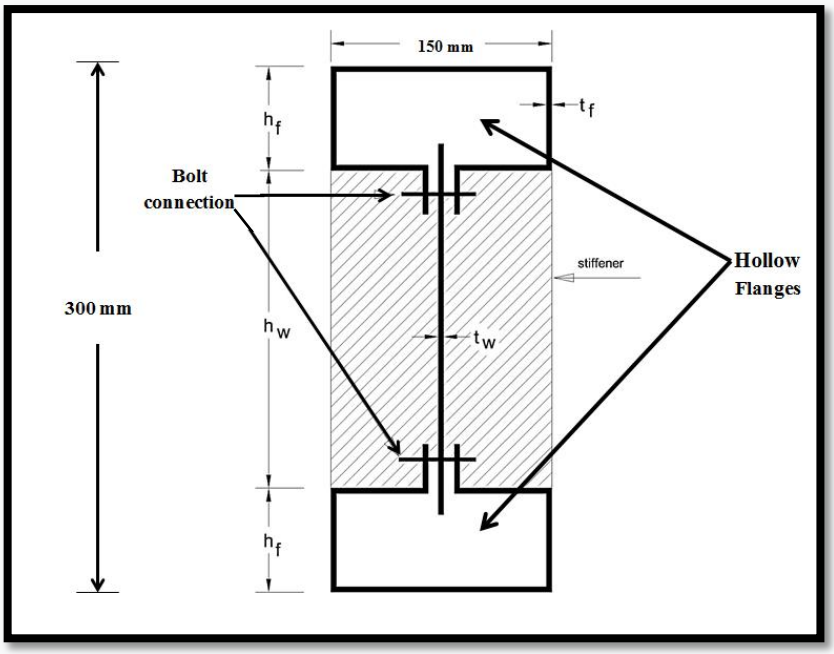

a)Details of Cross-Section of Beams.

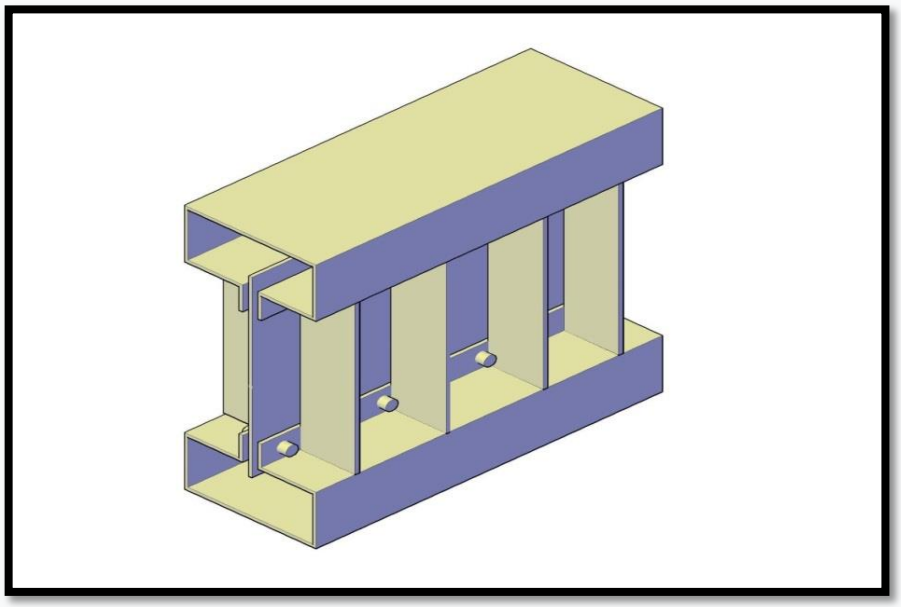

b) Three dimensional view of Cold-Formed Steel Beam Specimens.

Figure (3-3) : Details of Specimens.

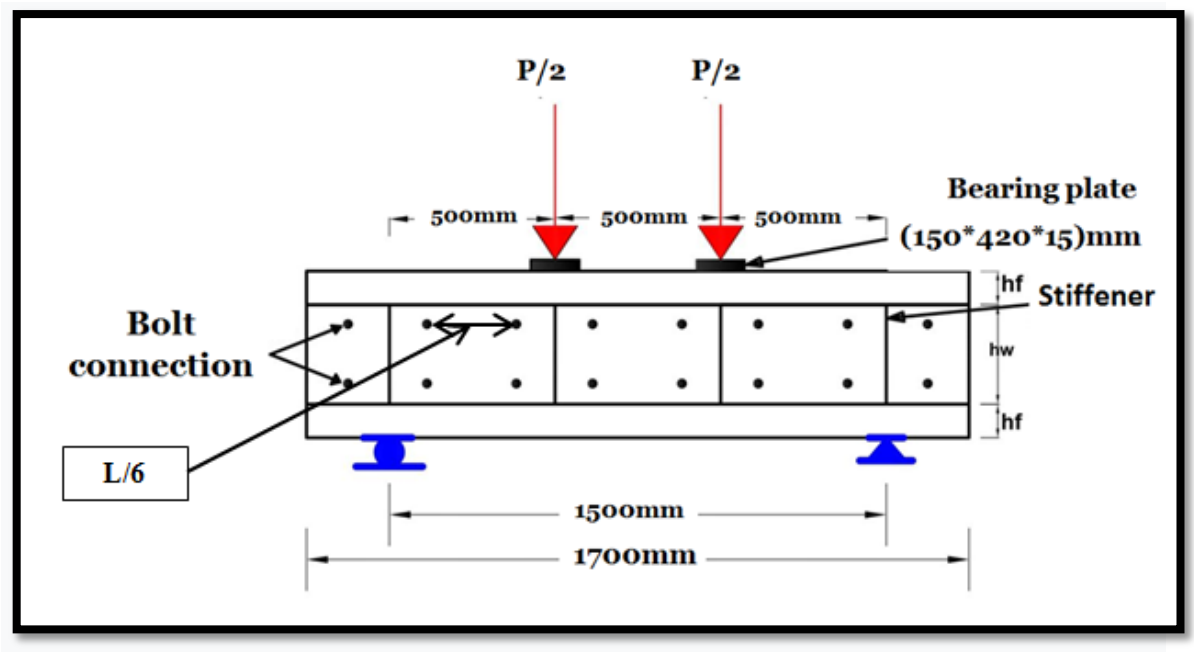

Figure(3-4) : Loading and Supporting Details of the Beam .

3.3.3 Steel Section Cutting and Forming

Cutting machine used to cut the steel sheet to achieve desirable measurement of sections. Hydraulic press brake plate machine used for bending and shaping process of channels and angles. The cutting machine and hydraulic press brake plate machine as shown in Plates(3-3) and (3-4)**,** respectively**.**

Plate(3-3): The Cutting Machine.

Plate(3-4): Press Brake Plate Machine.

After cutting the cold-formed steel plate and forming it into a channel, angles and flat plate, these parts are joined to form the beam, where each channel is welded with two angles to form the flange, and this flange is connected to the flat plate(web) by means of bolts to form the built-up hollow rectangular flange cold-formed steel I-beam sections(RHFCFS), as shown in plate(3-8), the distance between the bolts was at (L/6) of the span length from the supports[7], as shown in plate(3-7).

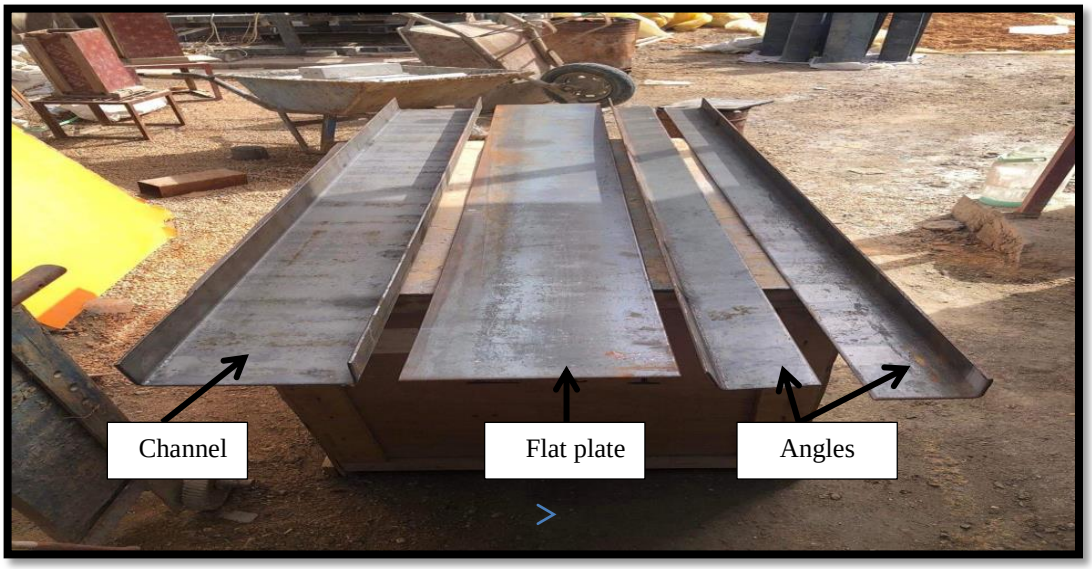

Plate(3-5): The Parts of Sections**.**

Plate(3-6): Connecting Parts of Sections**.**

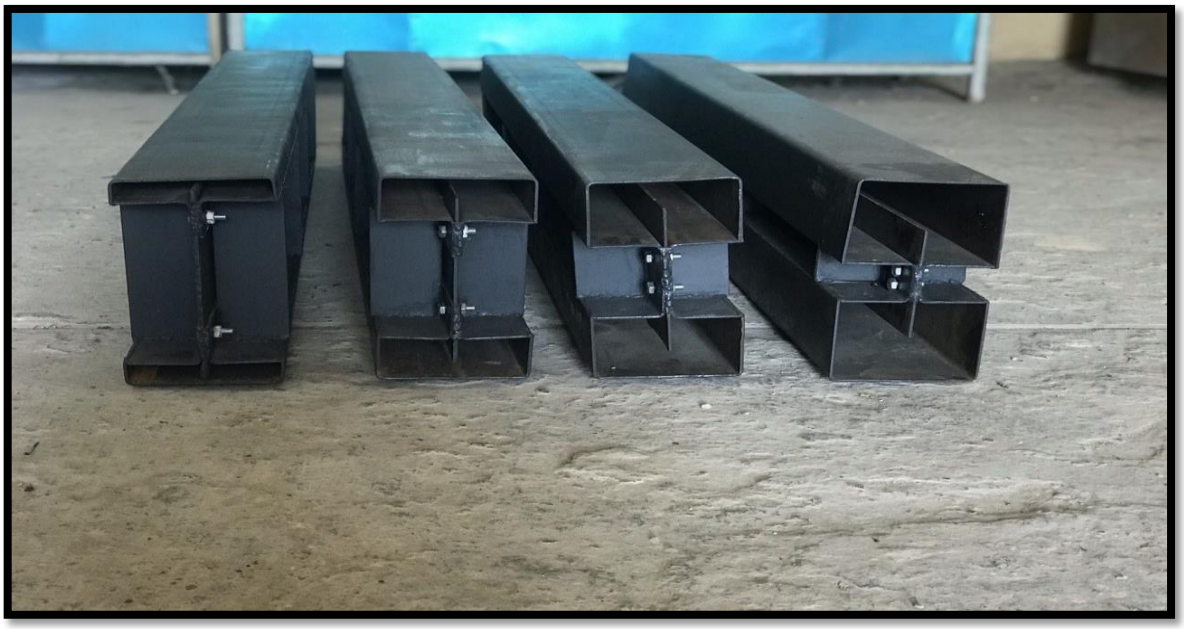

Plate(3-7): The Built-up Hollow Rectangular Flange Cold-Formed Steel I-Beam Sections(RHFCFS).

3.3.4 The Study Hypothesis

The experimental work was done in two groups:

- The group I was done by making four specimens with different depth of flange depending on the ratio of depth of flange to depth of cross section for beam, as shown in plate(3-8).

The flange depth (h_f) = the total depth of beam(H) × X

Where X equals to (0.1,0.2,0.3 and 0.4).

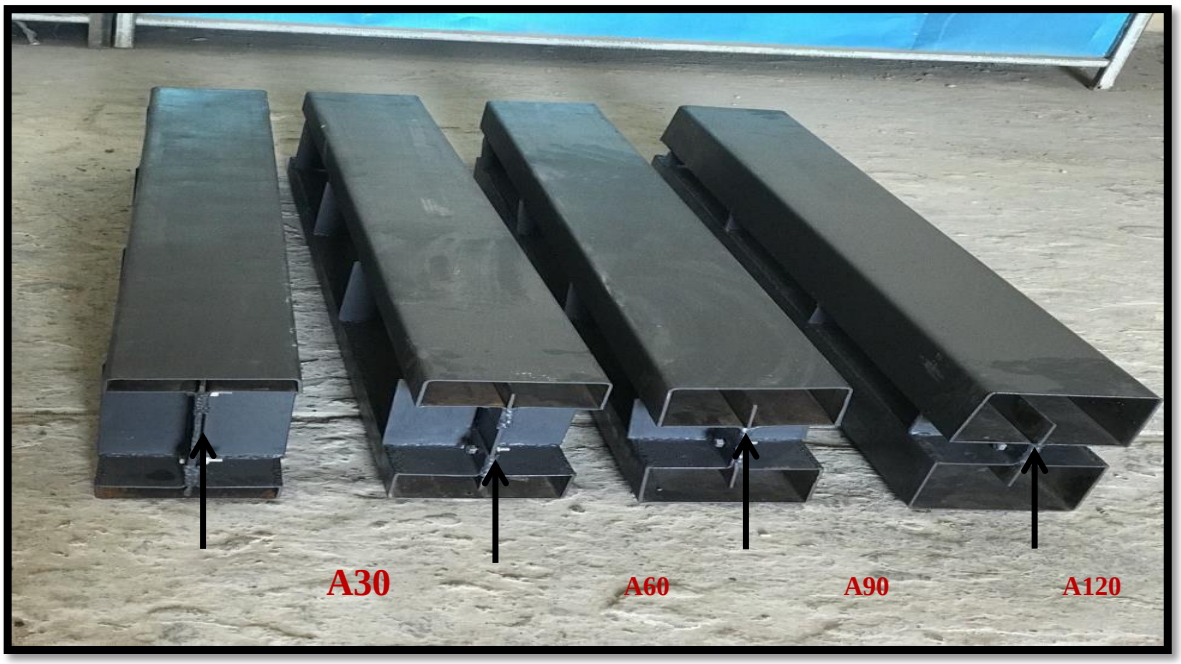

Plate(3-8) : Specimens of Group I.

All details of Specimen′s identification of group I and their dimensions shown in Tables (3-3) and(3-4) .

Table (3-3): Identification for flange depth of group I.

Specimen identification	Description
A30	**CFS I-beam with rectangular hollow flange (h_f=30mm)**
A60	**CFS I-beam with rectangular hollow flange (h_f=60mm)**
A90	**CFS I-beam with rectangular hollow flange (h_f=90mm)**
A120	**CFS I-beam with rectangular hollow flange (h_f=120mm)**

Table (3-4): Details for cross-section of specimens of group I.

Specimen identification	H mm	h_f mm	h_w mm	b_f mm	t_f mm	t_w mm	Location of connection
A30	**300**	**30**	**240**	**150**	**4**	**4**	**L\6**
A60	**300**	**60**	**180**	**150**	**4**	**4**	**L\6**
A90	**300**	**90**	**120**	**150**	**4**	**4**	**L\6**
A120	**300**	**120**	**60**	**150**	**4**	**4**	**L\6**

- The group II of the experimental work was done by making eight specimens from **A60** filled the hollow flange by different strengthen materials to improve the flexural behavior of specimens , as shown in plate (3-9). All details of Specimen′s identification of group II shown in Table(3-5).

Table (3-5): Details of tested specimens of group II.

Identification of specimens	Description
A60LC	**CFS I-beam with rectangular hollow flange (h_f=60mm) filled with light weight concrete.**
A60NC	**CFS I-beam with rectangular hollow flange (h_f=60mm) filled with normal concrete.**
A60RC	**CFS I-beam with rectangular hollow flange (h_f=60mm) filled with normal concrete (coarse aggregate has been replaced with100% recycled concrete).**
A60S	**CFS I-beam with rectangular hollow flange (h_f=60mm) filled with normal concrete 30% of the coarse aggregate has been replaced with sawdust.**

Table (3-5): Continue**.**

Identification of specimens	Description
A60FR	**CFS I-beam with rectangular hollow flange (h_f=60mm) filled with normal concrete 30% of the fine aggregate has been replaced with Fine rubber.**
A60CR	**CFS I-beam with rectangular hollow flange (h_f=60mm) filled with normal concrete 30% of the coarse aggregate has been replaced with Coarse Rubber.**
A60IF	**CFS I-beam with rectangular hollow flange (h_f=60mm) filled with normal concrete 30% of the gravel has been replaced with Iron Fillings.**
A60CSG	**CFS I-beam with rectangular hollow flange (h_f=60mm) filled with normal concrete 30% of the coarse aggregate has been replaced with Coarse Shattered Glass.**

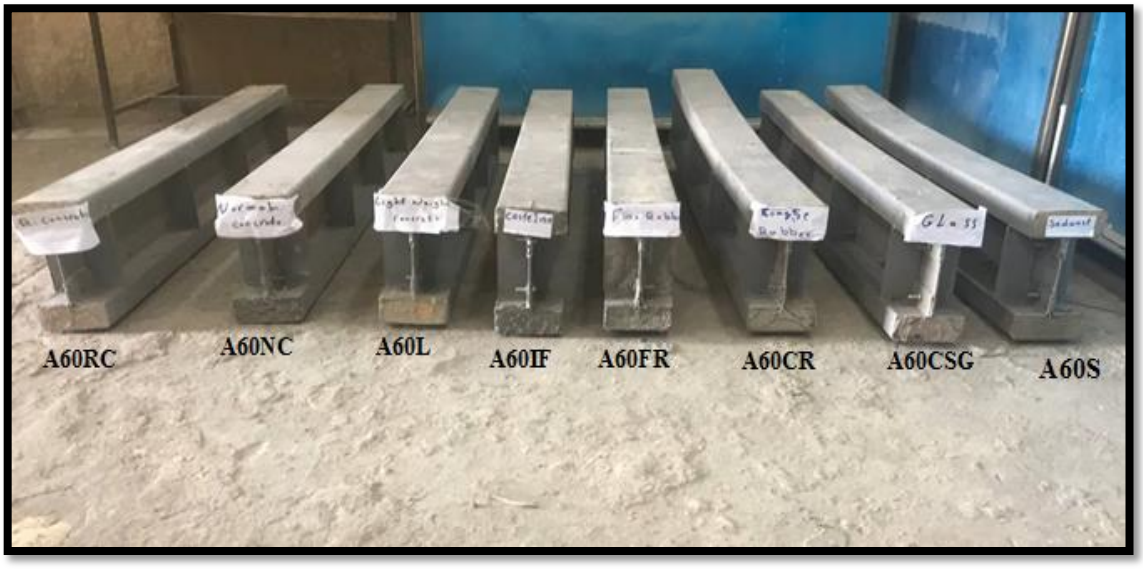

Plate(3-9): Specimens of Group II.

3.3.5 Stiffeners

Bearing stiffeners are placed under each concentrated load and supports to avoid side sway buckling, local buckling, compression buckling of the web and crippling. The stiffeners details are mentioned in Table(3-6).

Table (3-6): Details of stiffeners.

Specimens identification	Stiffener depth, mm	Stiffener width, mm	Thickness, mm
Group I			
A30	**240**	**69**	**4**
A60	**180**	**69**	**4**
A90	**120**	**69**	**4**
A120	**60**	**69**	**4**
Group II	**180**	**69**	**4**

3.4 Strengthening Materials

To increase load capacity, buckling resistance, and decrease deflection, eight alternative materials were proposed as fillers for the rectangular hollow flanges of CFS I-beam. Many criteria were considered, including low cost, lightweight, and great strength. The strengthening materials are :

- Light weight concrete(LWC) used to strength **A60L**.
- Normal concrete(NC) used to strength **A60NC**.
- Normal concrete (coarse aggregate has been replaced with100% recycled concrete)(RCC) used to strength **A60RC**.
- Normal concrete 30% of the coarse aggregate has been replaced with sawdust (SC) used to strength **A60S**.
- Normal concrete 30% of the fine aggregate has been replaced with Fine rubber (FRC) used to strength **A60FR**.

- Normal concrete 30% of the coarse aggregate has been replaced with Coarse rubber (CRC) used to strength **A60CR**.
- Normal concrete 30% of the gravel has been replaced with Iron fillings (IFC) used to strength **A60IF**.
- Normal concrete 30% of the coarse aggregate has been replaced with Coarse shattered glass (CSGC) used to strength **A60CSG**.

3.5 Strengthening Materials Properties

The materials that were used to strengthen cross sections consist of several different materials and using different equipment to mix them. A description of these materials is given below.

3.5.1 Cement

All sulphate resisting cement (I) was used in this study. Tables (B-1) and (B-2) respectively provide the chemical and mechanical properties of the cement used are given in Appendix B. These properties have been tested for sulphate resisting cement according to the Iraqi specification limits (IQ.S NO.5/1984)[37]. The chemical and mechanical properties of the cement used have been tested at University of Babylon/ College of Engineering/Construction Laboratory.

3.5.2 Coarse Aggregate

A (19mm) max. size coarse aggregate was used in this study according to (IQ.S NO.45/1984) and (Consultative Reference Guide (NO.500/1994)Weighted Method) [38] as shown in Table(B-3) in Appendix B. Table (B-4) shows the physical properties for coarse aggregate was used in this study. Testing was conducted at University of Babylon/ College of Engineering/Construction Laboratory.

3.5.3 Fine Aggregate

Sands of average weight that were transported from the Al-Najaf quarry were used as the fine aggregate in this study. As shown in Table (B-5) in Appendix B, the max. size of sand was (4.9mm) and in accordance with (IQ.S NO.45/1984) and (Consultative Reference Guide (NO.500/1994)Weighted Method) [38]. See (Table(B-6) in Appendix B) that shows the results of physical tests on the fine aggregate utilized throughout this investigation The Construction Laboratory at the College of Engineering at University of Babylon served as the site for the testing.

3.5.4 Water

In this study, tap water of Babylon city was used for mixing and curing of concrete, water which conformed to (IQS1703/1992).

3.5.5 Replacement Components

In this study, several re-used materials were used as a substitute for fine aggregate or coarse aggregate to reduce weight and cost and to study its effect on the flexural behavior of the sections. These materials are shown in the following Table (3-7). The properties of these materials are given in Appendix B.

Table (3-7): The Material definitions.

NO.	Symbol	The re-used materials	
1	**RC**	**Recycled Concrete**	
2	**S**	**Sawdust**	
3	**FR**	**Fine Rubber**	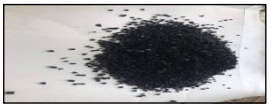

Table (3-7): Continue.

NO.	Symbol	The re-used materials	
4	**CR**	**Coarse Rubber**	
5	**IF**	**Iron Fillings**	
6	**CSG**	**Coarse Shattered Glass**	

3.6 Preparation of the Strengthening Material

3.6.1 Concrete Mix Design

In this study, used self-compact normal concrete and self-compact light weight concrete to strength the specimens. Several experimental mixes were made to attain the required compressive strength of a typical cylinder. It had a cement content of (kg/m^3), a water/cement ratio of (0.46), and an average value 0f slump flaw of (70 cm) as shown in plate (3-10). To achieve (30MPa) compressive strength in (28) days, a weighted average of (1:1.6:2.22) was used. According to the guidelines (ACI 211.1-95[39], table (3-8) shows the quantities of materials. Before starting the mixing process, sawdust, recycled concrete, and silica gravel were saturated with water (saturated surface dry) because these materials have the ability to absorb water, so we saturated them with water so that their water absorption does not affect the water of the mixture.

Plate (3-10): Slump Flow of Concrete Mix.

Table (3-8): The quantities of materials.

Material	Quantity (Kg/m^3)
Cement	**500**
Fine agg.	**775**
Coarse agg.	**825**
water	**190**
Super plasticizer (S.P)	**3.15**

3.6.2 Mixing

1. Each quantity was weighed before being put into clean packaging. After that, each mold (cube, prism, and cylinder) was greased**,** as illustrated in plate (3-11).

a) Material weights.

(b) All molds (cylinder, cube and prism).

Plate (3-11): Casting of control specimens.

2. The fine aggregates (or re-used material) and coarse aggregate (or re-used material) were then put to the mixer, and it was run for one minute. The cement was then added, and the mixture was processed again. Finally, water and super plasticizer were added to the mixture, which was allowed to run for three to four minutes, as illustrated in plate (3-12).

Plate (3-12): Operation of Concrete Mixing.

3. The area was leveled and the concrete surface was finished with a shovel after carefully placing the concrete into well-stacked, greased steel molds. The samples were then covered with a nylon sheet to prevent the water from evaporating. as illustrated in plate (3-13).

Plate (3-13): The Molds after Casting**.**

4. After that, the rectangular hollow flange for all the beams was filled with concrete. Each of the eight beams was filled with concrete according to the type of material used to strengthen it.

5. After leaving all steel beams and cast samples in the lab for (24 hours), the specimens were taken from the molds and allowed to cure for (28 days) by

covering them with nylon, as shown in plate (3-14). After a twenty-eight-day treatment period, remove the nylon from the samples.

Plate (3-14): The Molds in Curing.

3.6.3 Hardened Concrete Mechanical Properties

3.6.3.1 Compressive Strength Test

A hydraulic press machine was used to test the average three cube of (150 x 150 x 150) mm in line with (ASTM C39-86) [40] (1600kN). A compression test was conducted, as shown in plate (3-15), and Table (3-9) provides the cube's compression test results.

Plate (3-15): Compression Test for Cubic**.**

Table (3-9): Values of Compressive Strength Test**.**

Specimens	Test of Compressive Strength (MPa)At 28-days			Average value MPa
LWC	**28.79**	**37.81**	**26.97**	**31.19**
NC	**32.41**	**32.63**	**31.62**	**32.22**
RCC	**23.26**	**30.73**	**30.52**	**28.17**
SC	**19.19**	**21**	**19**	**19.73**
FRC	**21.79**	**18.59**	**22.3**	**21**
CRC	**18.75**	**14.79**	**16.24**	**16.6**
IFC	**35.24**	**37.78**	**38.4**	**37.14**
CSGC	**33.12**	**35.24**	**33.45**	**33.94**

3.6.3.2 Tensile Strength of Splitting.

The (ASTM C496-2004) was followed in performing the splitting tensile test, [41] regulation to test the cylinder (100 x 200) mm, as shown in plate(3-16). The values for splitting tensile strength are shown in Table 3-10. Tensile stress was computed using equation (3-1).

$$f_{sp} = 2P/\pi dL \quad \text{.....3-1}$$

Table (3-10): Values of Splitting Tensile Strength Test**.**

Specimens	Test of Splitting Tensile (MPa) at 28-days		Average value of Splitting Tensile (MPa) at 28-days
LWC	2.56	2.57	2.57
NC	3.04	3	3
RCC	3.11	3.11	3.11
SC	2.25	2.21`	2.23
FRC	2.06	2.03	2.05
CRC	1.4	1.68	1.54
IFC	3.58	2.97	3.3
CSGC	2.95	2.9	2.93

Plate (3-16): Splitting Tensile Test and the Machine.

3.6.3.3 Rupture Modulus (Flexural Strength) Test

Prisms with dimensions of (100 × 100× 400) mm are tested in accordance with ASTM C78-2002[42] . Plate (3-17) displays the modulus of rupture test specimens and machine, while Table (3-11) gives the value of tested specimens at 28 days. The rupture module determined by the equation (3-1).

$$Fr = 2PL/bd^2 \quad \text{.....3-2}$$

Table(3-11): Values of Flexural Strength Test.

Specimens	Test of Modulus of rupture (MPa)at 28-days		Average value of Modulus of rupture (MPa) at 28-days
LWC	1.52	1.79	1.66
NC	2.4	2.83	2.62
RCC	3.41	2.85	3.13
SC	3.17	2.95	3.06
FRC	2.58	2.11	2.35
CRC	1.58	2.34	1.96
IFC	3.21	2.47	2.84
CSGC	2.85	2.8	2.83

Plate (3-17): The Modulus of Rupture Test Specimens and Machine.

3.7 Instruments for Measuring

The beams were painted with gray color in order to show them in an appropriate view and to show the forms of failure. A LVDT sensor (Linear variable distance transformation) is used to measure the vertical deflection of the beam. A digital caliper for measuring deflection with a sensitivity of 0.01 mm, which is displayed in Figure (3-5), the locations of the contact gauge. Since webcam cameras are connected to the equipment via computer software, they were used during the study to record the load and demand meters for reading purposes. A computer program connects cameras to the device and assembles these cameras.

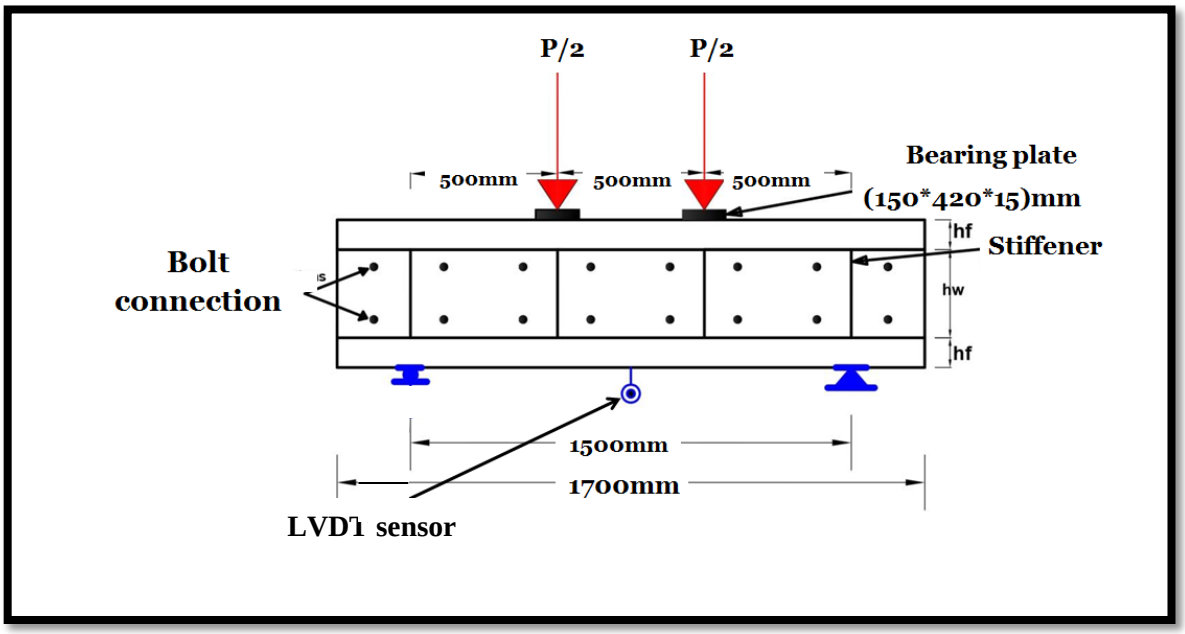

Figure (3-5): Location of LVDT sensor used in the tests.

3.8 Test Procedure

At University of Babylon/College of Engineering/Department of Civil Engineering/Construction Laboratory, conducted the tests. Under two equivalent concentrated loads, 12 simply supported beams were tested until failure, using a hydraulic testing equipment (480kN). Each beam was joined to a hinge at one end and a roller at the other. At supports and load-bearing locations, bearing plates were employed to prevent local steel yield. After

applying the load and self-weight, the initial reading of the deflection was registered at 5kN.

Plate (3-18): Instruments for Measuring.

CHAPTER FOUR

EXPERIMENTAL RESULTS AND

CHAPTER FOUR

EXPERIMENTAL RESULTS AND DISCUSSION

4.1 Introduction

The results for current experimental study were presented in this chapter. The results of experiments were typically split into two parts. The results of hollow flange cold-formed steel section subjected to four point bending condition were shown in the first part. The results of strengthened hollow flange with different types of materials under the same loading condition were shown in the second part.

4.2 Results of Test of Beams Specimens

As mentioned in Chapter Three, twelve beam specimens subjected to concentrated loading at two-thirds of the span points were tested experimentally and the results presented in this chapter. The general configuration of the examined specimens was depicted in Figure (3-4) in chapter three.

The experimental results include the maximum load capacity and mid span deflection. In addition, the failure mode for two groups were clarified. Table (4-1) summarized the results recorded experimentally for all tested specimens. The results of group I were compared with specimen A30. While the results of group II were compared with specimen A60.

Table (4-1): Experimental Results of Group I and II.

Specimens	Load(kN)			Deflection(mm)			
Group I	**Ultimate**	**%I**	**Service**	**Max.**	**%I**	**Service**	**%I**
A30	**217**	**-----**	**141**	**29.89**	**-----**	**14**	**----**
A60	**160**	**26**	**104**	**24.65**	**18**	**11**	**21**
A90	**177**	**18**	**115**	**17.25**	**42**	**8**	**43**
A120	**189**	**13**	**123**	**13.81**	**54**	**7**	**50**
Group II	**%II**			**%III**			**%III**
A60L	**196**	**23**	**127**	**4.84**	**80**	**2.5**	**77**
A60NC	**199**	**24**	**129**	**4.64**	**81**	**1.84**	**83**
A60RC	**195**	**22**	**127**	**4.13**	**83**	**2.31**	**79**
A60S	**225**	**41**	**146**	**8.69**	**65**	**3.53**	**68**
A60FR	**192**	**20**	**125**	**5.65**	**77**	**2.25**	**79**
A60CR	**190**	**19**	**124**	**5.6**	**77**	**2.51**	**77**
A60IF	**206**	**29**	**134**	**3.44**	**86**	**1.69**	**84**
A60CSG	**215**	**34**	**140**	**5.66**	**77**	**1.93**	**82**

*%I: decreasing in load and deflection comparing with **A30**.

*%II: increasing in load compared with **A60**.

*%III: decreasing in deflection compared with A60.

4.3 Experimental Results of Group I

4.3.1 Hollow Flange Depth

All specimens were loaded progressively at a rate of (0.1 kN/sec), Figures (4-1) to (4-4) introduced the load-deflection curves at mid–span of group I. Service deflection depending on the beam length (L/360) was the allowable deflection for all specimens.

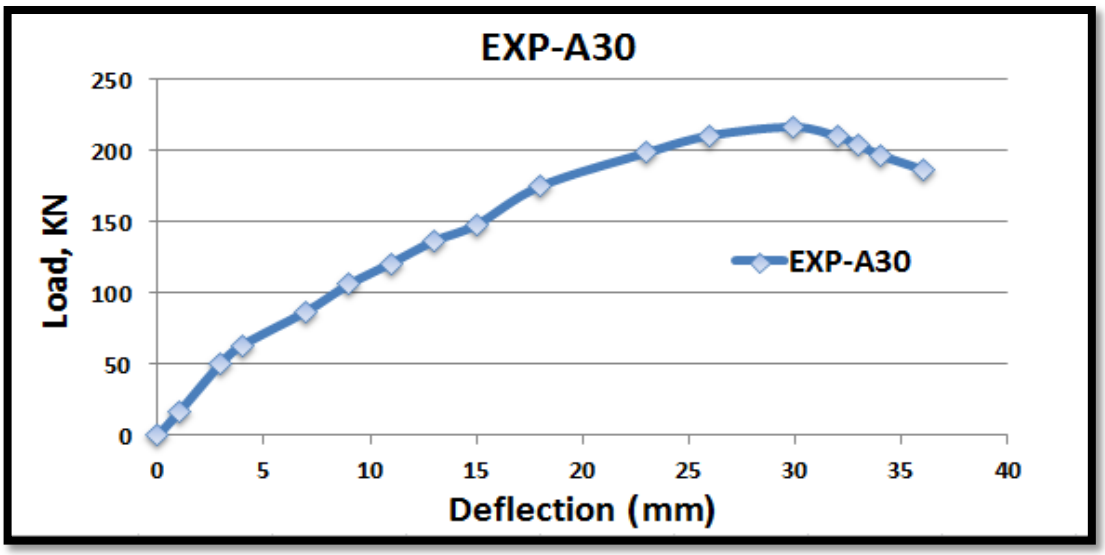

Figure (4-1): Curve of Load-Deflection for **A30** .

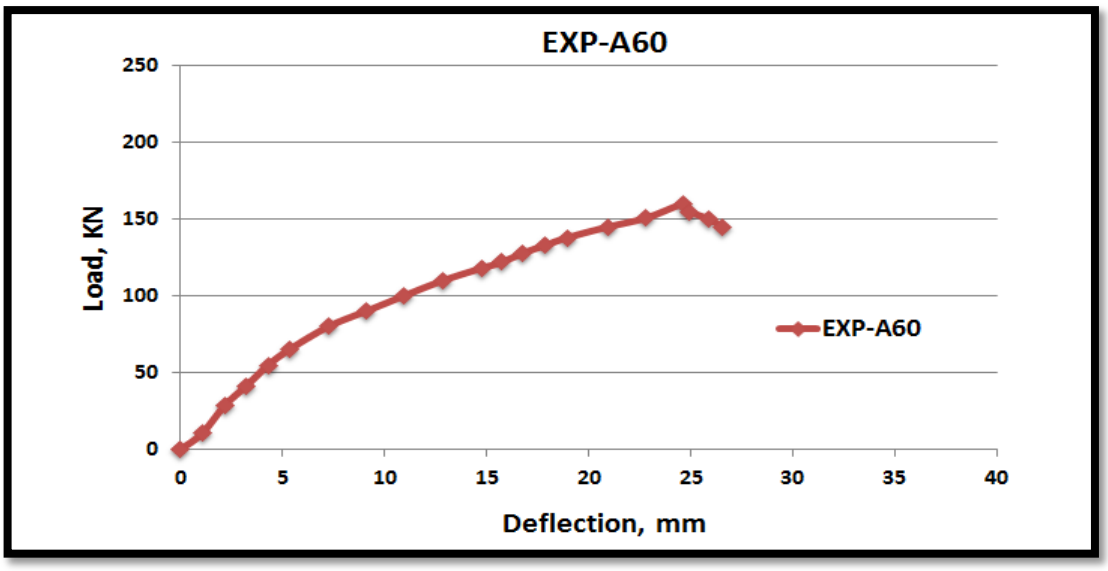

Figure (4-2): Curve of Load-Deflection for **A60**.

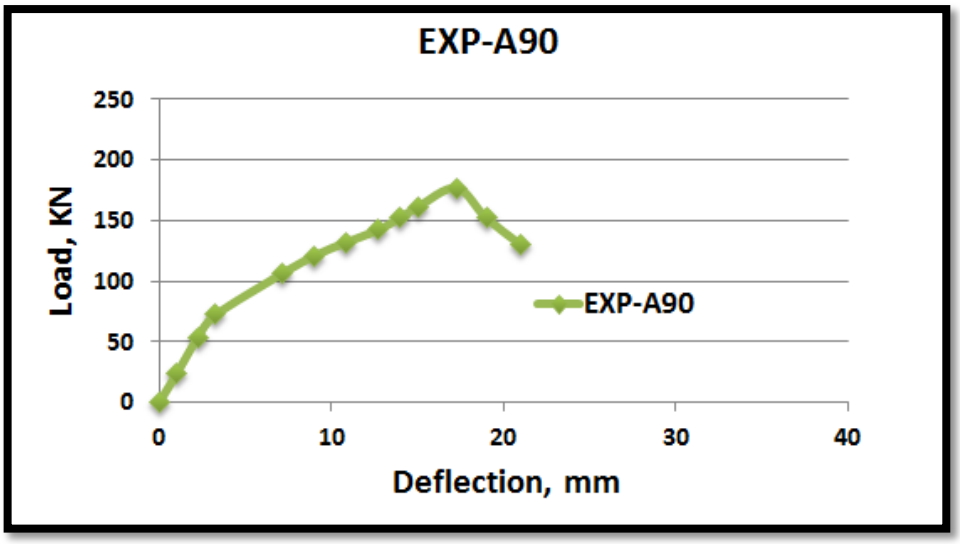

Figure (4-3): Curve of Load-Deflection for **A90**.

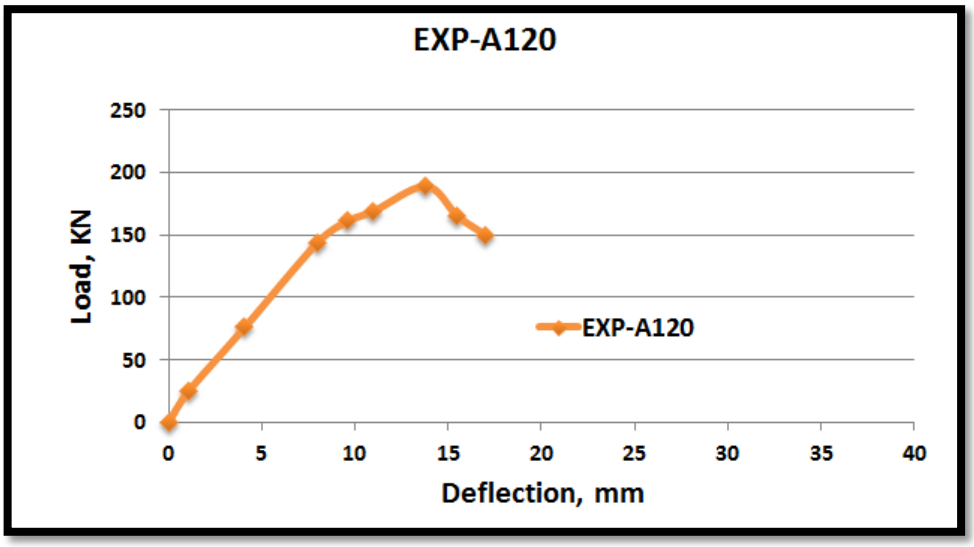

Figure (4-4): Curve of Load-Deflection for **A120**.

Figure (4-5) showed the deflection and load curves for group I. The section load capacities of HFBs will have been increased as a result of the web and flange plates separating as a result of interrupted bolt due to effect of increasing for hollow flange depth. This indicates that the hollow flange sections were more efficient due to their distinctive geometry and low weight. After completing the calculation of the deflection results, and after calculating the service deflection was calculated at 0.65 of the ultimate load, and then it was compared with the allowed deflection, which was equal to

(L/360 =4.16mm), it was found that the deflection of group I was higher than the allowable one as shown in Figure (4-6).

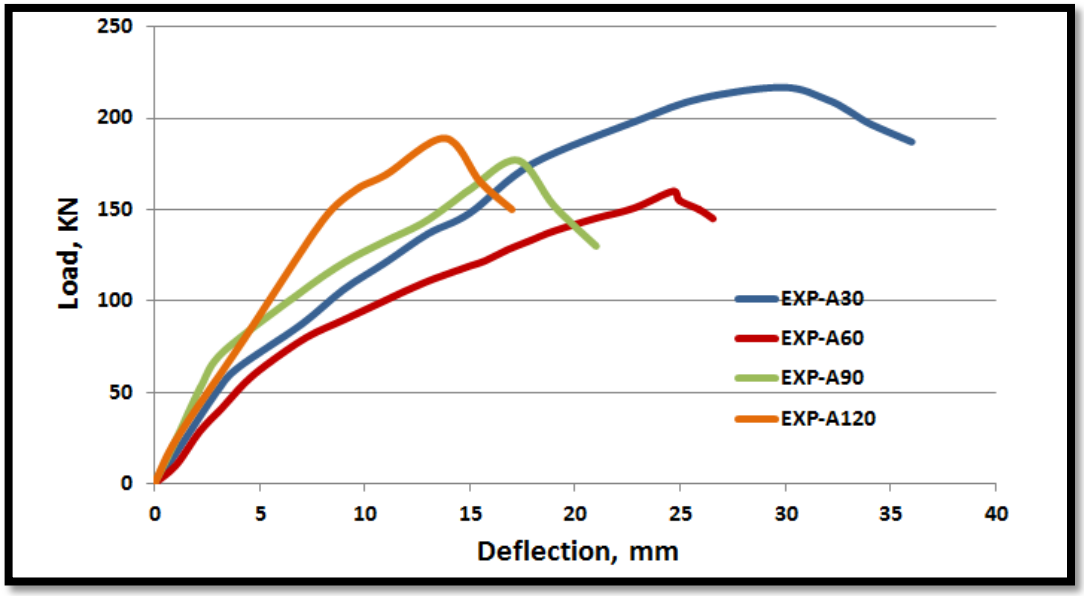

Figure (4-5): Curve of Load-Deflection for Group I.

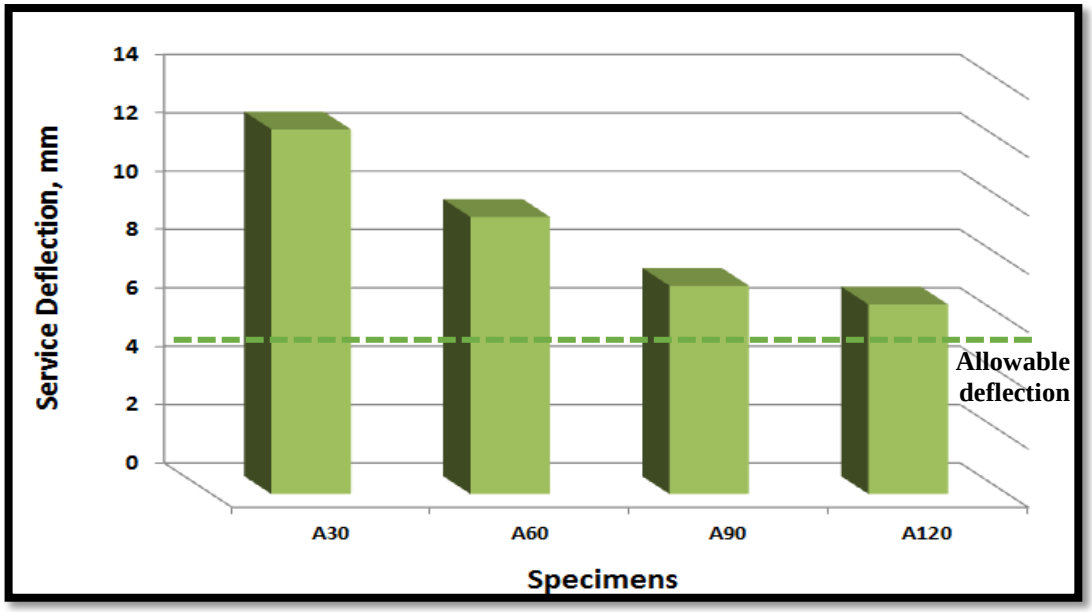

Figure (4-6): Comparing the Deflection of Group I with Allowed Deflection.

4.3.2 Failure Mode of Group I

After completing the tests, it was useful to look at the pictures of all the specimens in order to study the different modes of failure such as local buckling, flexural failure, distortional buckling and torsional buckling.

Specimen A30

For this specimen a 217KN and 29.89mm were reported as ultimate load and maximum deflection. The failure in specimen A30 due to flexural and distortional buckling as shown in Plate (4-1). The reasons for this failure were may be to the depth of the web in this section was greater than the rest of the sections, when the depth of the cold-formed steel sections increased, also the sections were exposed to a higher rate of buckling than bending and also because the maximum stresses were concentrated in the compression flange, the concentration of these stresses led to the distortional buckling. In this beam, after a certain load, the web descended until it contacted the flange, this made the web and the flange work by carrying the load as one piece, so that this section bore higher than the rest, but with a higher undesirable deflection.

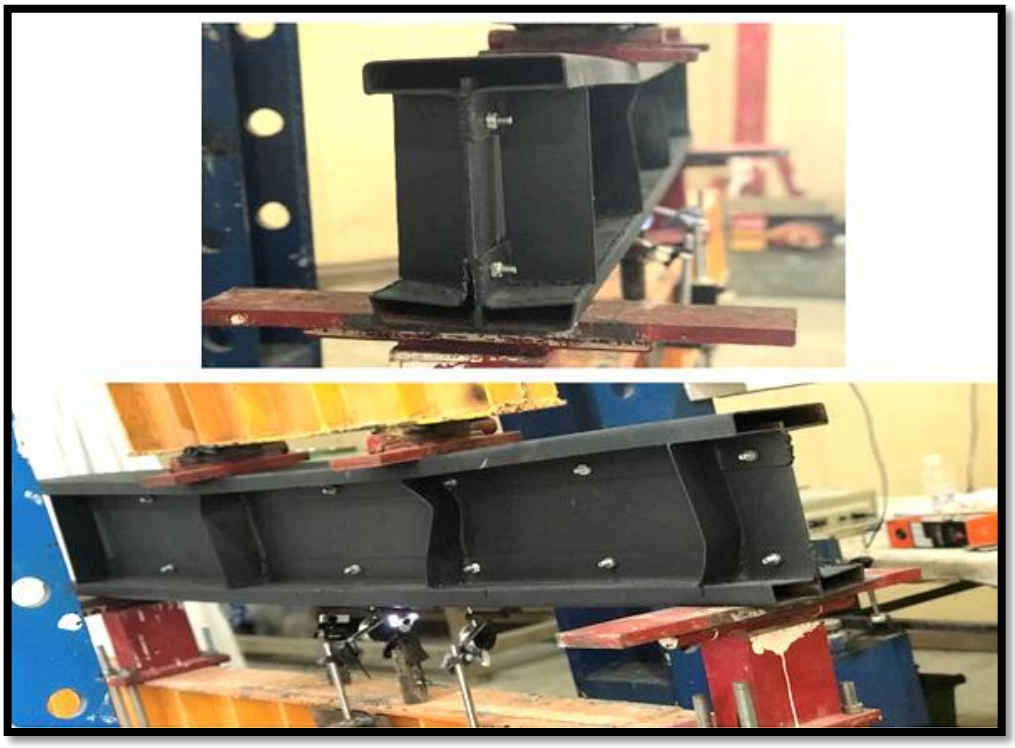

Plate (4-1): Failure Mode for Specimen **A30**.

Specimen A60

Ultimate load was reported a 160kN and 24.65mm maximum deflection. In some circumstances, for this specimens it was even feasible to lower the value of the section capacity as the stiffener location could result in a different load mechanism that changes the failure location to weaker location, this reason may be cause the buckling in stiffeners as shown in Plate (4-2). Where the amount of decrease in strength in specimen **A60** compared with specimen **A30** was (26) % and the decrease in deflection in specimen **A60** compared with specimen **A30** was (17.5) % .

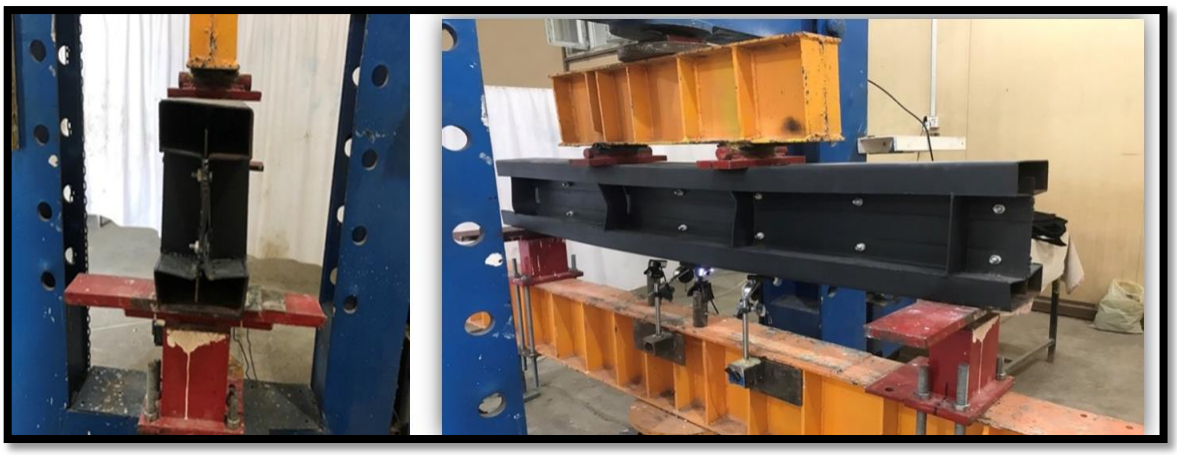

Plate (4-2): Failure Mode for specimen **A60**.

Specimens A90 and A120

Loading failure were reported at about (177KN and 189KN) and (17.25mm and 13.81mm) maximum deflection for A90 and A120, respectively. When the specimens reach the failure stress in the material with the flange buckling failure. This failure may occur due to applying the loads on the section, with the aid of the geometrical imperfection which causes yielding in material. It can be realized from specimen A90 as shown in Plate(4-3) as the same for specimens A120 as shown in Plate (4-4). Where the amount of decrease in strength in this specimen **A90** compared with specimen **A30** was (18.3%), and the decrease in deflection in this specimen compared with specimen A30 was (42%). The amount of decrease in strength in this specimen **A120**

compared with specimen **A30** was (13%), and the decrease in deflection in this specimen compared with specimen **A30** was (54%).

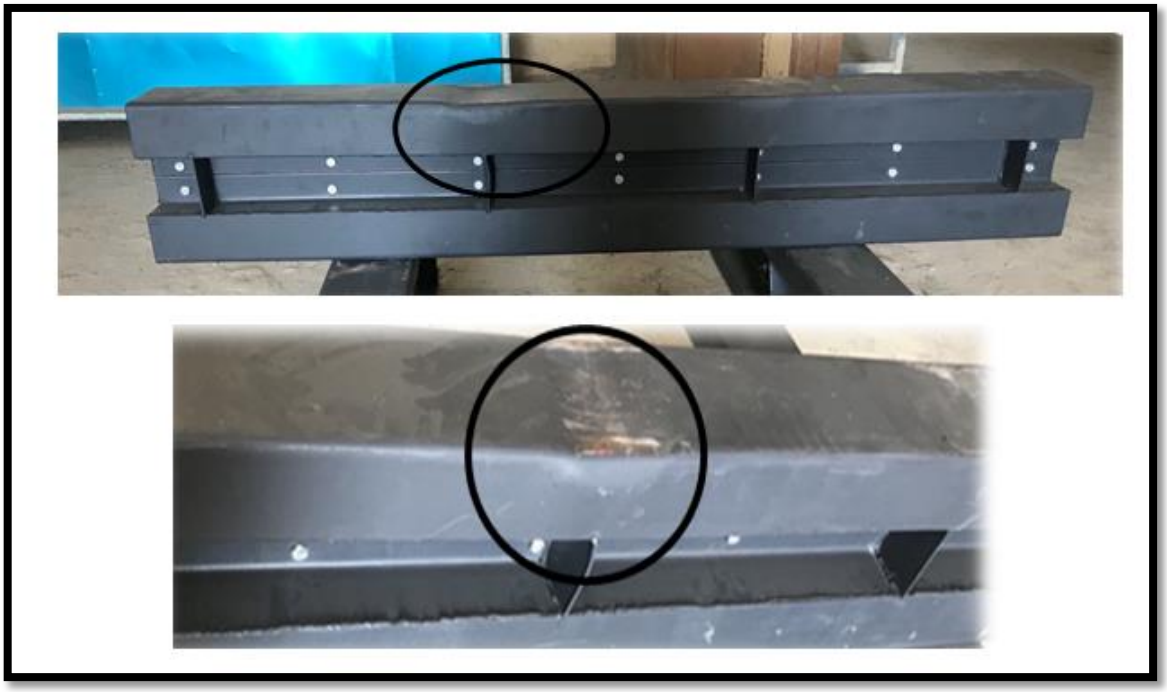

Plate (4-3): The Failure Mode(local buckling) of Specimen **A90**.

Plate (4-4): The Failure Mode(local buckling) of Specimen **A120**.

4.4 Experimental Results of Group II

4.4.1 Strengthening Materials

According to type of strengthening materials was divided the filled hollow flange specimens into two parts, the first one using light weight concrete, normal concrete and normal concrete replaced the coarse aggregates with recycled concrete, while the second part using replacement fine or coarse aggregates in normal concrete with sawdust, iron fillings, fine and coarse rubber and coarse chattered glass.

4.4.1.1 Concrete

Figures (4-7) to (4-9) present load-deflection curves at mid-span and third-span for specimens A60L, A60NC and A60RC. They are noticeable that all the tested specimens with strengthened hollow flange have increased in strength capacity by (18%, 20% and 18%), respectively, compared with specimen A60. The three figures also showed the decrease in deflection about (80%, 81% and 83%) for A60L,A60NC and A60RC, respectively, compared with specimen A60.

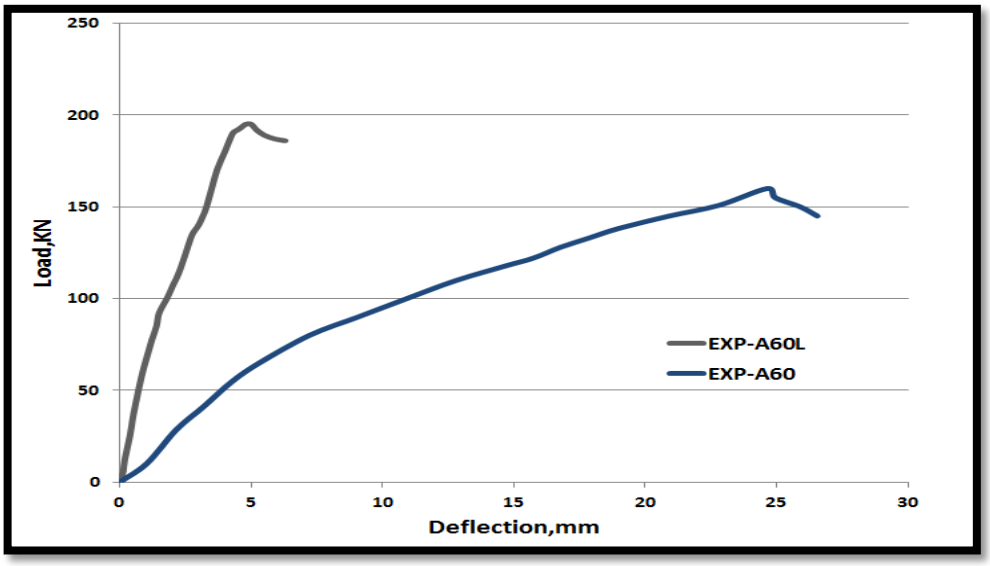

Figure (4-7): Curve of Load-Deflection for **A60L**.

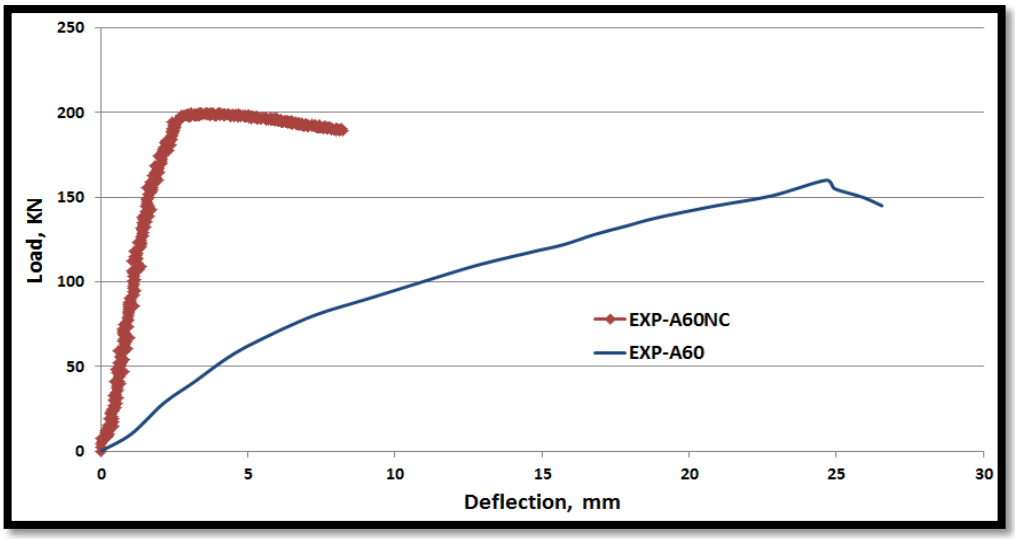

Figure(4-8): Curve of Load-Deflection for A60NC.

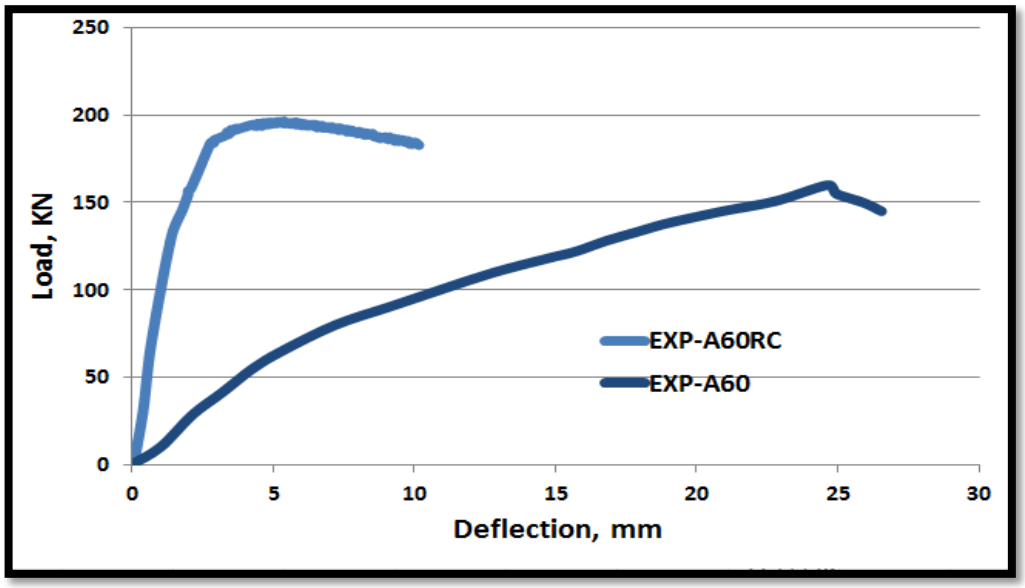

Figure(4-9): Curve of Load-Deflection for **A60RC**.

4.4.1.2 Replacement of Concrete Components

Figures (4-10) to (4-14) presented load-deflection curves at mid-span for specimens A60S, A60FR, A60CR, A60IF and A60CSG. They were noticeable that all the tested specimens with strengthened hollow flange have increasing in strength capacity by (29%, 17%, 16%, 22% and 26%), respectively, compared with specimen A60. The five figures also showed the decrease in deflection about (65%, 77%, 77%, 86% and 77%) for

A60S,A60FR, A60CR, A60IF and A60RC, respectively, compared with specimen A60.

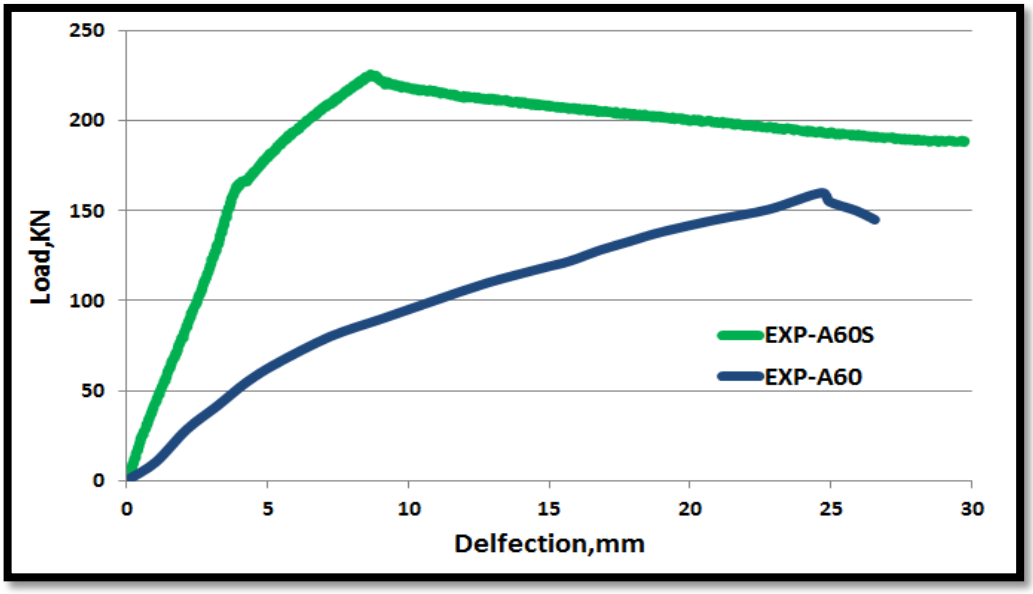

Figure(4-10): Curve of Load-Deflection for **A60S**.

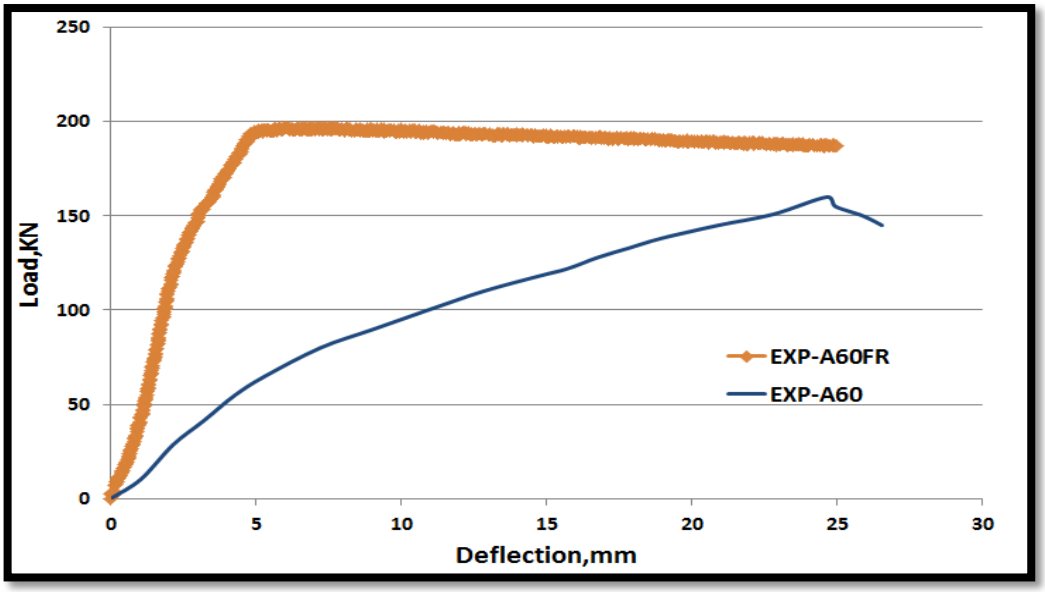

Figure (4-11): Curve of Load-Deflection for **A60FR**.

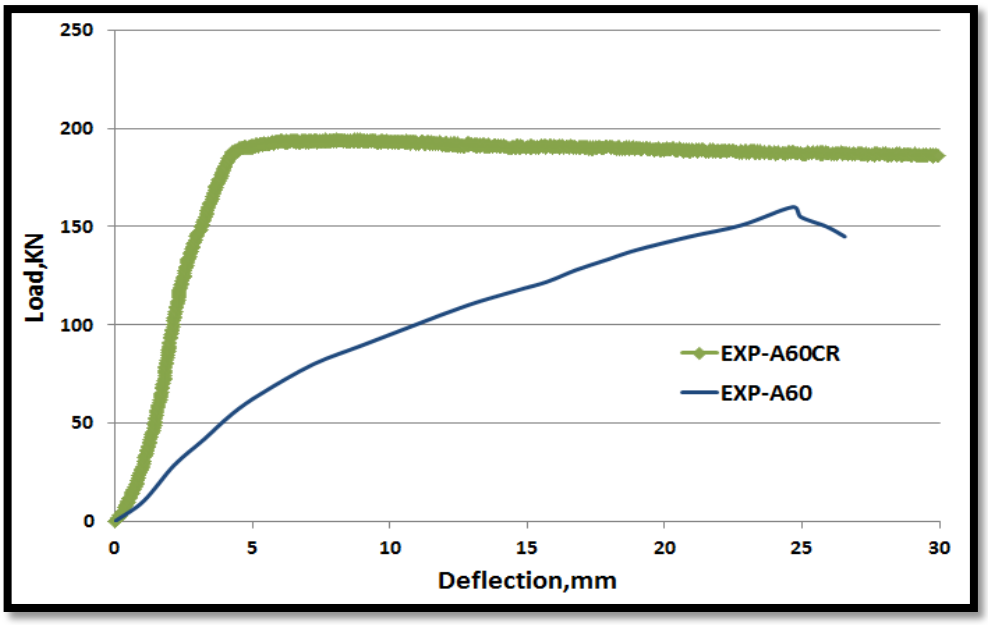

Figure (4-12): Curve of Load-Deflection for **A60CR**.

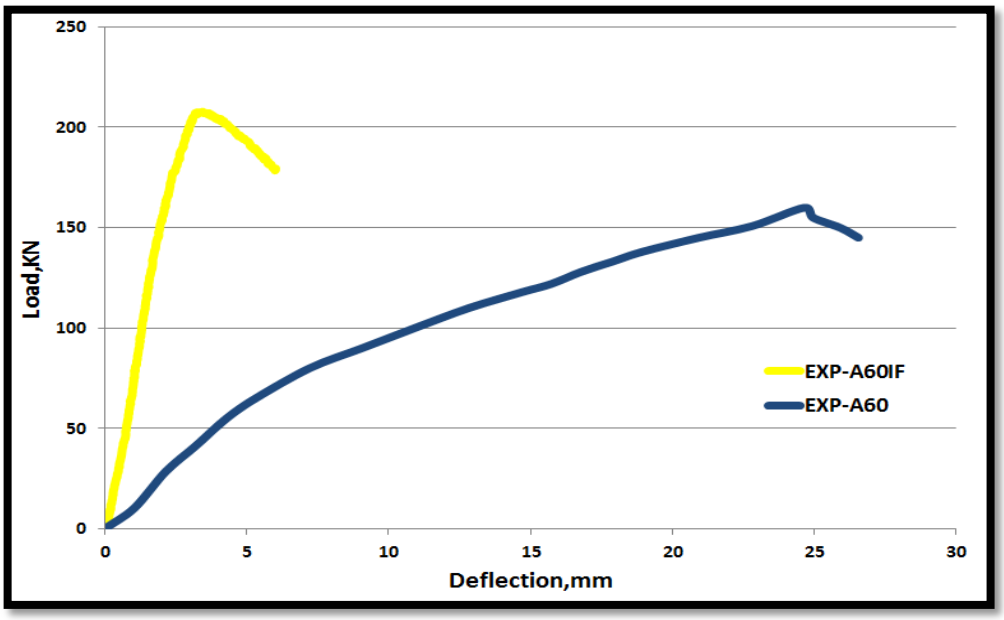

Figure (4-13): Curve of Load-Deflection for **A60IF**.

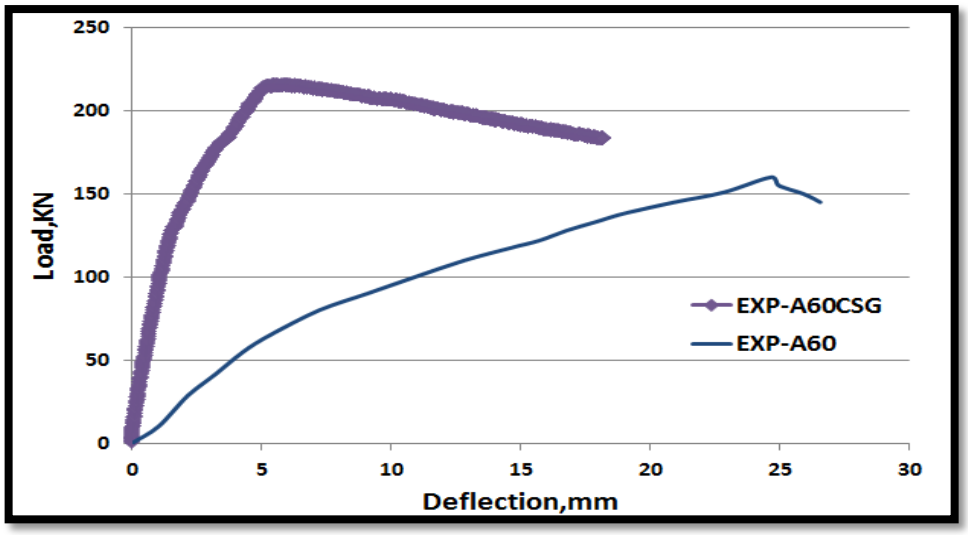

Figure (4-14): Curve of Load-Deflection for **A60CSG**.

When comparing the results of load-deflection for group II with the allowed deflection (L/360 = 4.16mm) , it was found that all specimens had a service deflection less than the allowable deflection as shown in Figure(4-16), this means that strengthening the hollow rectangular flanges improved the beam behavior and made the deflection within the permissible limits of the specifications.

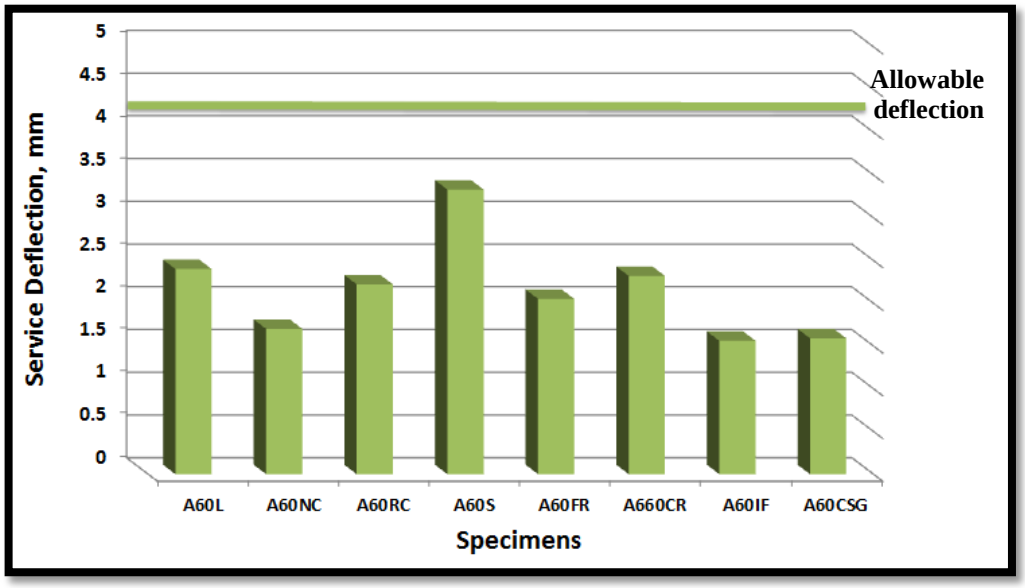

Figure (4-15): Comparing the Deflection of Group II with Allowed Deflection.

All the beams in this group gave an increase in the bearing capacity with a decrease in the deflection as expected according to the compression and

tensile tests, except for two beams, **A60S** and **A60CSG**, where **A60S** was the highest of all the beams in terms of bearing capacity, and perhaps the reason is due to the behavior of the sawdust in the concrete after a certain age, as shown in [42] Which showed the improvement of concrete behavior when adding sawdust treated with water as a substitute for sand at a certain percentage, as it reduces the density of concrete and increases the compressive and tensile strength at a certain age, It gave results similar to control concrete, in this research[10], sawdust was used with cement mortar and lightweight concrete as strengthening materials for hollow flange, and the compressive results of sawdust with cement mortar (18.82MPa) and light weight concrete (30MPa) were used. With this difference in compressive strength, the beam strengthened with sawdust gave a difference in load bearing by (8.5%) for the beam strengthened with light weight concrete, this means that sawdust has a good effect on concrete properties. Strengthening the flange with normal concrete 30% of the coarse aggregate has been replaced with sawdust improved the behavior of the beam, as it increased the bearing capacity and decreased the deflection, and this improved the flexural behavior. **A60CSG** was the second most load-bearing beam, and the concrete used to strengthen it was one of the highest values in terms of compressive and tensile strength , due to the presence of broken glass as a substitute for coarse aggregate by (30%), as the broken glass improves the bonding between the components of the concrete and increases its resistance as the age of the concrete increases as mentioned in [43] , it was found that when replacing the coarse aggregate by (60%) with broken cullet glass with the same gradation of the aggregate, it improves the bonding between the concrete components and increases the tensile and compressive strength until it reaches twice the resistance of the control concrete at the age of two years. As for the rest of the beams, they gave an increase in the bearing capacity and a decrease in the deflection, according to the results of the tensile and

compression tests, in sequence from the highest to the lowest, after comparing them with A60, the increase in bearing capacity ranged between (16% and 29%), and a decrease in deflection ranging between (65% and 86%). This means that strengthening the rectangular hollow flange with different materials improved the behavior of the beams, as it increased the bearing capacity and decreased the deflection, and this improved the flexural behavior, as shown in Figure (4-16).

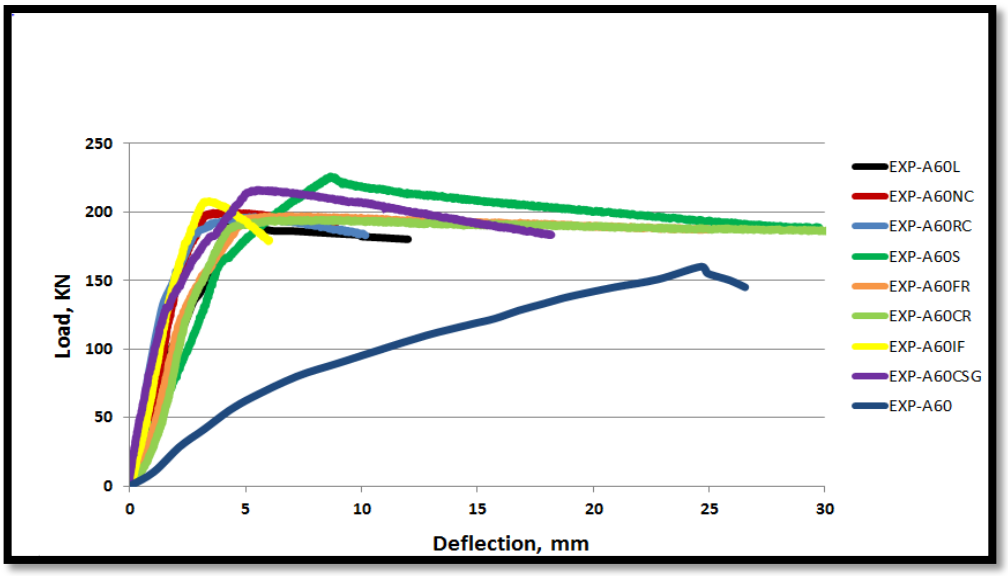

Figure (4-16): Curves of Load-Deflection for Group II at the mid-span.

4.4.2 Failure Mode of Group II

Flexural failure was the failure type for specimens A60S, A60FR and A60CR in this group, while the yield failure was the control failure for specimens A60L, A60NC, A60RC, A60IF and A60CSG as shown in Plates (4-5) to (4-12).

Plate (4-5): The Failure of Specimen **A60L**.

Plate (4-6): The Failure of Specimen **A60NC**.

Plate (4-7): The Failure of Specimen **A60RC**.

Plate (4-8): The Failure of Specimen **A60S**.

Plate (4-9): The Failure of Specimen **A60FR**.

Plate (4-10): The Failure of Specimen **A60CR**.

Plate (4-11): The Failure of Specimen **A60IF**.

Plate (4-12): The Failure of Specimen **A60CSG**.

4.4.3 Concrete crack

The eight beams of group II were strengthened with different types of concrete, it was noticed that cracks occurred in the face of the concrete visible from the flange in the Lower flange (tension zone) only, as shown in plate(4-13). These cracks occurred as a result of bending moments in this region, as well as due to weak tensile strength of the concrete and may be due to de-bonding between concrete and steel, the use of shear connections can improve this connection.

Plate (4-13): Concrete Cracks.

4.5 Ductility Index

Ductility is the ability of a beam to resist plastic deformation without reducing its capacity of carrying loads till failure . Alternatively, the ratio of ultimate stage deformation to service deformation is known as ductility. Deformations include strain curves and deflections, for instance. The deflection at the service limit is at service load (approximately 65 percent of maximum load)[45]. Table(4-2) shows the ductility ratio for all specimens.

Table(4-2): Ductility Index of all specimens.

	Specimens	Deflection(mm)		Ductility ratio	I%*
		Δs	Δu	Δu/Δs	
Group I	A30	14	29.89	2.14	----
	A60	11	24.65	2.24	5
	A90	8	17.25	2.2	3
	A120	7	13.81	2	-7
Group II	A60L	2.5	4.84	2	-11
	A60NC	1.84	4.64	2.52	13
	A60RC	2.31	4.13	1.8	-20
	A60S	3.53	8.69	2.5	12
	A60FR	2.25	5.65	2.51	12
	A60CR	2.51	5.6	2.24	0
	A60IF	1.69	3.44	2.04	-9
	A60CSG	1.93	5.66	2.93	31

* I%: compared with **A30** for group I and with **A60** for group II.

From table (4-5) it can be noticed that specimen **A120** in group I, gave the lower value of ductility index compared to others. In group II, the specimens **A60NC**, **A60S**, **A60FR** and **A60CSG** more ductile than other specimens, their ductility increased by 12.5%, 11.61%, 12.1 and 30. % respectively when compared with **A60.**

4.6 Stiffness Index

When a component bends under load, stiffness means the amount of load that we need in order for deflection to occur in the middle of the beam of

1mm. The value of this parameter is computed using equation (4-1) and listed in Table (4-3) for all specimens.

K′ = P/Δ ……..4-2 [46]

Where:

K′: stiffness parameter.

P: 0.75 of ultimate load.

Δ: deflection at 0.75 of ultimate load.

Table (4-3): Stiffness Parameter of all specimens.

Specimens	0.75 P, KN	Δ, mm	K′, KN/mm	I% *
A30	**162.75**	**22.42**	**7.26**	**----**
A60	**120**	**18.49**	**6.5**	**-10**
A90	**132.75**	**12.94**	**10.26**	**41**
A120	**141.75**	**10.36**	**13.68**	**88**
A60L	**147**	**3.63**	**40.5**	**523**
A60NC	**149.25**	**3.48**	**42.9**	**560**
A60RC	**146.25**	**3.1**	**47.18**	**626**
A60S	**168.75**	**6.52**	**25.88**	**298**
A60FR	**144**	**4.24**	**33.96**	**422**
A60CR	**142.5**	**4.2**	**33.94**	**422**
A60IF	**154.5**	**2.58**	**59.88**	**821**
A60CSG	**161.25**	**4.25**	**37.94**	**484**

***** I%: increasing in stiffness ratio compared with **A30** for group I and with **A60** for group II**.**

After calculating the stiffness ratio of each specimens found in group I, the deeper the flange increase the value of the stiffness ratio, except for A60, as

for group II, the stiffness ratio for all beams when compared with A60 for all of them increased in high proportions as shown in Table (4-4).

4.7 Efficiency of Specimens

The experimental side of this study has been completed and results have been collected. The load-to-weight ratio is a tool for calculating the efficiency of sections. This ratio means the amount of weight required to obtain an increase in the strength capacity of the sections, which means the higher this ratio, the better the performance of the sections. Table(4-4) shows the results of twelve specimens. [5]

Table (4-4): The efficiency of specimens.

Specimens	Ultimate load, kN	Total weight of beam, Kg	Efficiency
A30	**217**	**51.2**	**4.24**
A60	**160**	**53.6**	**3**
A90	**177**	**56.4**	**3.14**
A120	**189**	**60**	**3.15**

The efficiency was calculated for the sections of group I and it was found that beam A30 was the most efficient among all beams and was the least weight and this increased its efficiency, while the efficiency was not calculated for the sections of the group II, because their weights were greatly increased by adding strengthening materials, and this will reduce their efficiency [47].

4.8 Modulus of Toughness

A modulus of toughness of material is a measure of how much energy it can retain during plastic deformation. It is defined as the highest strain energy density that a material is capable of withstanding prior to breaking. The modulus of toughness is crucial because a sample capacity to absorb energy without breaking increases with its modulus. It is safer to choose a more ductile material with a greater toughness modulus when building a structure that may experience unintentional overload. The energy absorbed by the specimens was computed for three locations, namely A-Y, A-U, and A-F, in order to obtain the toughness of the specimens for each loading stage. A-Y toughness describes the yield load, whereas A-U toughness begins after the yield load and terminates before reaching the ultimate load. The A-F toughness is a failure toughness that begins with the ultimate load and ends with failure, [47], as shown in Figure (4-17) Table(4-5) shows the value of modulus of toughness for all specimens.

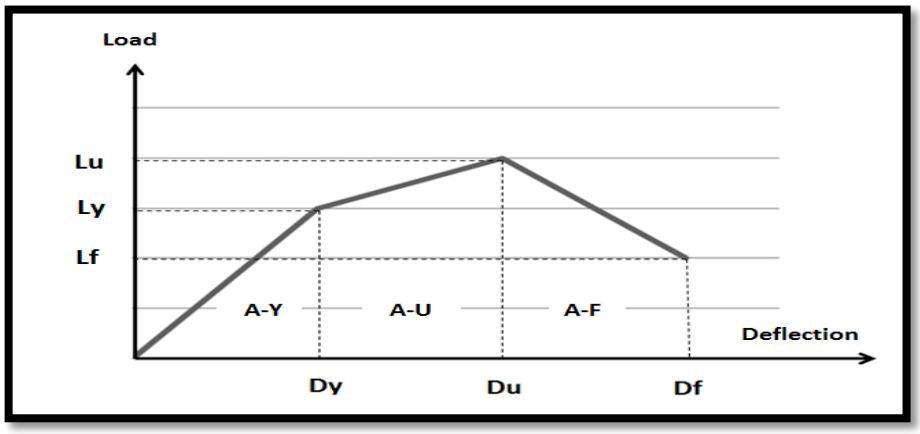

Figure (4-17): Model of Toughness .

Table (4-5): The Values of Modulus of Toughness.

Specimens	Modulus of Toughness KN.mm		
	A-Y	A-U	A-F
A30	1808	2382	858
A60	1066	1097	480
A90	470	1047	668
A120	734	840	802
A60L	277	321	1291
A60NC	146	490	701
A60RC	330	485	914
A60S	533	761	4216
A60FR	402	1101	2993
A60CR	365	1712	4151
A60IF	231	241	461
A60CSG	408	617	2342

After calculating the modulus of toughness for each beam in the three regions, it was found the group I for all specimens that the modulus of toughness in the elastic-plastic region was more than the other two regions. While in group II, the modulus of toughness was observed in the failure region higher than the rest of the regions, this means that these sections had the ability to absorb more stresses at the failure stage as shown in Figure(4-18).

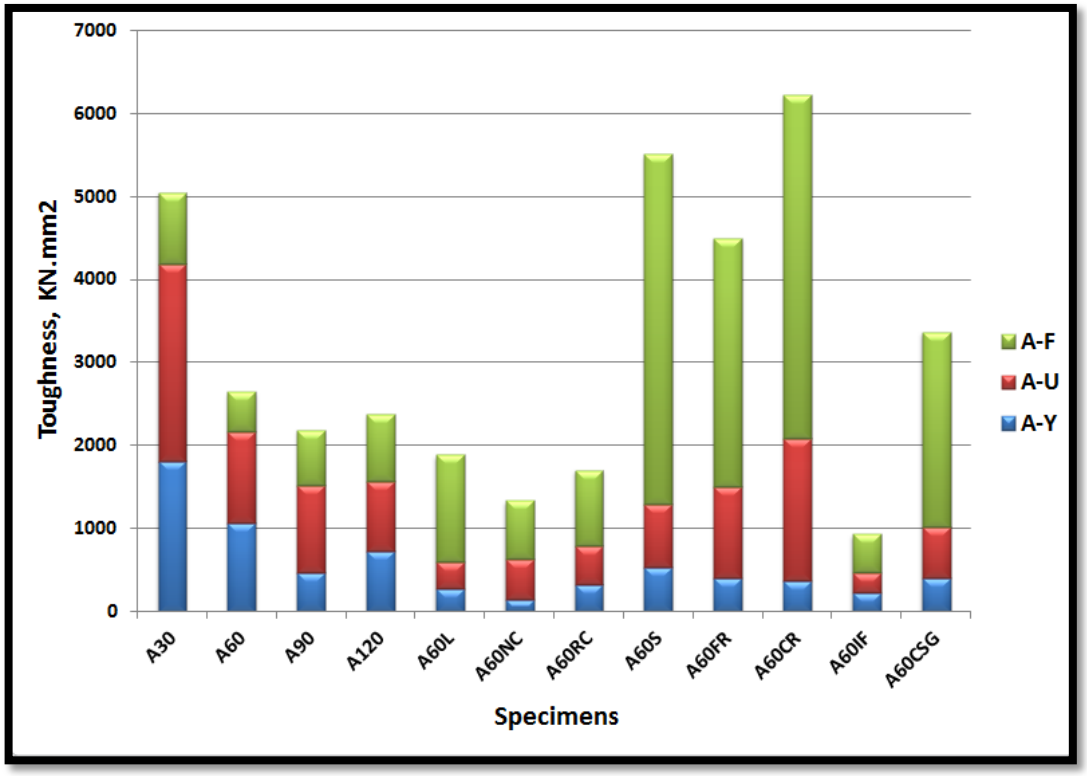

Figure (4-18): Toughness of all Specimens.

CHAPTER FIVE

NUMERICAL ANALYSIS BY FINITE ELEMENT

CHAPTER FIVE

NUMERICAL ANALYSIS BY FINITE ELEMENT

5.1 Introduction

This chapter discusses the finite element modeling approach that was employed in the current investigation. The finite element approach is widely used to simulate the behavior of structural components, and it has evolved into a sophisticated tool **ABAQUS** commercial software. This work employs **(CAE) 2017 ABAQUS** is a powerful numerical instrument that is commonly utilized. For components and simulation of systems and their application is established well in multi physics disciplines. It is used to solve temporary situations of several degrees and physics.

Several built-in models for forecasting material and process behavior are included in **ABAQUS**. The ability to incorporate user-defined models. Two **ABAQUS** built-up models can help model the response of concrete: the smeared concrete model and the model of concrete-damaged plasticity, which are covered in more detail in Appendix C.

5.2 Specifications of Numerical Simulation Model

The main parts of a flexural members in group I were: Two flanges, Web, Bolts connectors (Bolts and Screw) to connect flanges with web and eight stiffeners, in group II : Two flanges, Web, bolts connectors(Bolts and Screw), eight stiffeners, and strengthen material filled the hollow flanges. In order to present a realistic model of flexural members under four bending points, it was very important to simulate the actual material behavior of each part. Effective material models that can reasonably accurately simulate each part's real behavior were introduced by the ABAQUS material library. The details of dimensions, and properties of material of the modeled flexural members is exactly the same as the experimental work members**.**

5.2.1 Part and Assembly

All specimens are modeled to study the load capacity and behavior of rectangular hollow flange cold- formed steel I-beam. All tested beams are modeled by using three-dimensional deformable solid extrusion elements in the modeling of stiffeners, flange, web, loading and support plates parts of CFS beam and three-dimensional deformable solid revolution elements for bolts and screws as shown in **plate (5-1).**

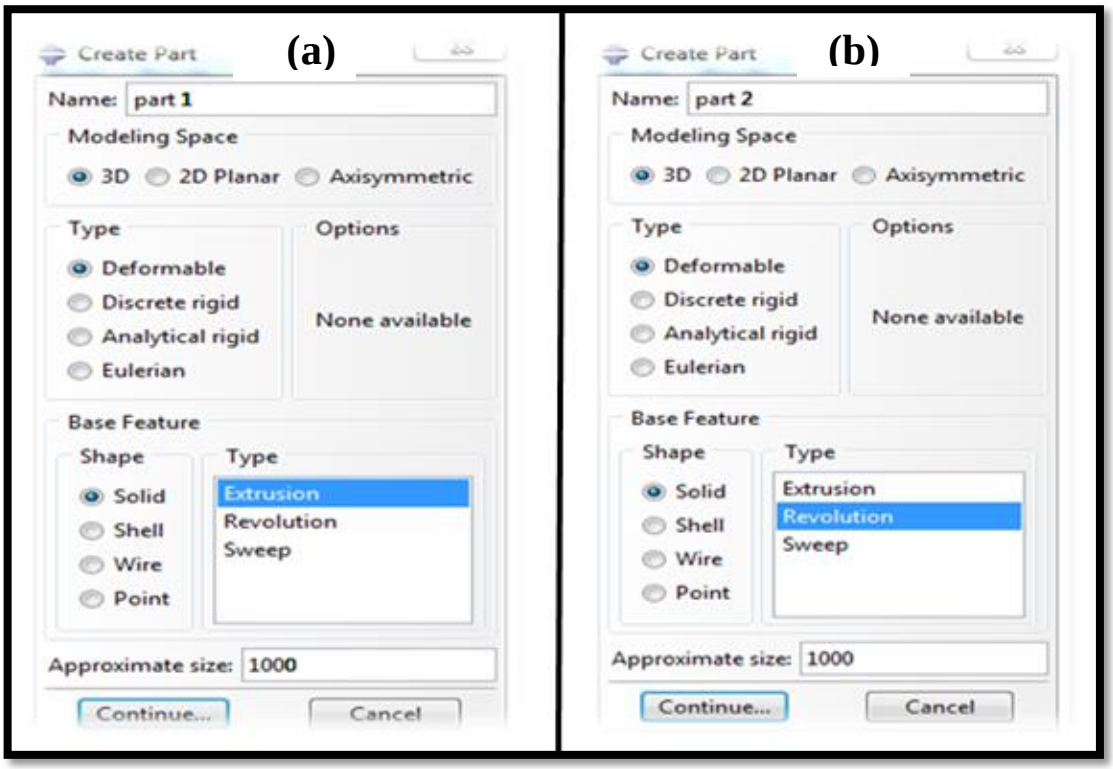

Plate (5-1): Modeling of Finite Element Part. (a) Modeling of Finite Element Part for stiffeners, flange, web, loading and support plates and (b) Modeling of Finite Element Part for Bolts and Screw.

All these parts of CFS beam were drawn separately and then assembled and merged these parts to get CFS beam. The assembly of parts which used in modeling specimens is shown in Figure (5-1).

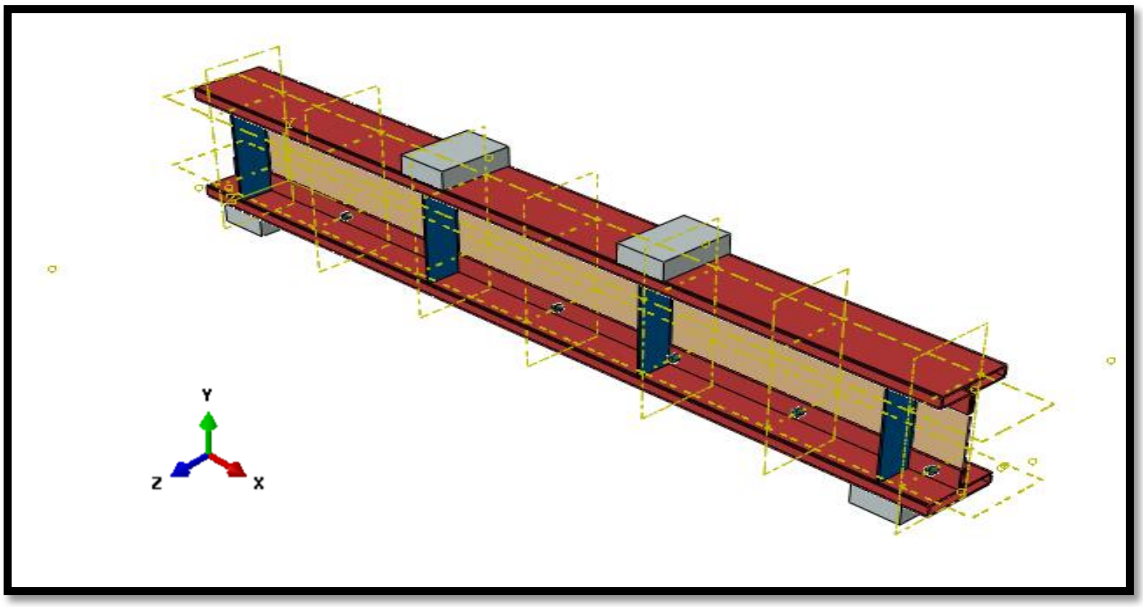

Figure (5-1): Assembled Parts of CFS Beam.

5.2.2 Property Module

The performance of any structure under load in three dimensional FEA was dependent on the property of material which was used to create the member "Poisson's ratio, modulus of elasticity, and stress-strain relationship of material". Stiffeners, flanges and web parts of CFS beam have the same martial. Bolts, screws, loading plates and support plates have the same martial, so that material created under the mechanical properties of material (elastic and plastic properties). Table (5-1) shows the properties of steel section. Tables (5-2) and (5-3) show the elastic and plastic properties of concrete. Young's modulus in table(5-2) was calculated from the equations in Table C-1 in Appendix C. The relationships of stress-strain for strengthening materials were mentioned in Figures(5-2) to (5-9).

Table (5-1): Elastic and Plastic Properties of Steel Section.

Elastic properties	**Young′s modulus (MPa)**	**Passion′s ratio**
	200000	**0.3**
Plastic properties	**Yield stress(MPa)**	**Plastic strain**
	266.7	**0**
	375	**0.15**

Table (5-2): Elastic Properties of concrete.

Specimens	Elastic	Young′s modulus (MPa)	Passion′s ratio
A60L	**fc′=31.19MPa**	**30948**	**0.15**
A60NC	**fc′=32.22MPa**	**31251**	**0.15**
A60RC	**fc′=28.17MPa**	**30017**	**0.15**
A60S	**fc′=19.73MPa**	**26975**	**0.15**
A60FR	**fc′= 21MPa**	**27485**	**0.15**
A60CR	**fc′= 16.6MPa**	**25613**	**0.15**
A60IF	**fc′= 37.14MPa**	**32612**	**0.15**
A60CSG	**fc′= 33.94MPa**	**31743**	**0.15**

Table (5-3): Plastic Properties of Concrete.

Dilation angle	Eccentricity	Fbo/fco	K	Viscosity parameter
25	**0.1**	**1.16**	**0.667**	**0.0015**

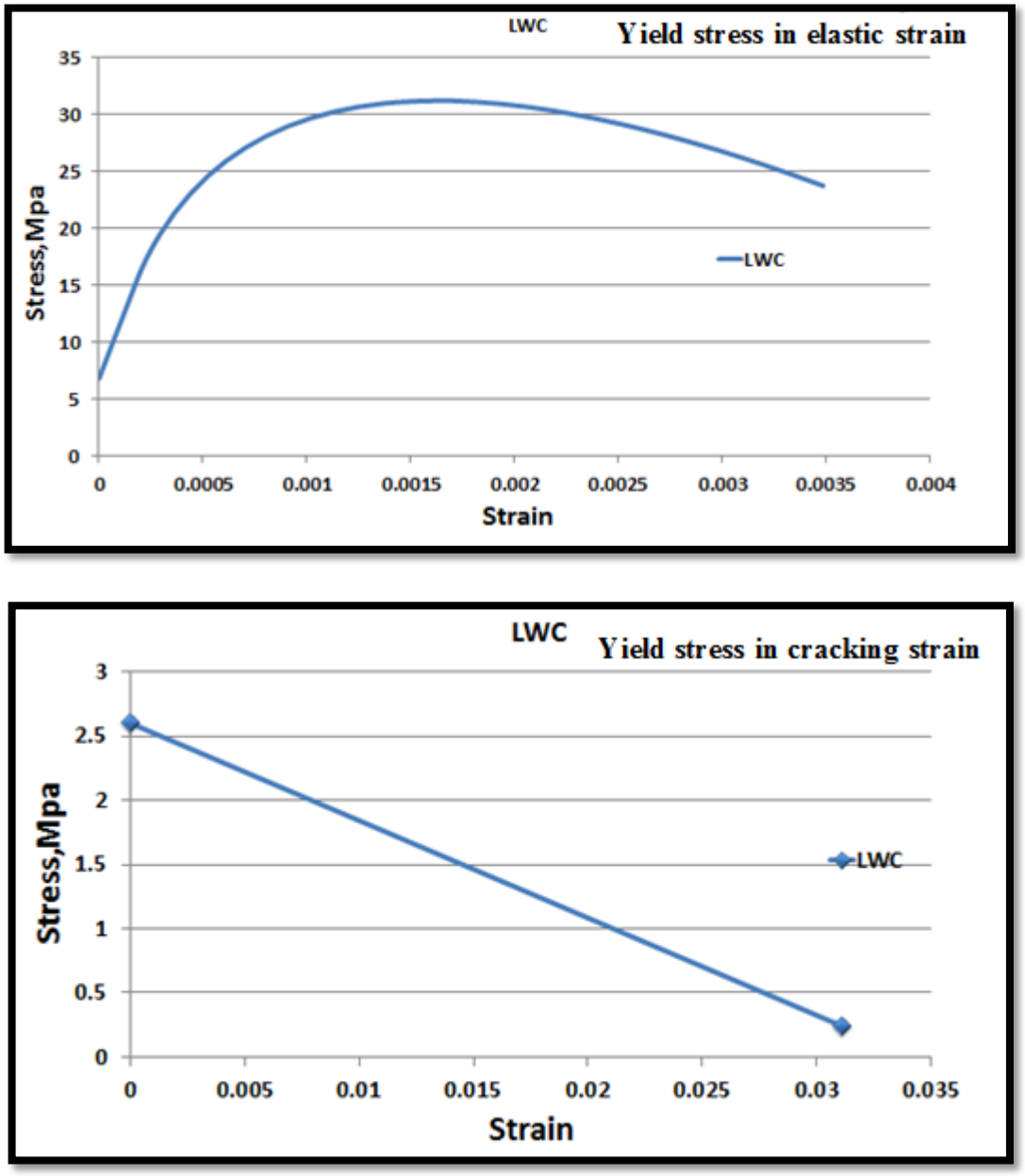

Figure (5-2): Relationship of Stress-Strain for **A60L**.

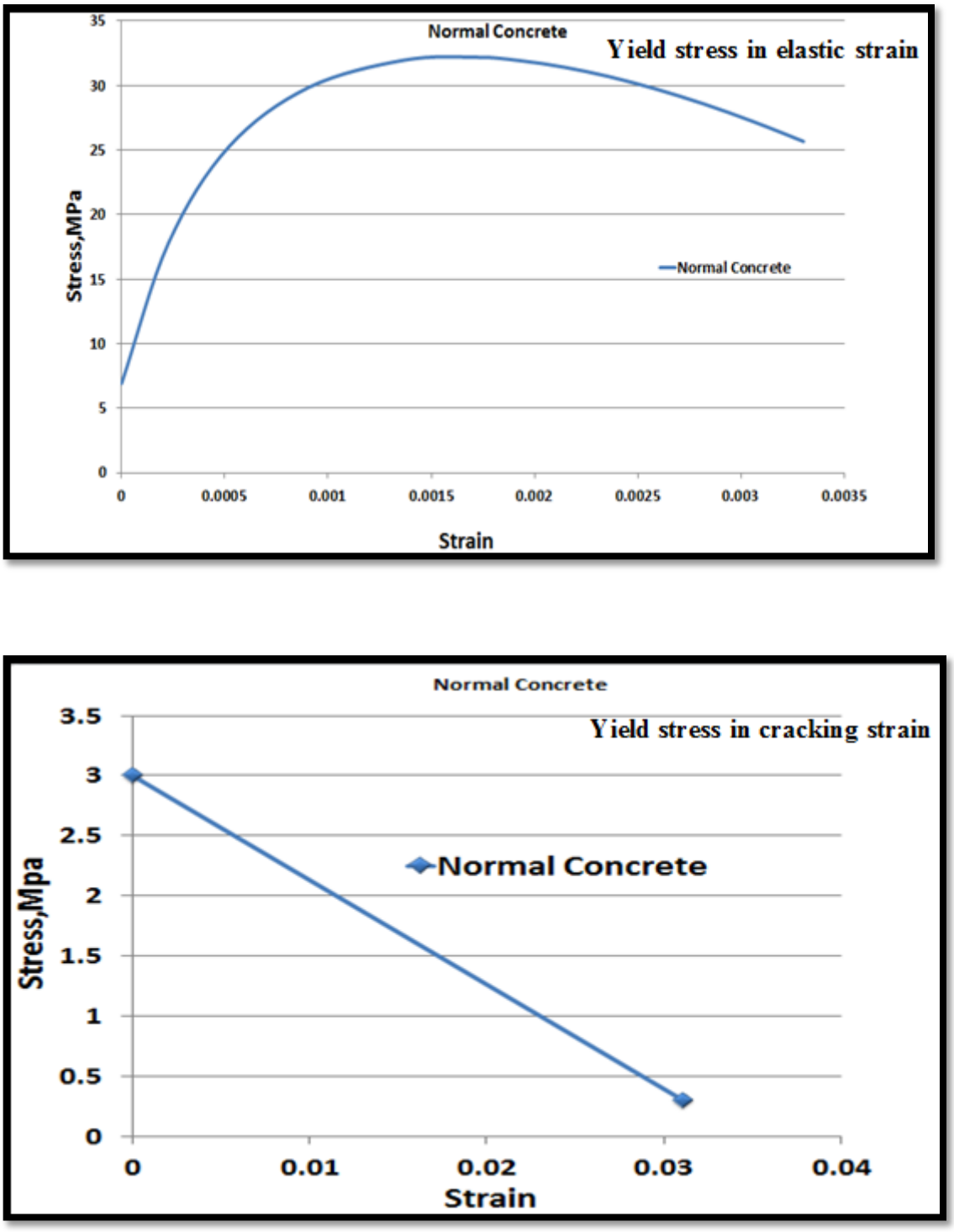

Figure (5-3): Relationship of Stress-Strain for **A60NC**.

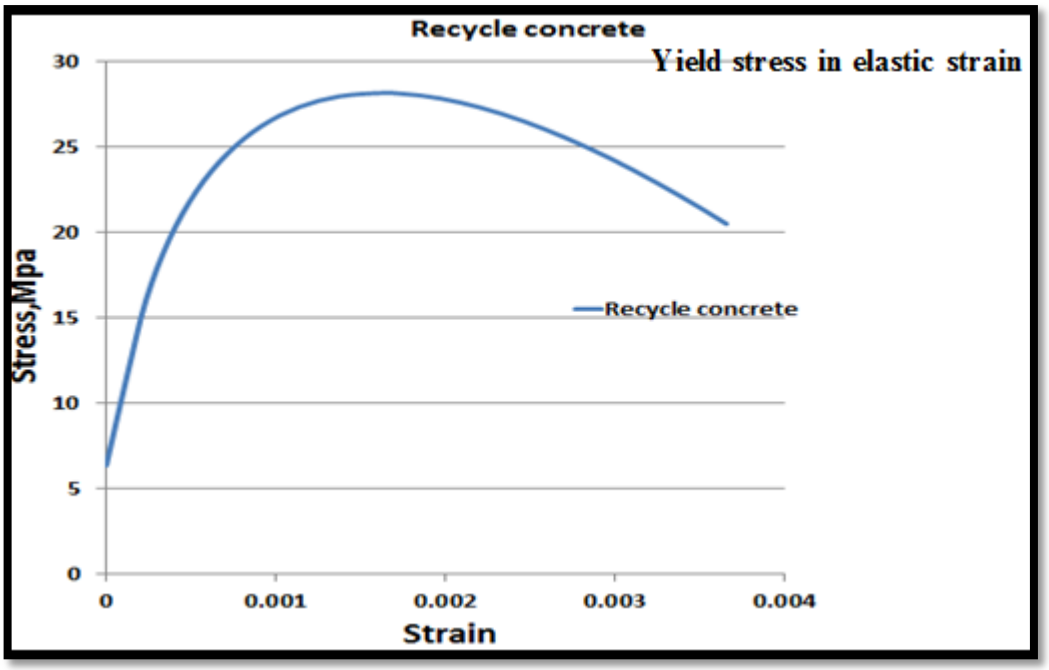

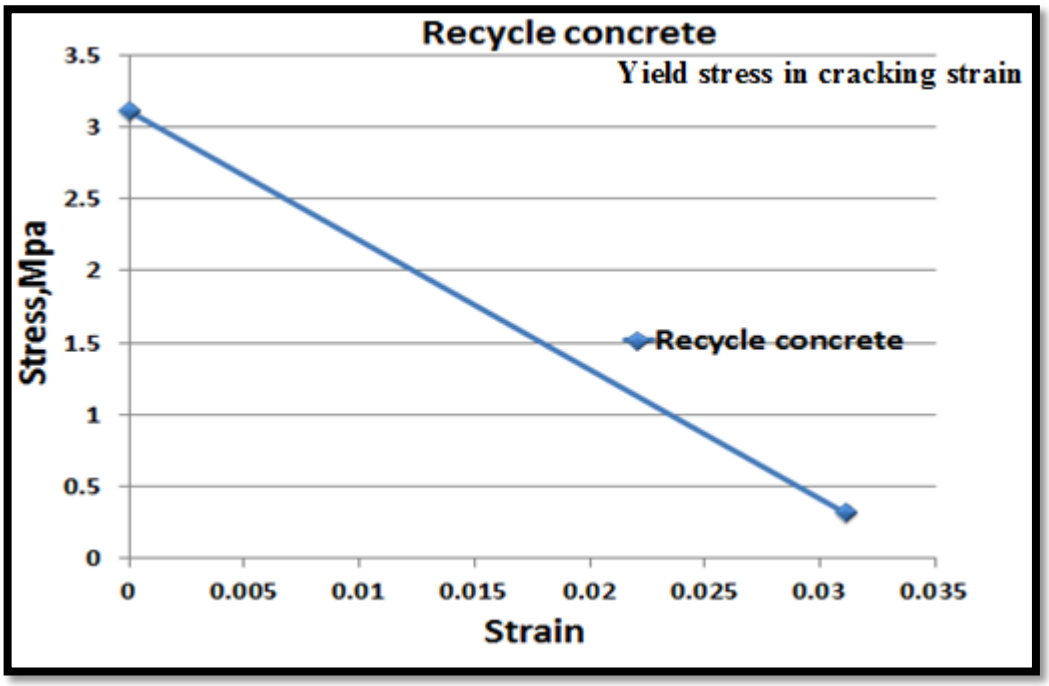

Figure (5-4): Relationship of Stress-Strain for **A60RC**.

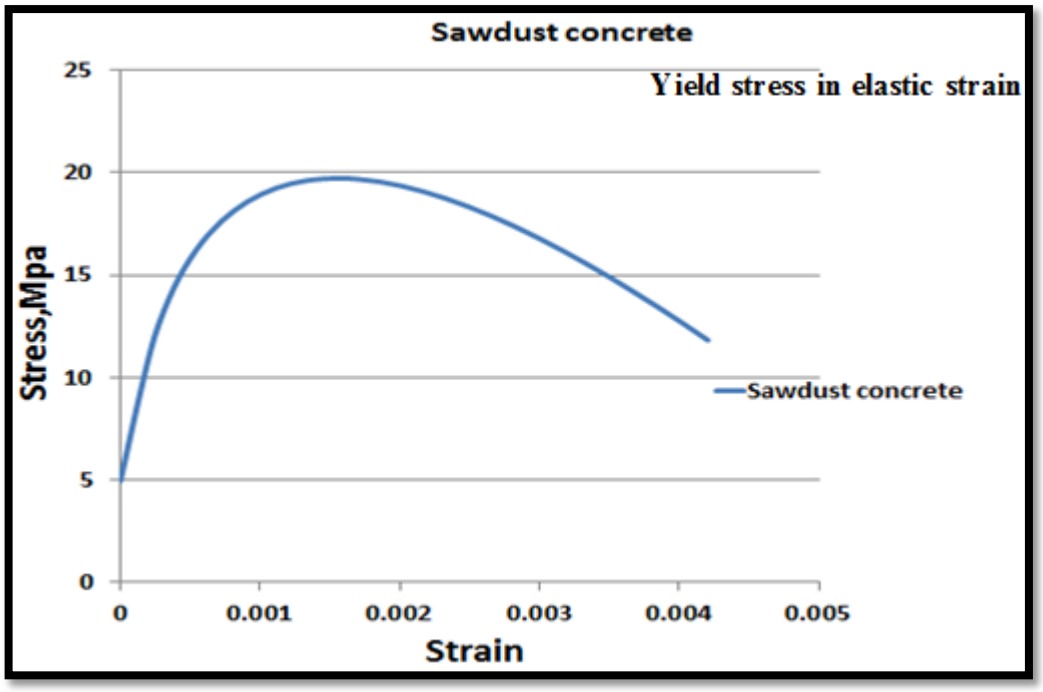

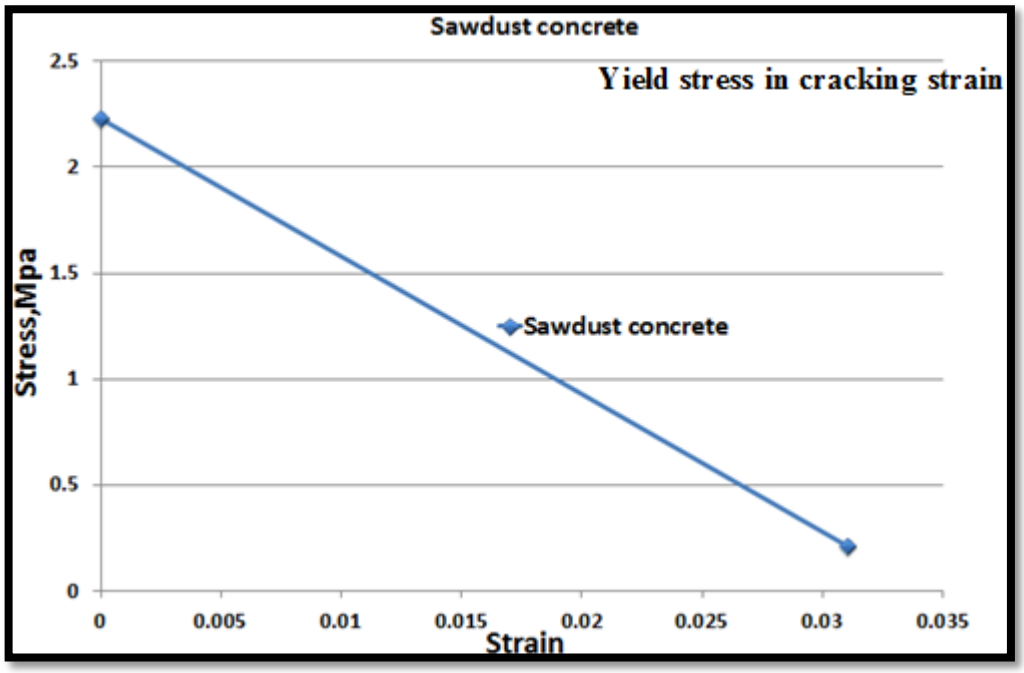

Figure (5-5): Relationship of Stress-Strain for **A60S**.

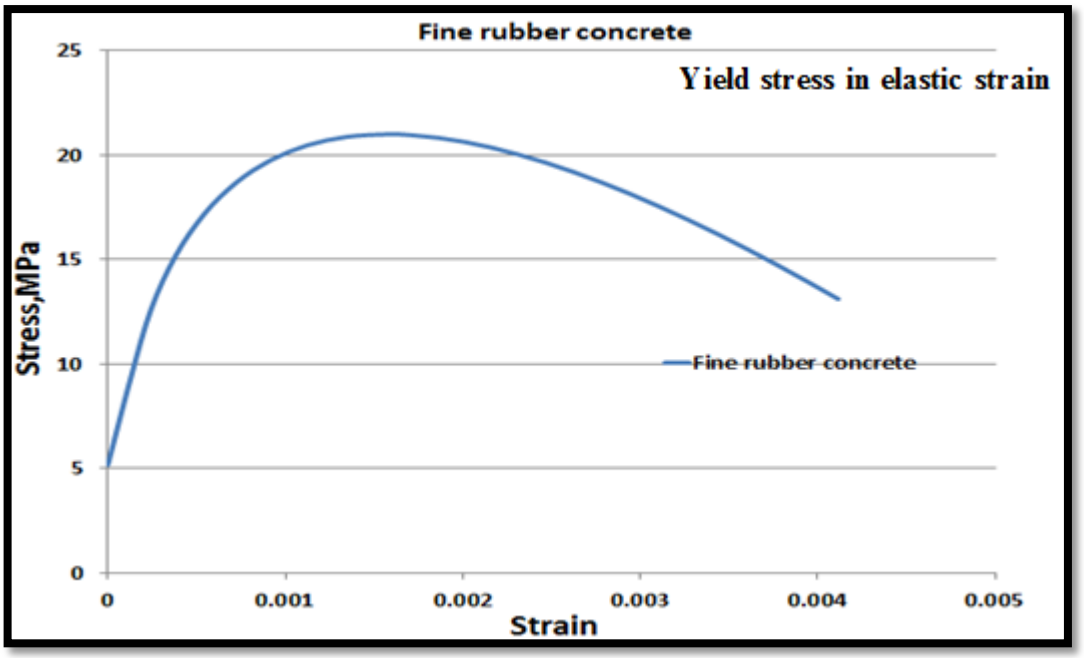

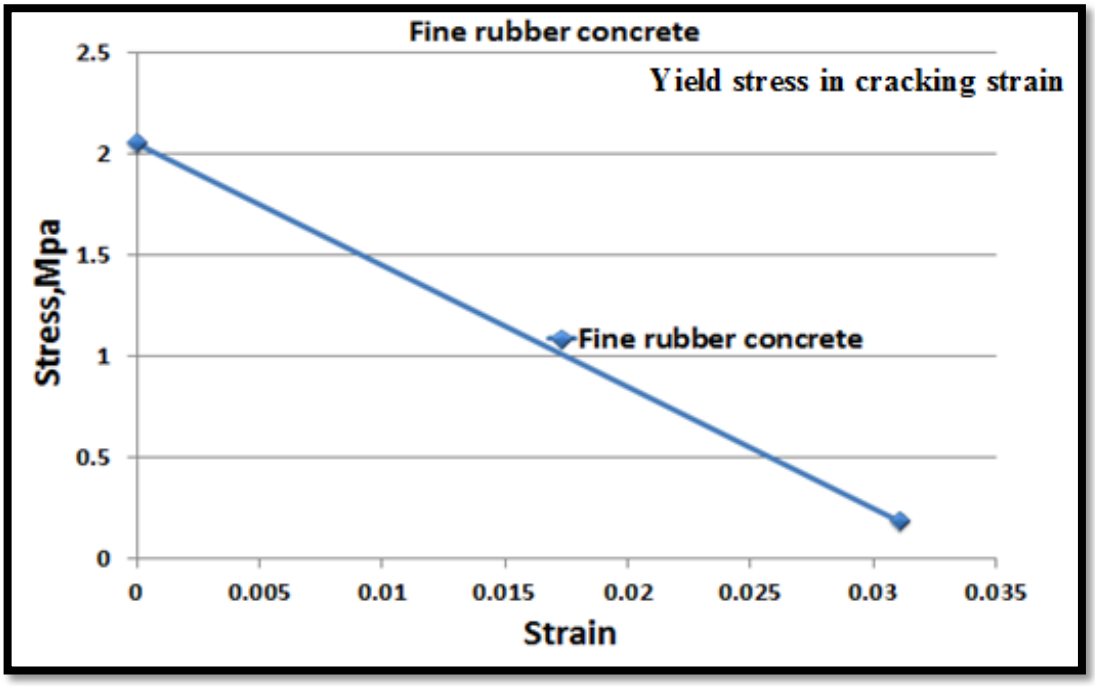

Figure (5-6): Relationship of Stress-Strain for **A60FR**.

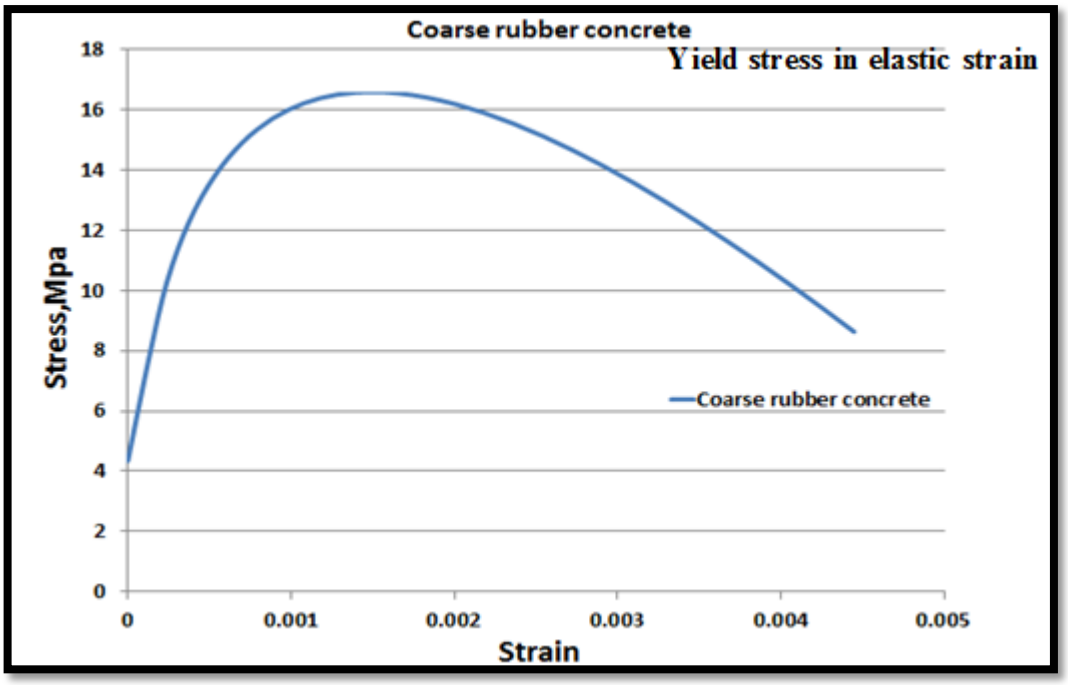

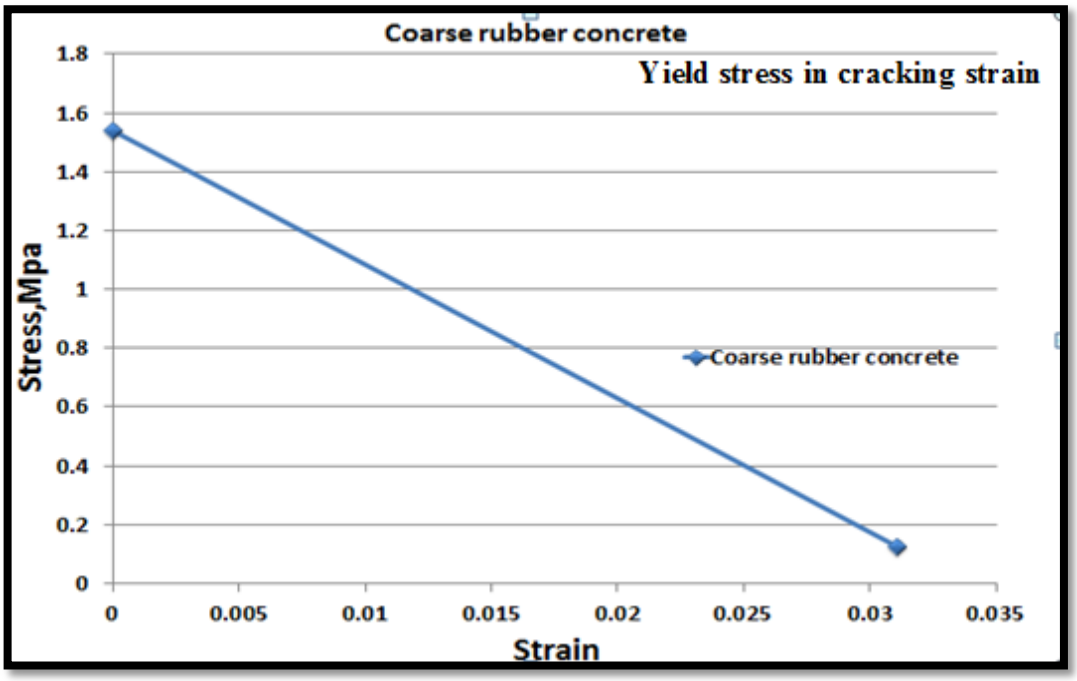

Figure (5-7): Relationship of Stress-Strain for **A60CR**.

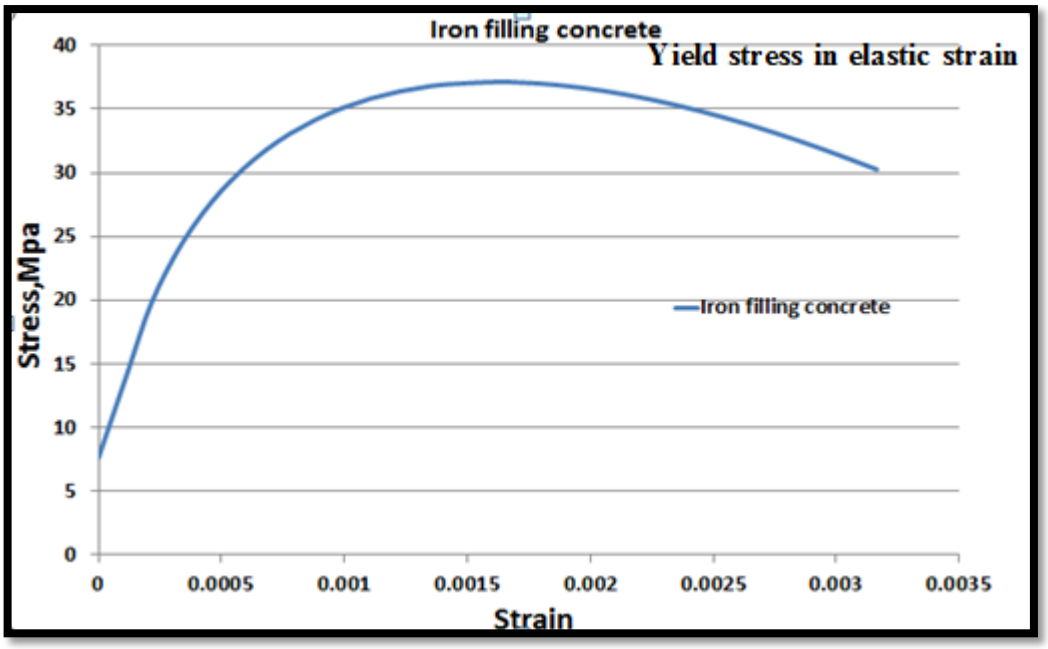

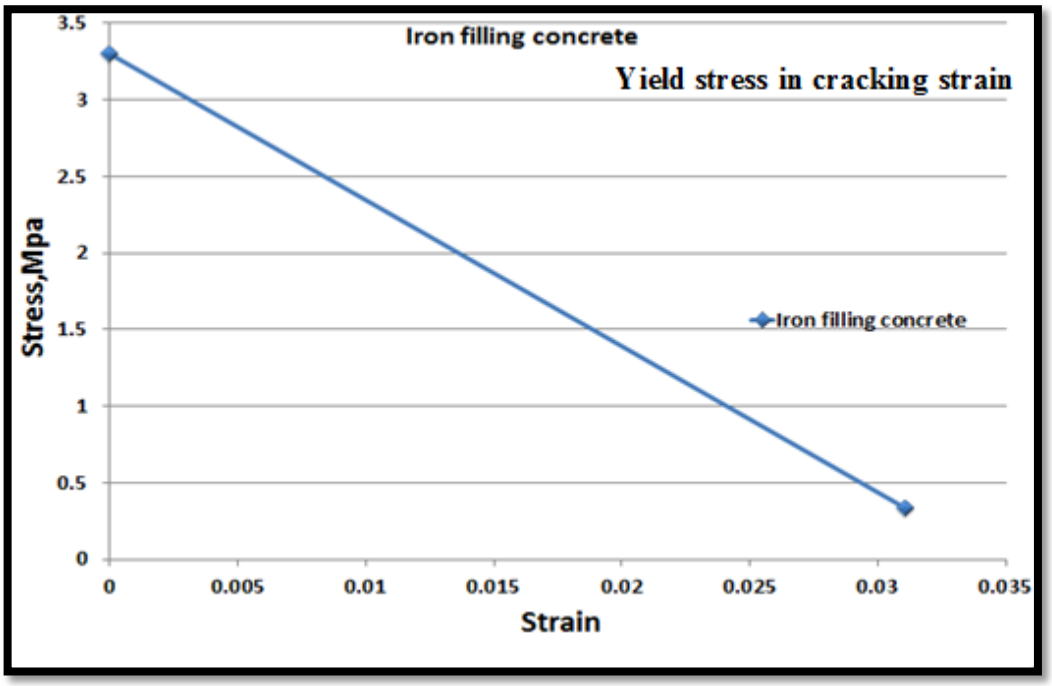

Figure (5-8): Relationship of Stress-Strain for **A60IF**.

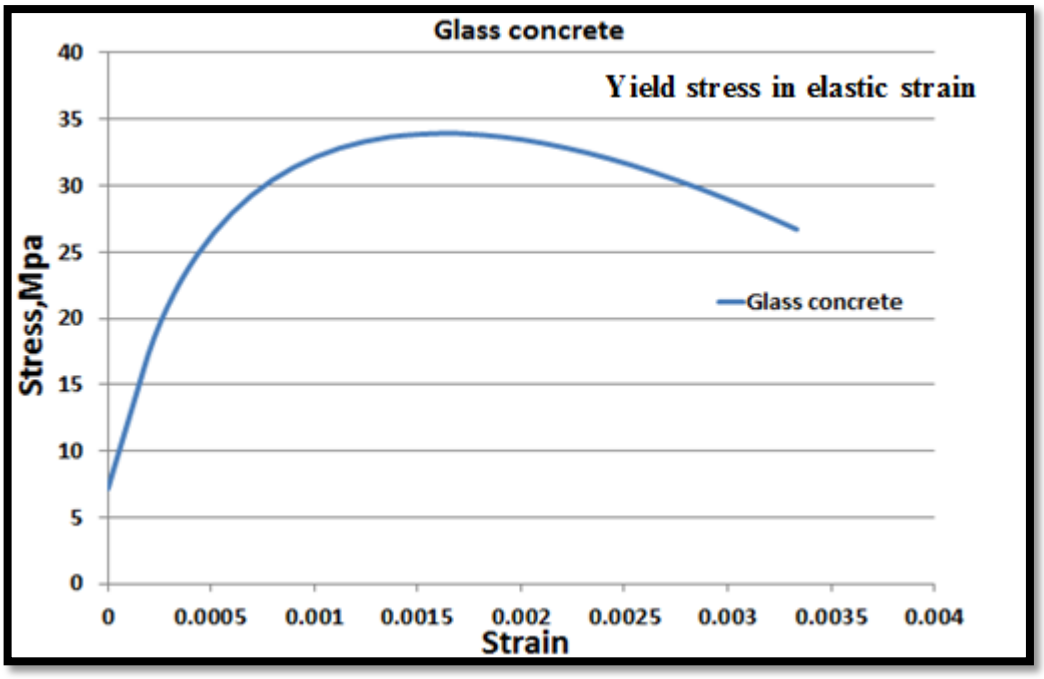

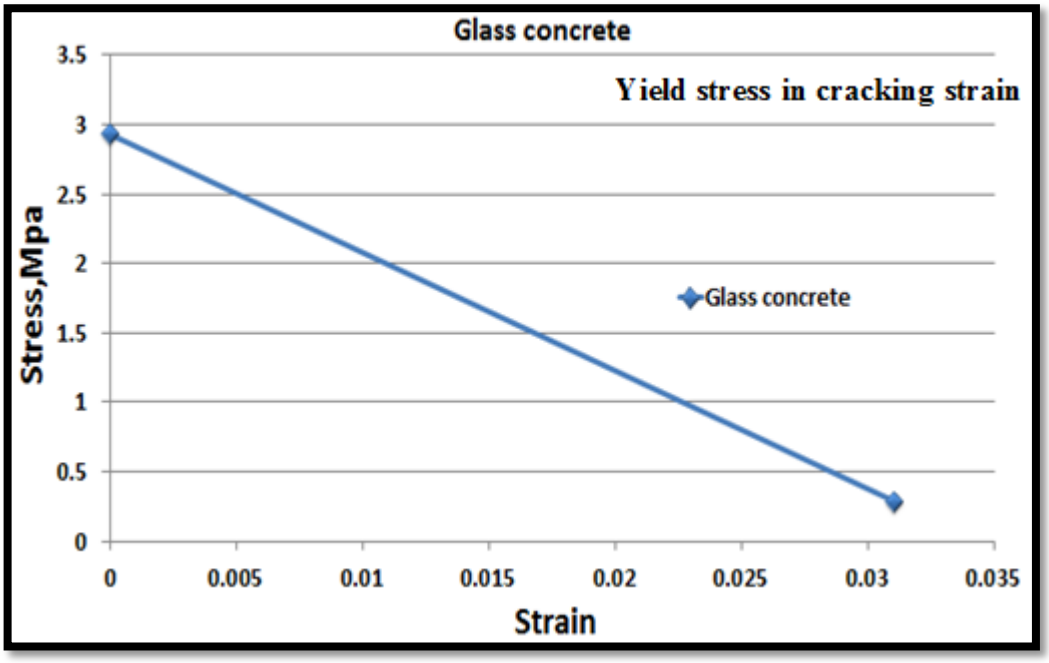

Figure (5-9): Relationship of Stress-Strain for **A60CSG**.

5.2.3 Interaction of Module

The modeling contact finite element formulation is based on the kinematics technique: contact without penetrated and friction conditions are specified kinematic ally at the nodes. In actuality, two lines of nodes made of different materials must be produced. These lines must be as near together as feasible in order to create a connection between the nearest front-nodes. The concrete and steel beam were supposed to have a coefficient of friction of 0.8, and this value was reached after multiple experiments to determine the number that minimizes the difference between the experimental and numerical findings.

The connection between the flange and the web, between the bolt parts and between the support plate and load plate with the beam was interaction, while the connection between the welded flange parts and between the stiffeners and the web was full bond tie.

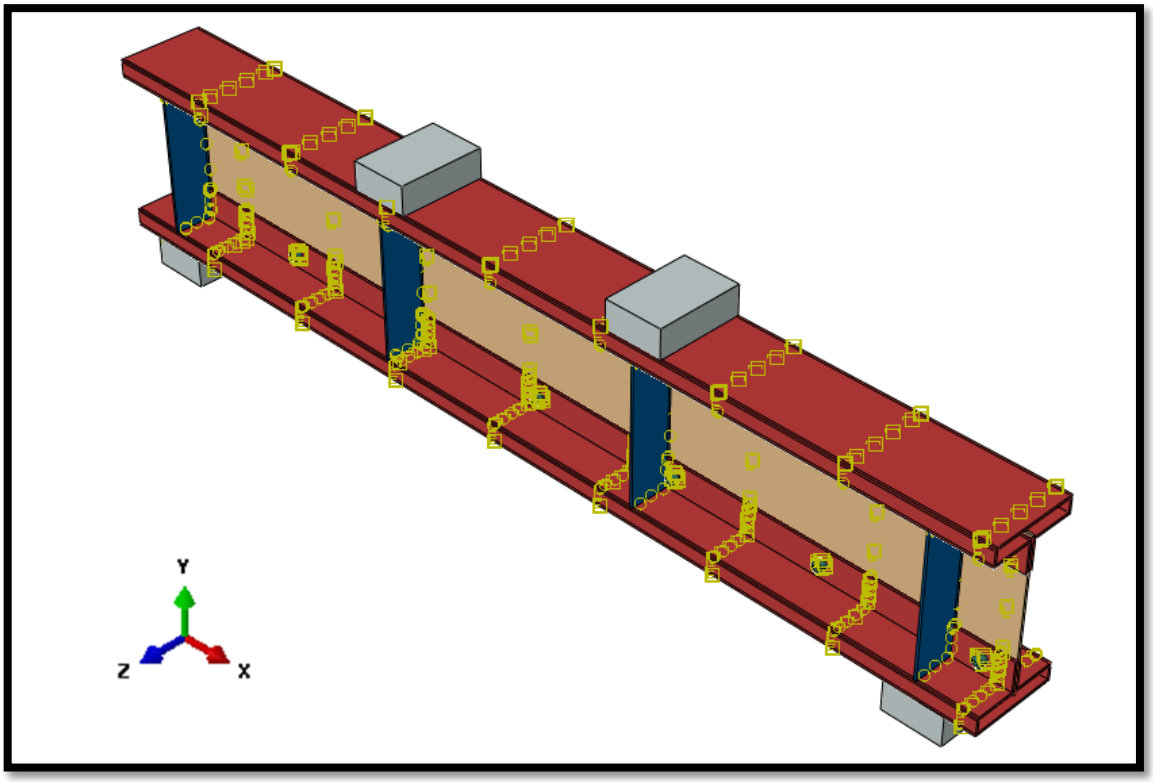

Figure (5-10): Interaction of Model.

5.2.4 Boundary and Loading Condition Module

The experimental work and finite element model for all beams loaded at identical locations, with the load represented as a vertical displacement of the bearing plate using the boundary condition (displacement/rotation) option and confined the (X) displacement and (Y,Z) rotation. The supports were modeled based on experimental findings, with constrained displacement in the direction (X,Y,Z) axis for hinge support case using boundary condition (Symmetry/Anti symmetric / Encastre) and free displacement in the direction z axis for roller support case using boundary condition (displacement/rotation) as shown in figure (5-11).

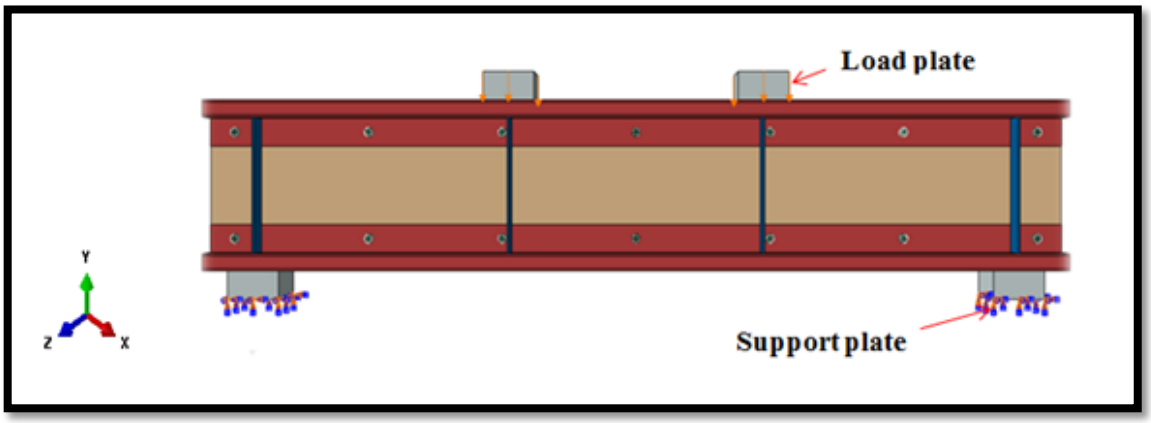

Figure (5-11): Boundary and loading Module.

5.2.5 Meshing and Convergence Study

There are numerous different elements that can be used in ABAQUS, and it's critical to choose the proper one for the job. The solid component (cold formed steel beam and strengthen materials) was controlled using the "eight-node three-dimensional linear brick element" with reduced integration. as shown in Figure(5-12). ABAQUS, on the other hand, provides a wide range of options, components of a three-dimensional (3D) continuum. The advantage of using linear brick elements over quadratic brick elements is that they can be used in contact, whereas quadratic brick components require more time to install and calculate constant nodal loads across the slave

surface. While the goal to avoid shear, choose decreased integration over full integration. Full integration delivers poor outcomes due to the locking phenomenon. As a result, the chosen for the vast majority of applications, element type is a reliable solution. Each node in a three-dimensional solid element has three degrees of freedom. To model the steel plates of loading and supporting of the three-dimensional solid element (C3D8R) was used in these positions.

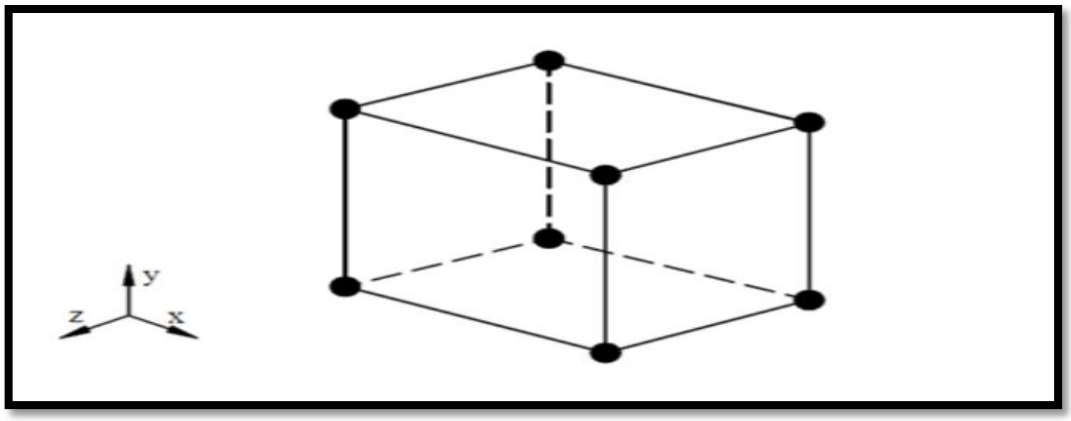

Figure(5-12): C3D8R Element type used in FE simulation(Wu. 2015)[49] of steel beam and strengthen materials.

The primary goal of the convergence study was to determine the ideal model mesh size with the fewest possible elements and the highest possible degree of convergence of the results, even with an increase or decrease in the mesh size. This was practically achieved by modeling beam A30 with the same material properties but with a decrease in element sizes of 50, 25, 20, 15, and 10 so that the reduction in mesh size had a minor impact on the results, as shown in Figures (5-13), (5-14) and (5-15) . The convergence study, showed that it can ignore the difference when the size of mesh decreased from 20mm to 15mm, therefor; the 15mm was used.

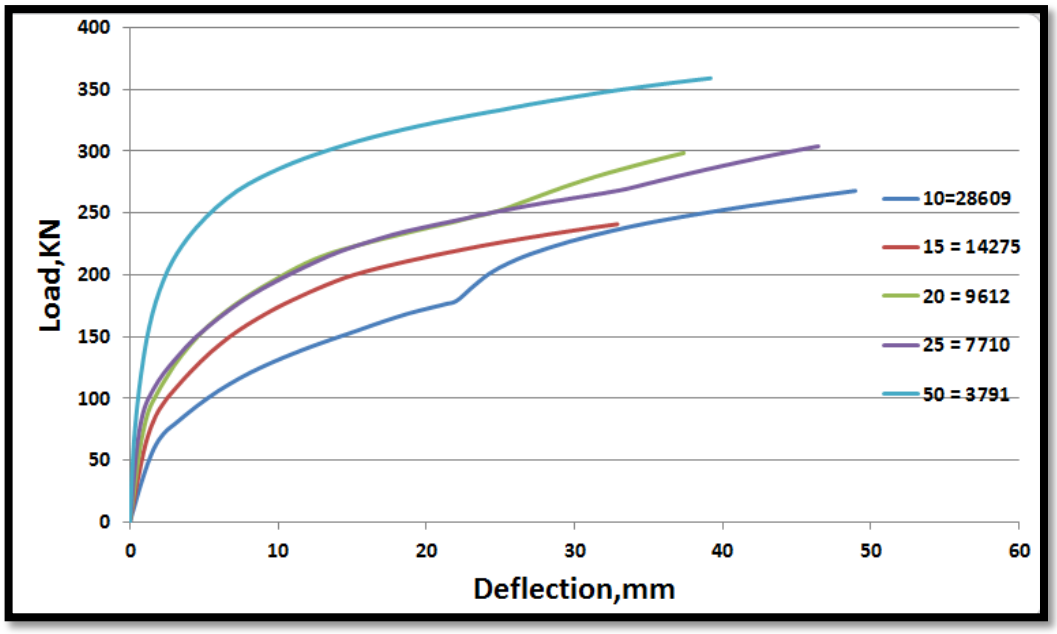

Figure(5-13): Load- deflection curves of **A30** for mesh trial.

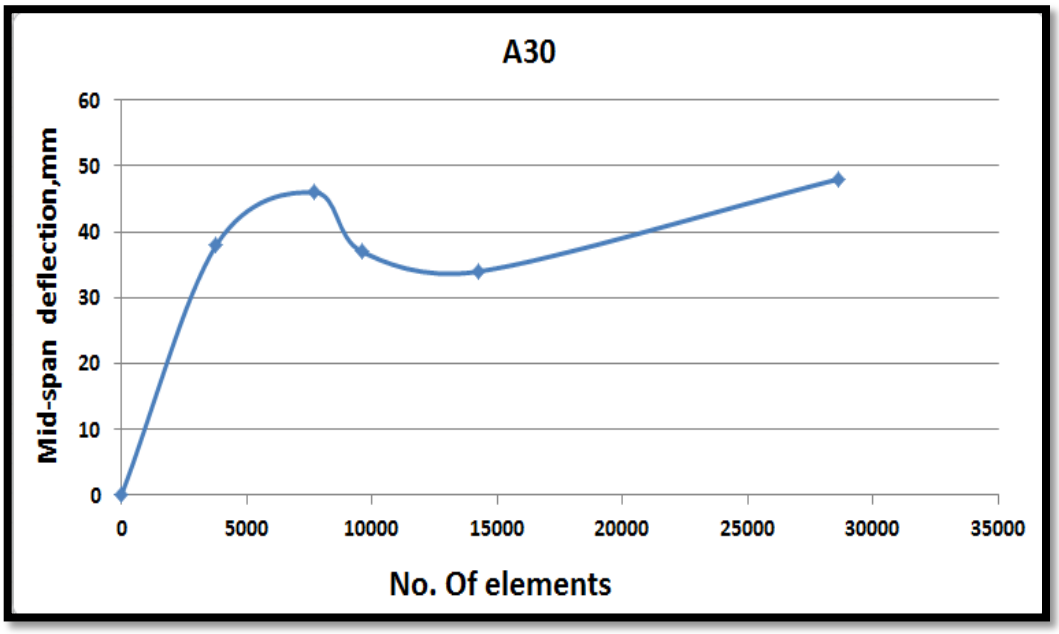

Figure(5-14): Result of Converges Study.

Mesh size 10

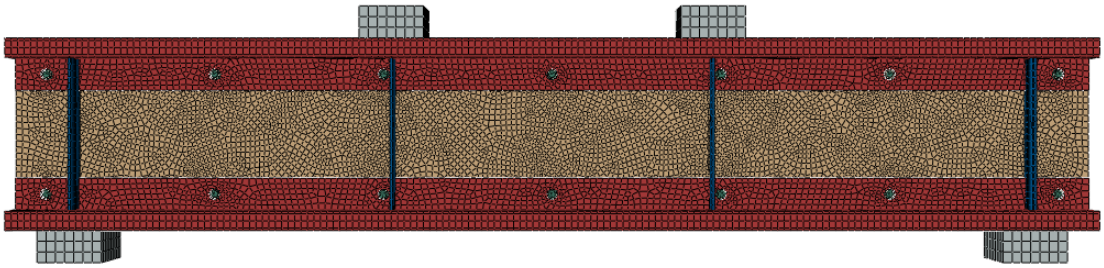

Mesh size 15

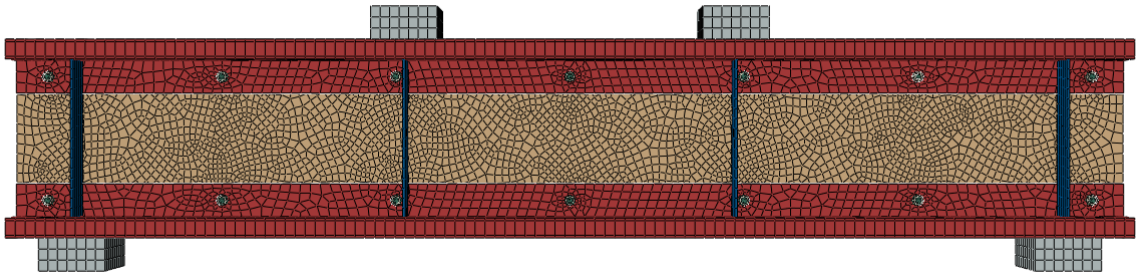

Mesh size 20

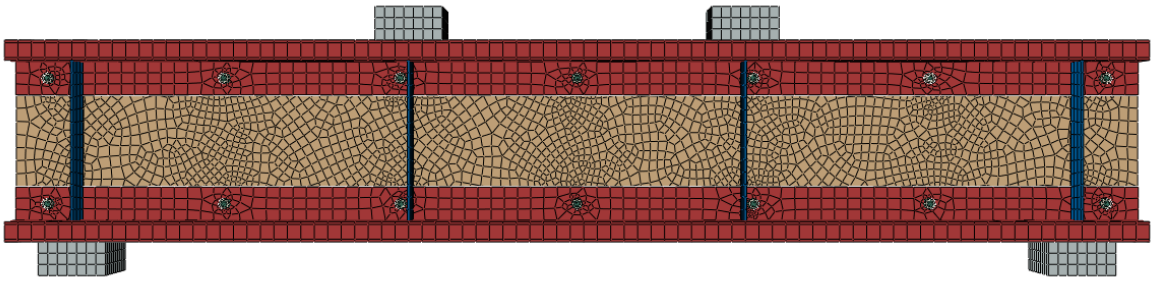

Mesh size 25

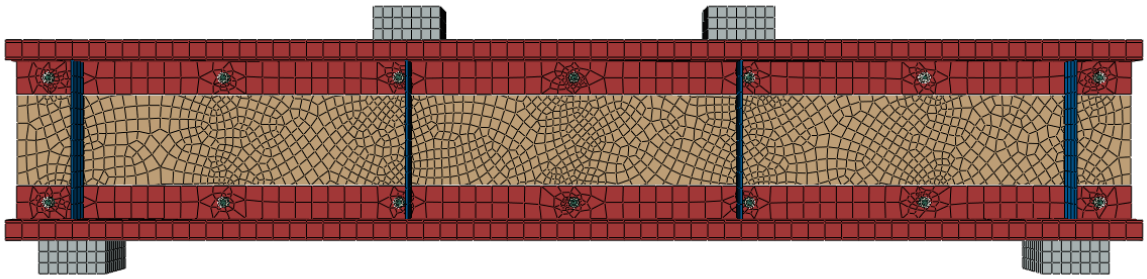

Figure(5-15): Finite Element Mesh.

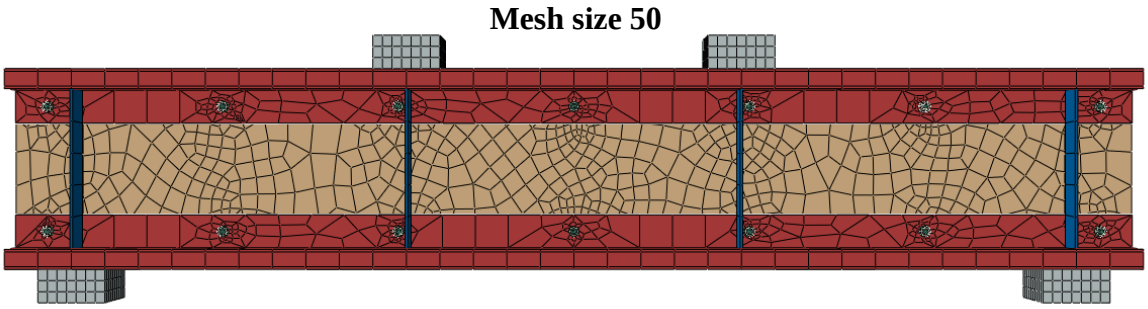

Figure (5-15): Continue.

5.3 Finite Element Analysis Results

For each tested beam, the results of **FEA** using the **ABAQUS** software were compared to the experimental results. **ABAQUS** results comprising ultimate load, maximum deflection and load-deflection curves.

5.3.1 Deformation Response

The behavior of the examined members during the loading was described by the load-deflection relationships, and it was an essential indication that the FE model was accurate. On the other hand, it responded with a stiffer response than the experimental specimens. Many factors could contribute to increase stiffness in FEM. The creation of the flanges in the experiments, the handling of concrete, the negative effects of the environment, etc., were the most important factors. The manner in which certain beam components were simulated may also have contributed to the simulated beams' higher initial load-mid span deflection response. The bond between the components of a beam was represented by the embedded region constraint in ABAQUS. This perfect representation may actually contribute to the deceptive initial increased stiffness of the numerical model since the actual interaction was flawed in reality. Figures (5-16) and (5-17) illustrate the load-mid span deflection of group I and group II, respectively.

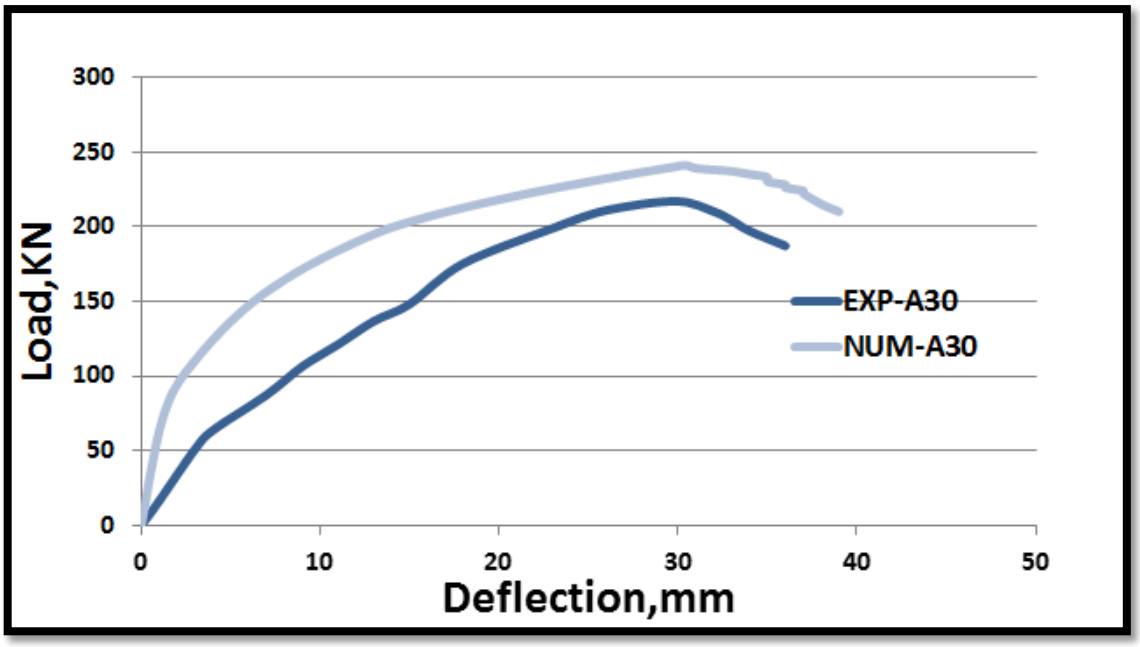

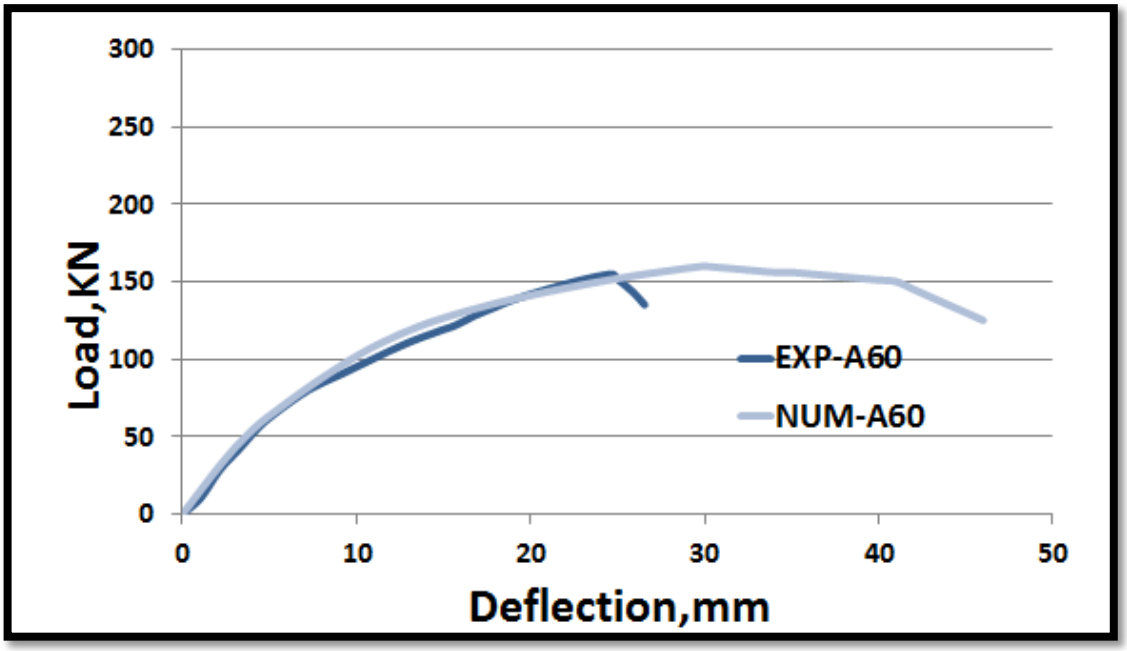

Figure (5-16): Experimental and Numerical Load-Mid span Deflection Curves of Group I.

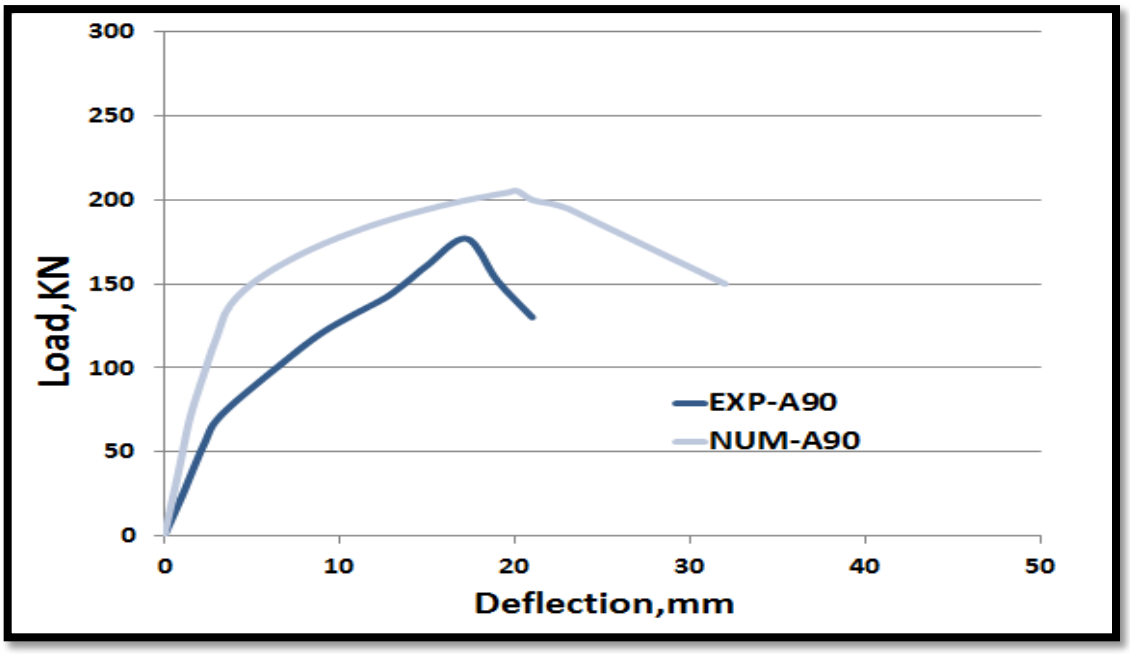

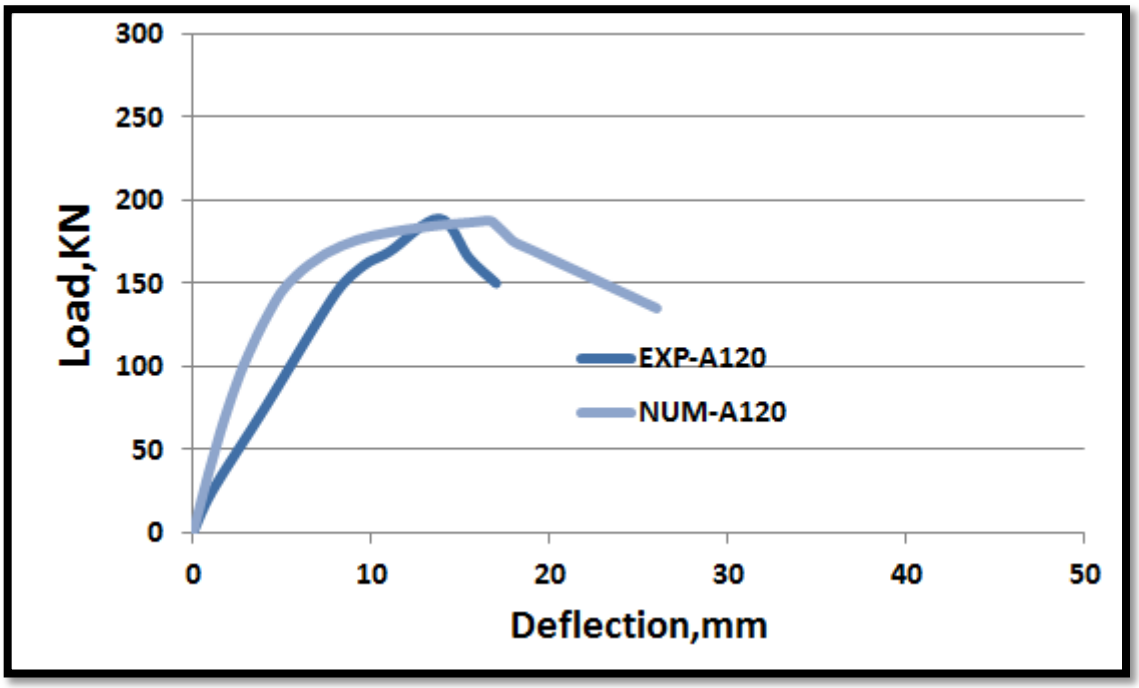

Figure (5-16): Continue**.**

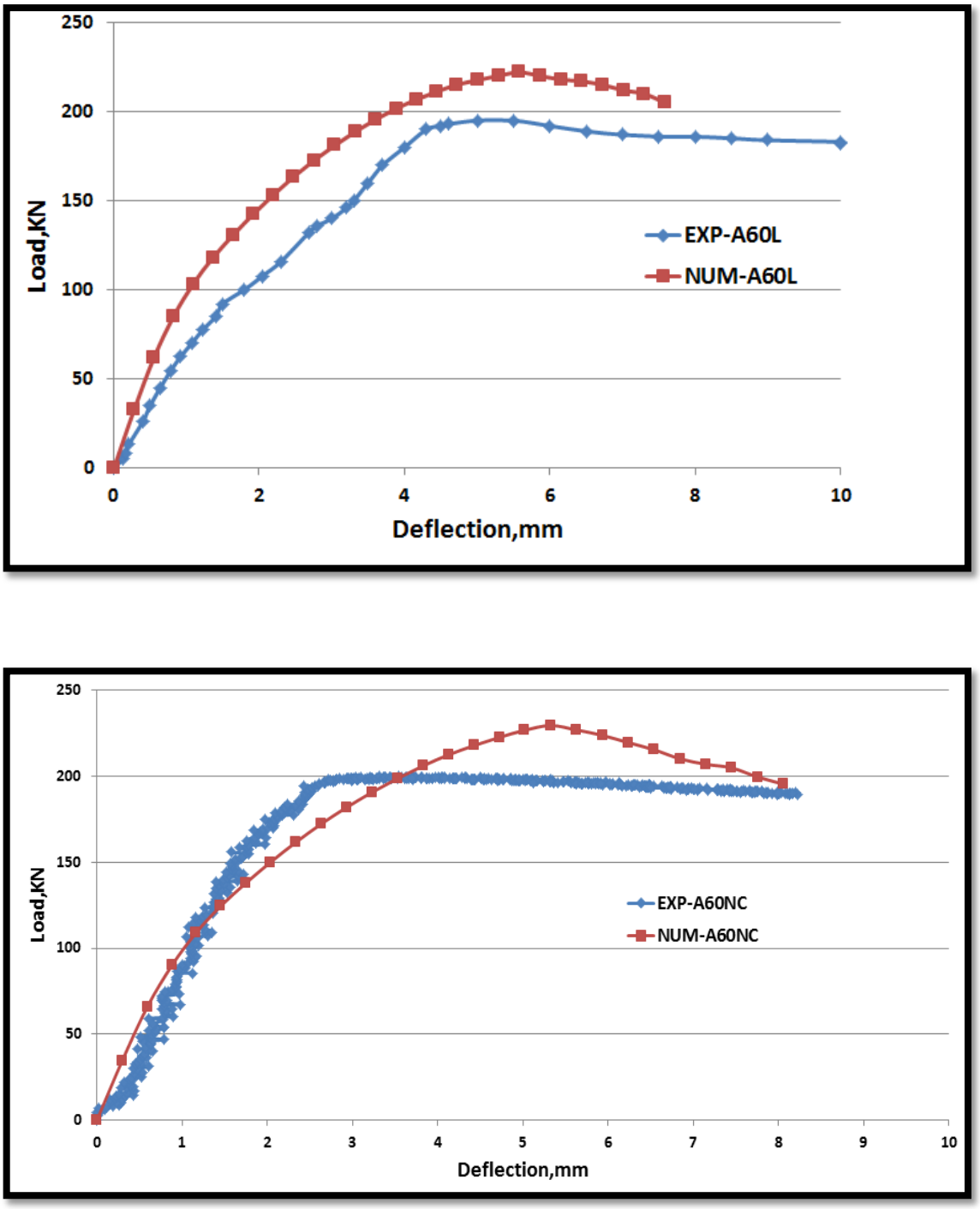

Figure (5-17): Experimental and Numerical Load-Mid span Deflection Curves of Group II.

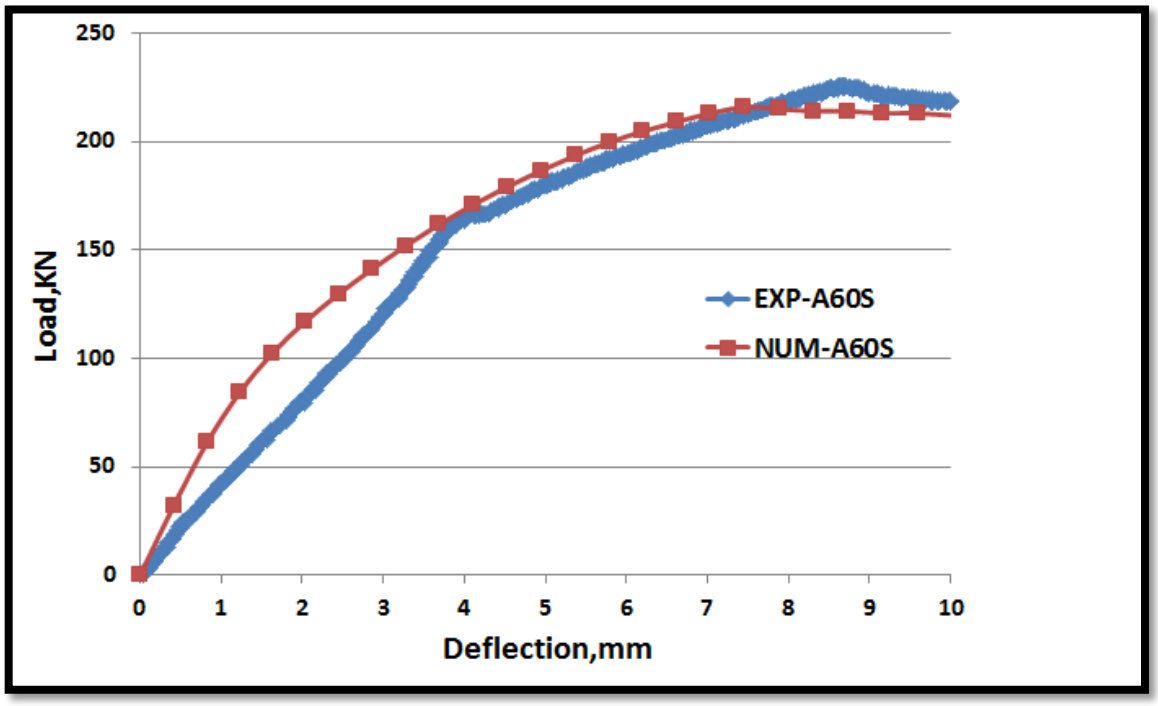

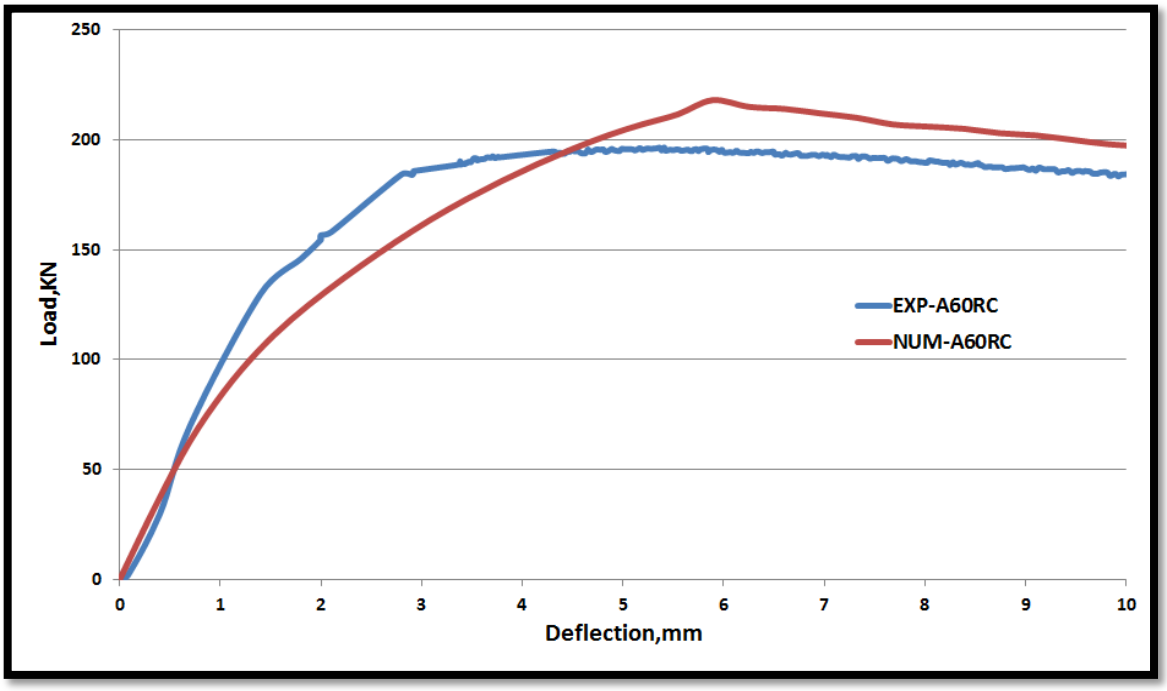

Figure (5-17): Continue.

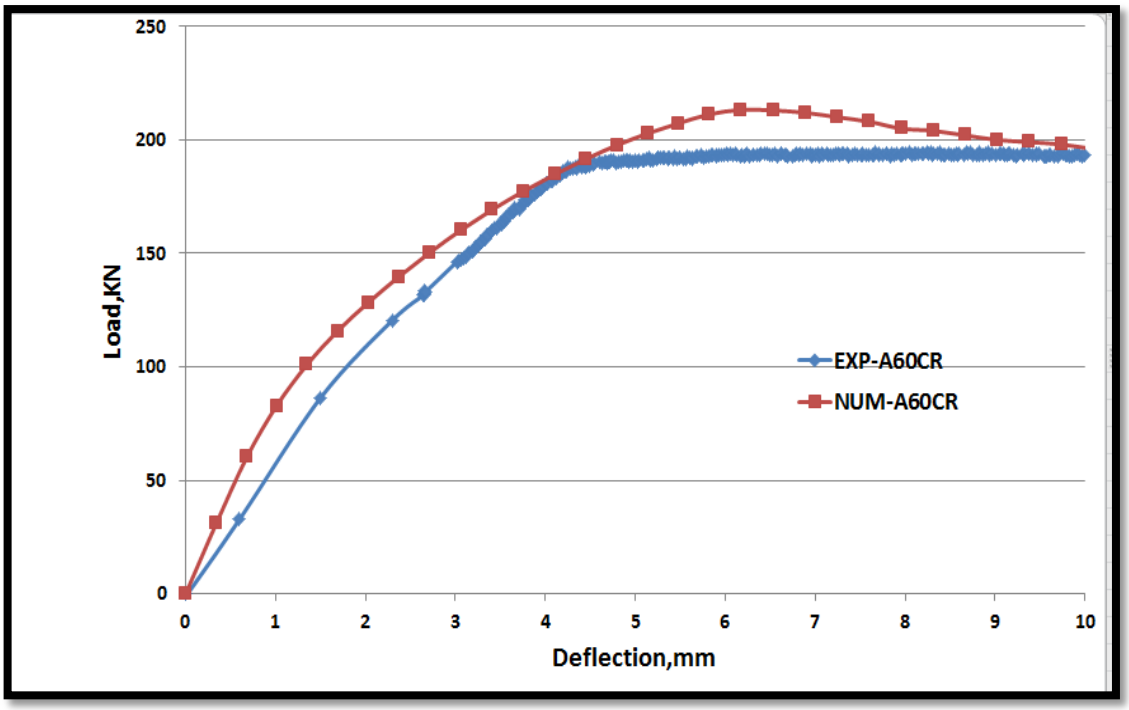

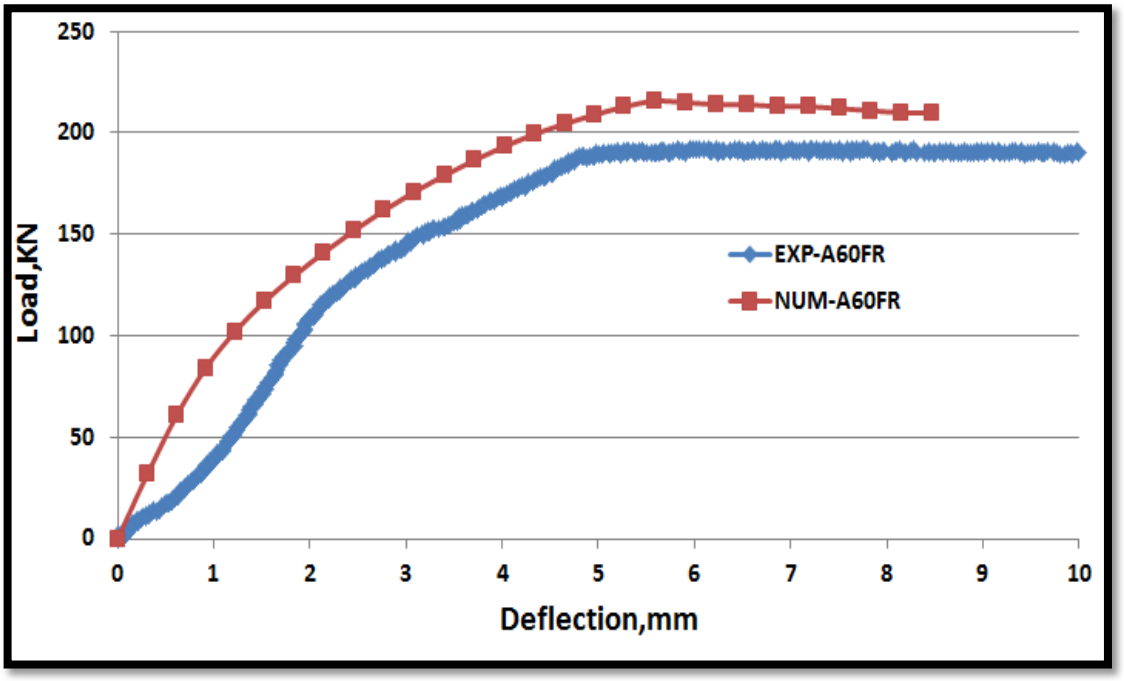

Figure (5-17): Continue.

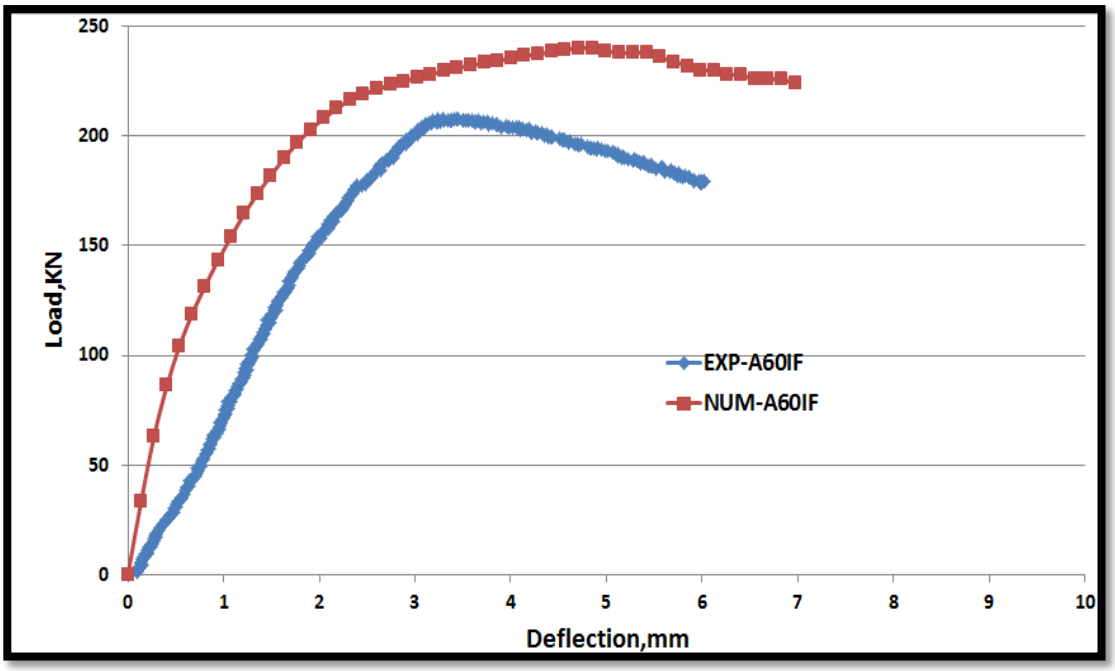

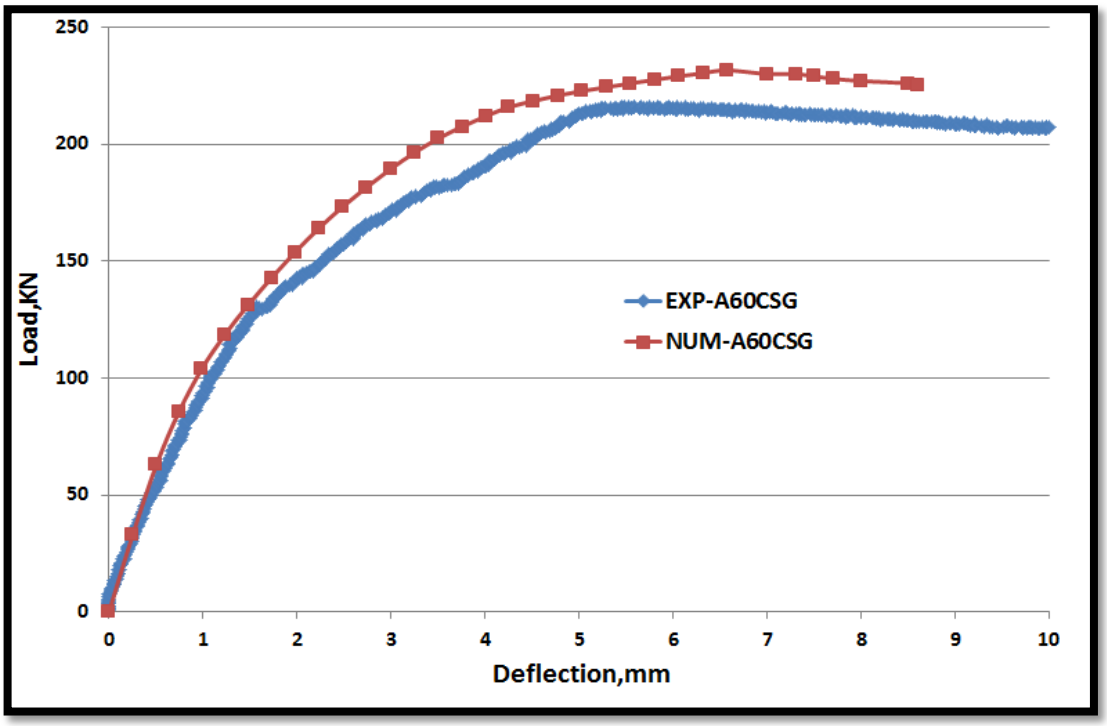

Figure (5-17): Continue.

5.3.2 Ultimate Loads of Specimens in Finite Element

The ultimate load and corresponding deflection from finite element analysis and the comparison between experimental and numerical deflection at ultimate load were shown in Table(5-4). The max. difference in results was varying between (1%) decrease to (11%) increase ultimate load. While the difference in max. deflection at mid span was starting from (-14%) to (40%) .

Table(5-4): Experimental and FEM Ultimate Loads of all specimens.

Specimens	Ultimate loads, P_u,kN		A %	Max. deflection, Δ_u, mm		B %
	Exp.	Num.		EXP.	Num.	
A30	217	241	11	29.98	30.4	1
A60	160	160.08	0.05	24.65	28.98	18
A90	177	205	16	17.25	20.2	17
A120	189	187	-1	13.81	16.63	20
A60L	196	192.7	-2	4.84	5.58	15
A60NC	199	193.3	-3	4.64	5.3	14
A60RC	195	193.2	-1	4.13	5.8	40
A60S	225	190.4	-15	8.69	7.44	--14
A60FR	192	190.2	-1	5.65	5.5	-3
A60CR	190	188	-1	5.6	6.17	10
A60IF	206	194.1	-6	3.44	4.7	36
A60CSG	215	193.4	-10	5.66	6.57	16

* $A = \frac{pu)num.-pu)exp.}{pu)exp.} * 100\%$

** $B = \frac{\Delta u)num.-\Delta u)exp.}{\Delta u)exp.} * 100\%$

5.3.3 Deflection at Service Load and Ductility Index

Table (5-5) illustrated the comparison of numerical and experimental deflection at service load and ductility factor for all beams. The service load was equivalent to 0.65 of the ultimate load [49].The FE analysis' service deflection values and ductility factors were in accepted agreement with the experimental values. For service deflection and ductility factor, the deviations as average were roughly 0% and 62%, respectively.

Table(5-5): Exp. and FEM Results of Service Deflection and Ductility Index

Specimens	Service Deflection(mm)			Ductility Index, μ		
	$(\Delta s)_{FEM}$	$(\Delta s)_{EXP}$	A%	$(\mu)_{FEM}$	$(\mu)_{EXP}$	B%
A30	6.56	14	- 53	4.6	2.14	53
A60	10.5	11	-5	2.8	2.24	20
A90	3.5	8	-56	5.8	2.2	62
A120	3.9	7	-44	4.3	2	53
A60L	2.1	2.1	0	2.7	2.3	15
A60NC	2.02	1.84	10	2.7	2.52	7
A60RC	2.4	2.01	19	2.42	2.42	0
A60S	2.65	3.53	-25	2.81	2.5	11
A60FR	2.14	2.25	-5	2.6	2.51	3
A60CR	2.35	2.41	-2	2.63	2.32	12
A60IF	1.09	1.39	-21	4.3	2.47	43
A60CSG	1.96	1.93	2	3.4	2.93	14

* $A = \frac{\Delta s)_{FEM.} - \Delta s)_{EXP.}}{\Delta s)_{EXP.}} * 100\%$

** $B = \frac{(\mu)_{FEM.} - (\mu)_{EXP.}}{(\mu)_{FEM.}} * 100\%$

5.3.4 Mode Failure of Steel Beams and Crack of Concrete

The FEM-generated modes failure were very similar to those discovered during the experimental investigation. Plates (5-2) and (5-3) illustrate the modes failure of group I and group II, respectively. Plate (5-4) illustrated the crack patterns of concrete.

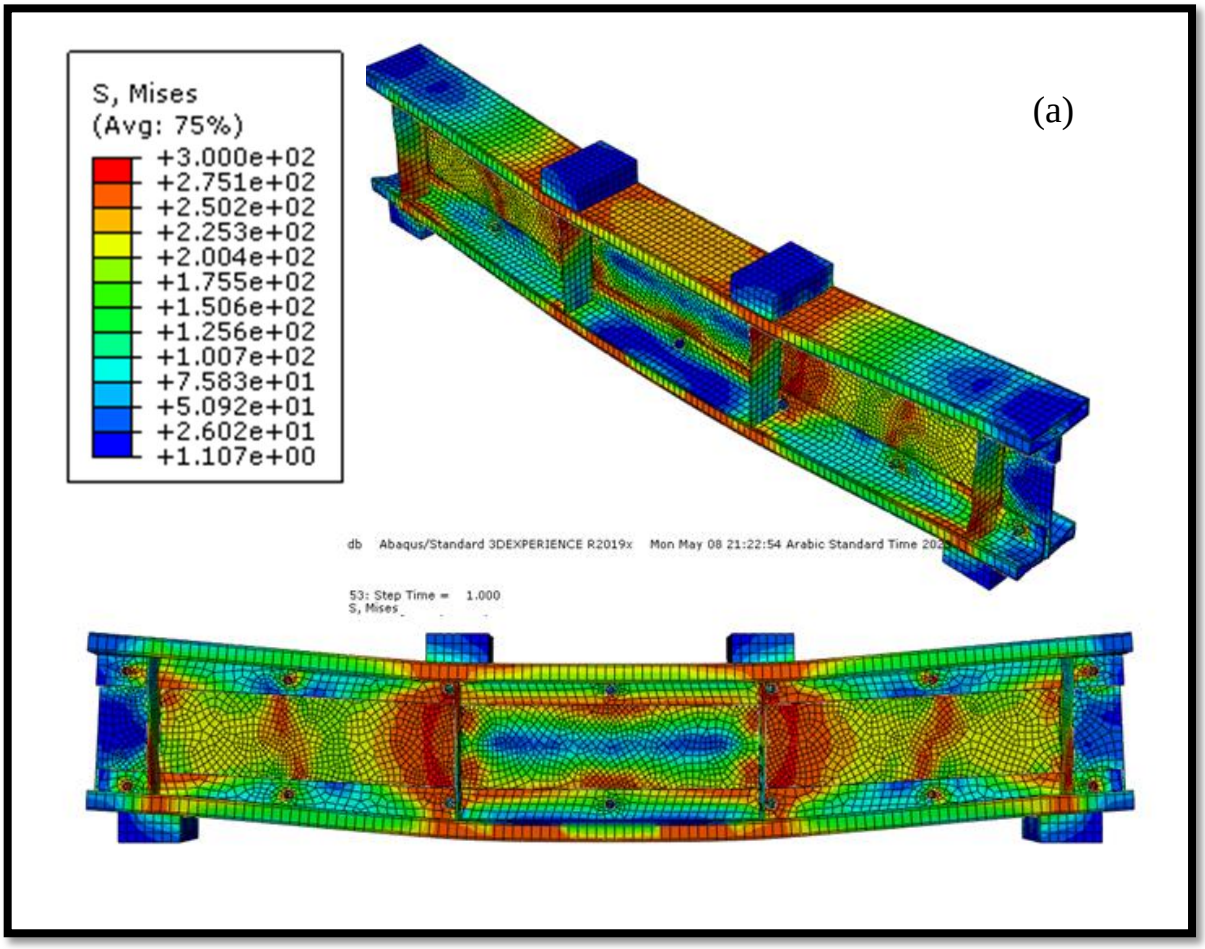

Plate (5-2): Stress Distribution at Ultimate Load for Group I (a) **A30**, (b) **A60**, (c) **A90** and (d) **A120**.

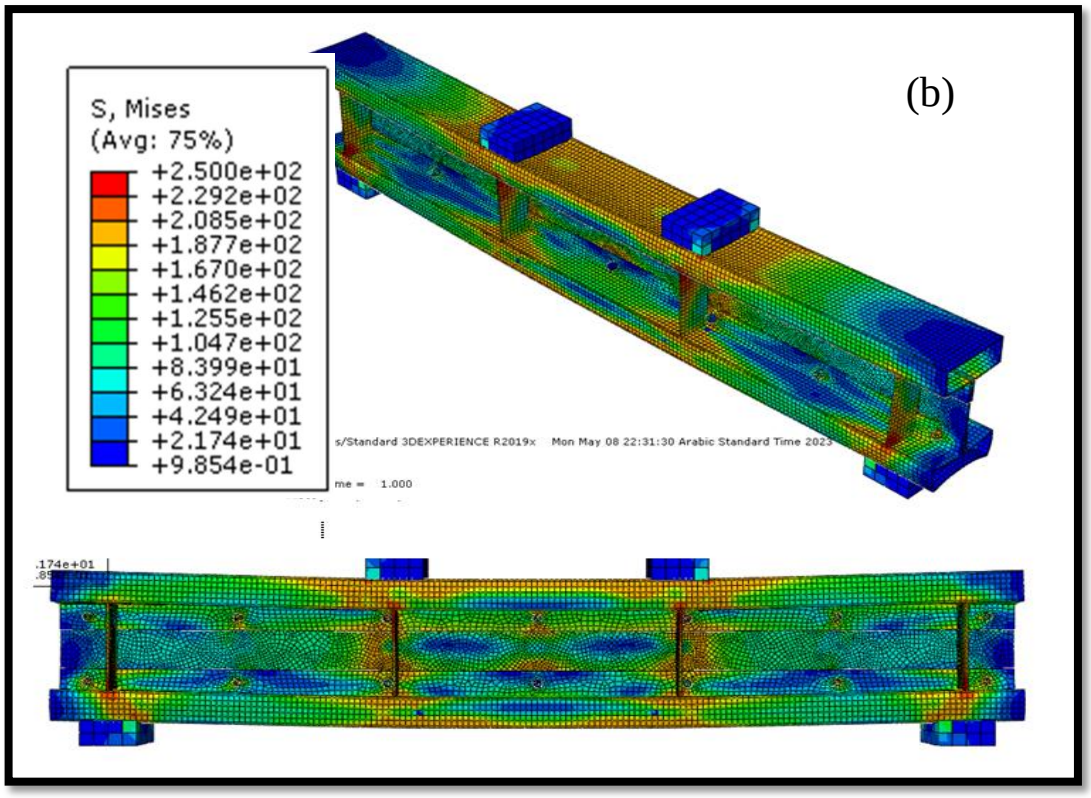

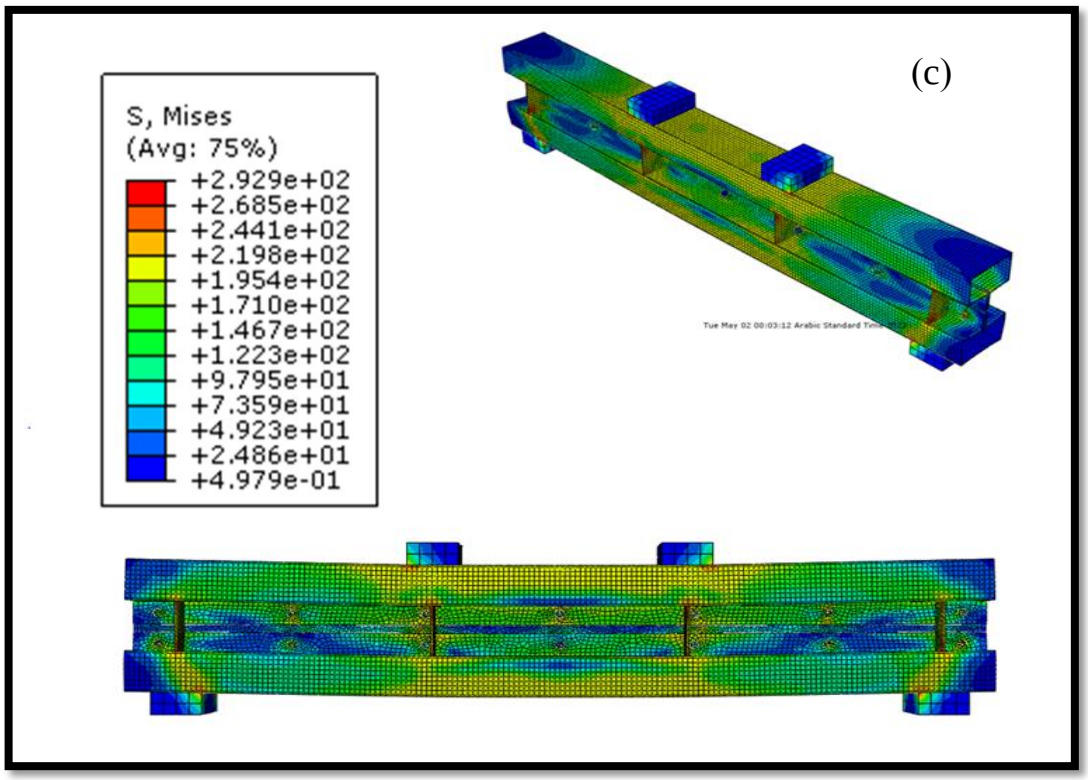

Plate (5-2): Continue.

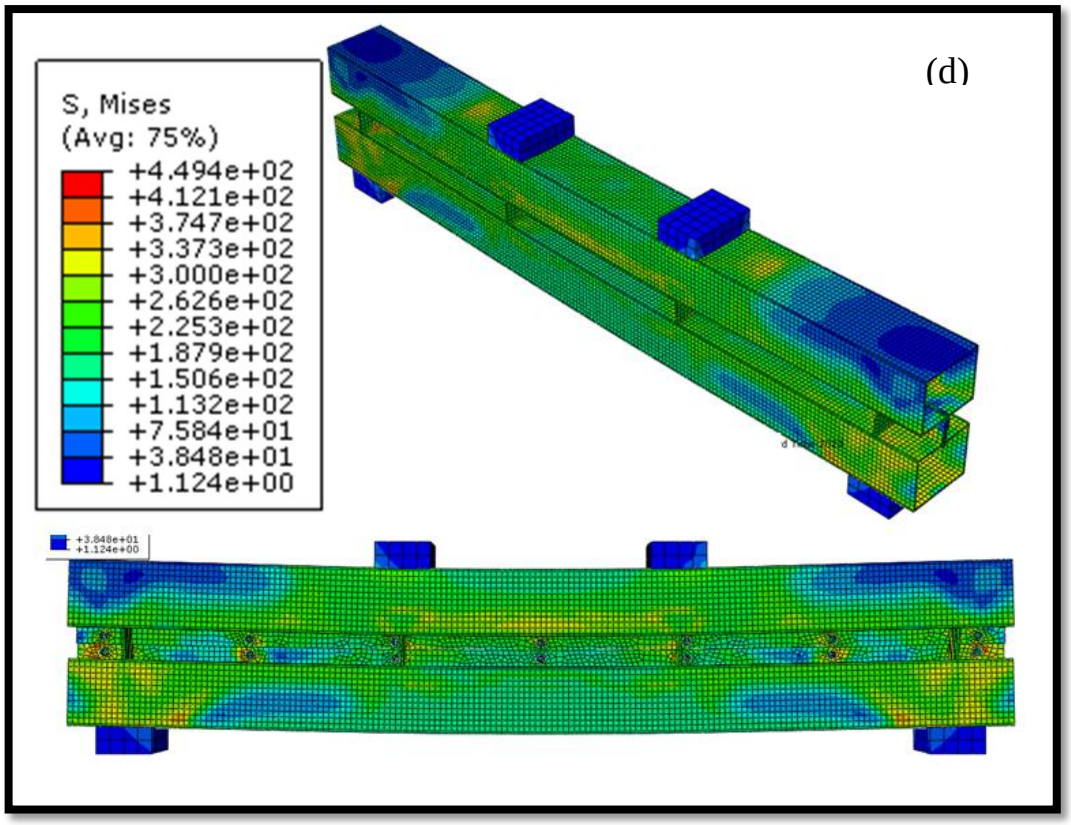

Plate (5-2): Continue.

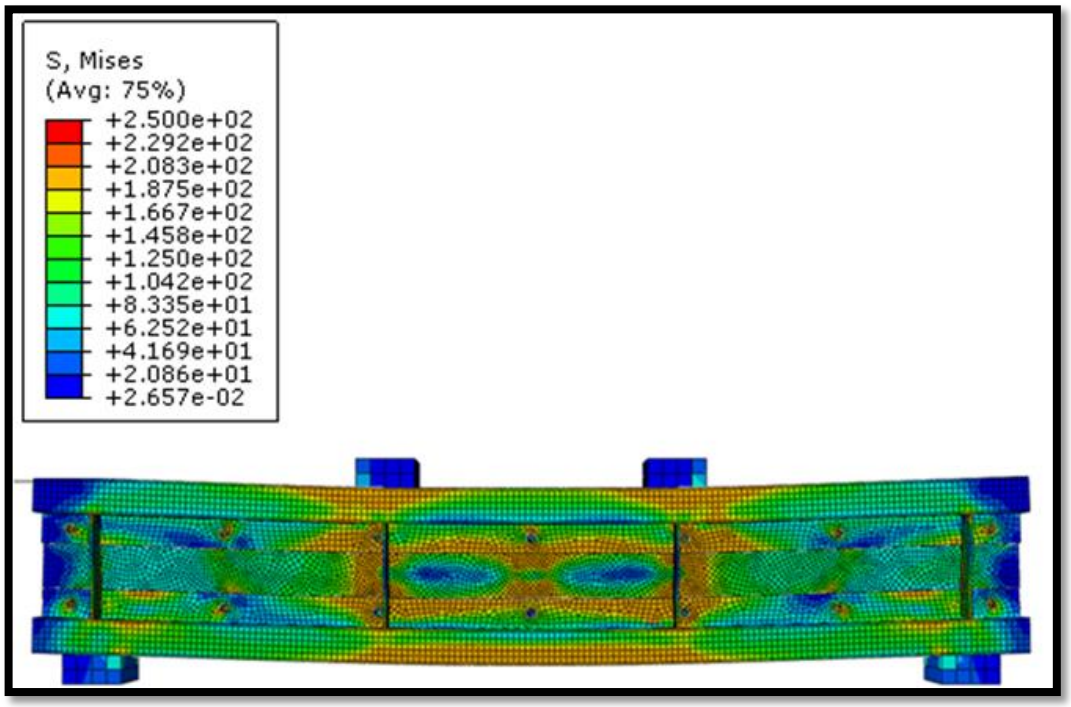

Plate (5-3): Stress Distribution at Ultimate Load for Group II.

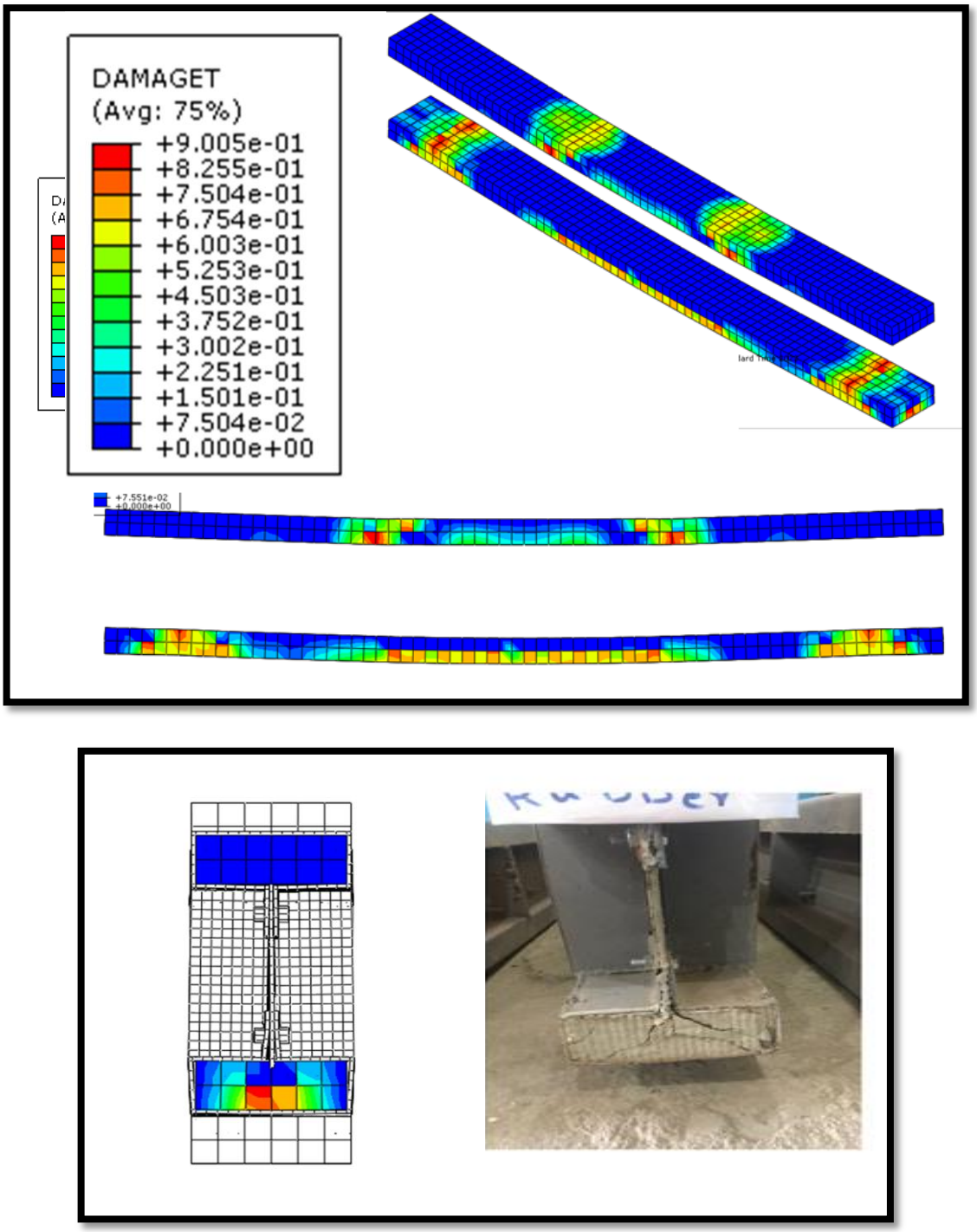

Plate (5-4): Crack Pattern of Finite Element Model for Concrete.

Finally, when compared to the experimental failure mode, the reported failure mechanism predicted in FEM for all specimens was identical.

5.4 Parametric Study

Two important parameters were investigated in the experimental work, including the depth of flange and eight types of strengthening in an attempt to increase the strength of rectangular hollow flange cold-formed steel I-beams

under two concentrated loads. Using the finite element simulation model in this work, which has been shown to be capable of forecasting the experimental ultimate load within an acceptable percent and modes of failure. In order to provide a more complete and accurate knowledge of the behavior of beams with hollow flange , a parametric analysis carried out. It included the assessment of the behavior of hollow flange beams involving the connection type between web and flange, the thickness of plate, strengthening the compression flange only with normal concrete, strengthening the beam with ultra- high strength concrete and different depth of flange in the same beam. Table(5-6) shows the result of parametric study. Figure (5-18) Shows the load-mid span deflection for all parametric study.

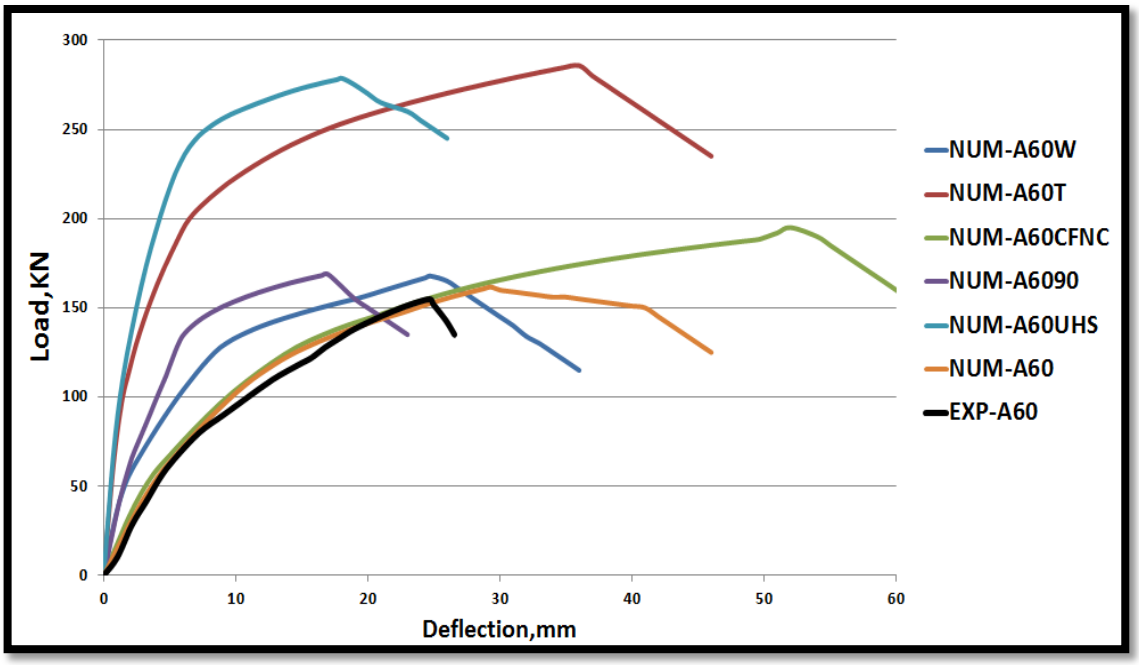

Figure(5-18): Load- max Deflection for All Parametric Study.

5.4.1 Effect of Connection Type

The bolt connection between web and flange well studied during the experiments. Therefore, in order to get a full view of the effects of connection type on flexural behavior of hollow flange beam, weld connection will be studied here. A60W beam consist of two flange and web, two flange connected to web by welding. When comparing A60W with A60, the bearing capacity increased by 5% and the deflection increased by 0.6%.

Table (5-6): The Result of Numerical Analysis of A60W

Specimens	Ultimate applied load(kN)	Mid-span deflection(mm)	Failure Mode
A60W	**168**	**24.8**	**Flexural**

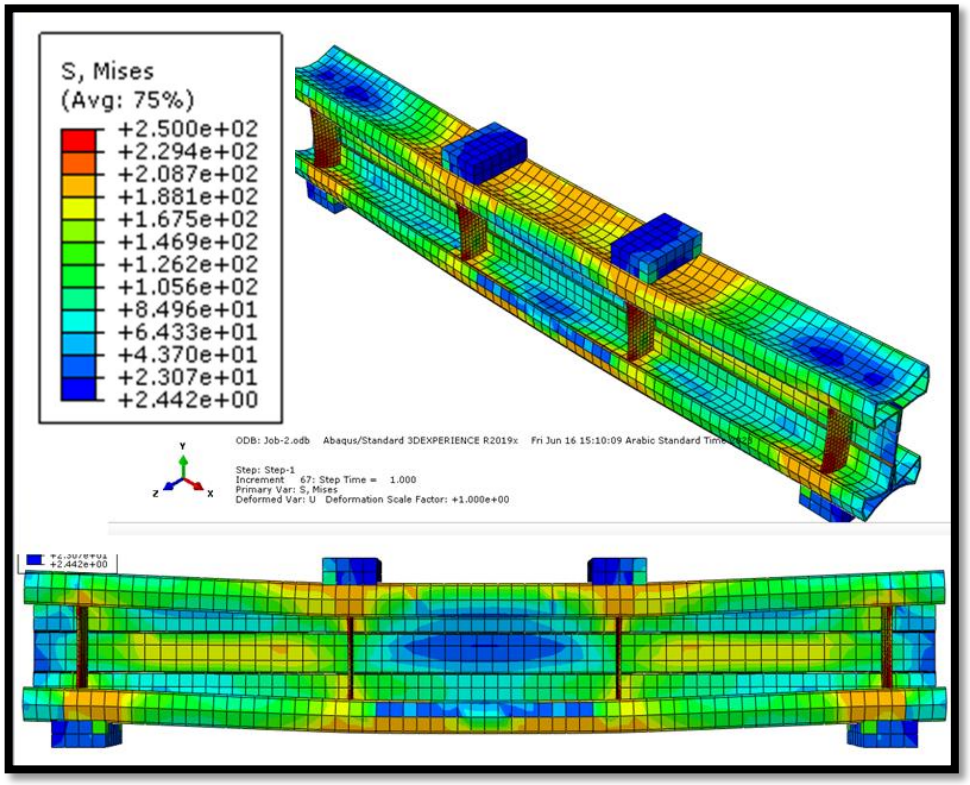

Plate (5-5): Stress Distribution at Ultimate Load for **A60W**.

5.4.2 Effect of Thickness of Steel Plate

In this case, the effect of thickness on the flexural behavior of the beam A60 was studied. In this case, A60T6 beam consists of two flange and web, the flanges connected to web by bolt, the thickness of steel plate(flanges and web) is 6mm. When comparing A60T with A60, the ultimate capacity increased by 44% and the deflection increased by 30.7%.

Table (5-7): The Result of Numerical Analysis of A60T6

Specimens	Ultimate applied load(kN)	Mid-span deflection(mm)	Failure Mode
A60T6	**285.77**	**35.6**	**Flexural**

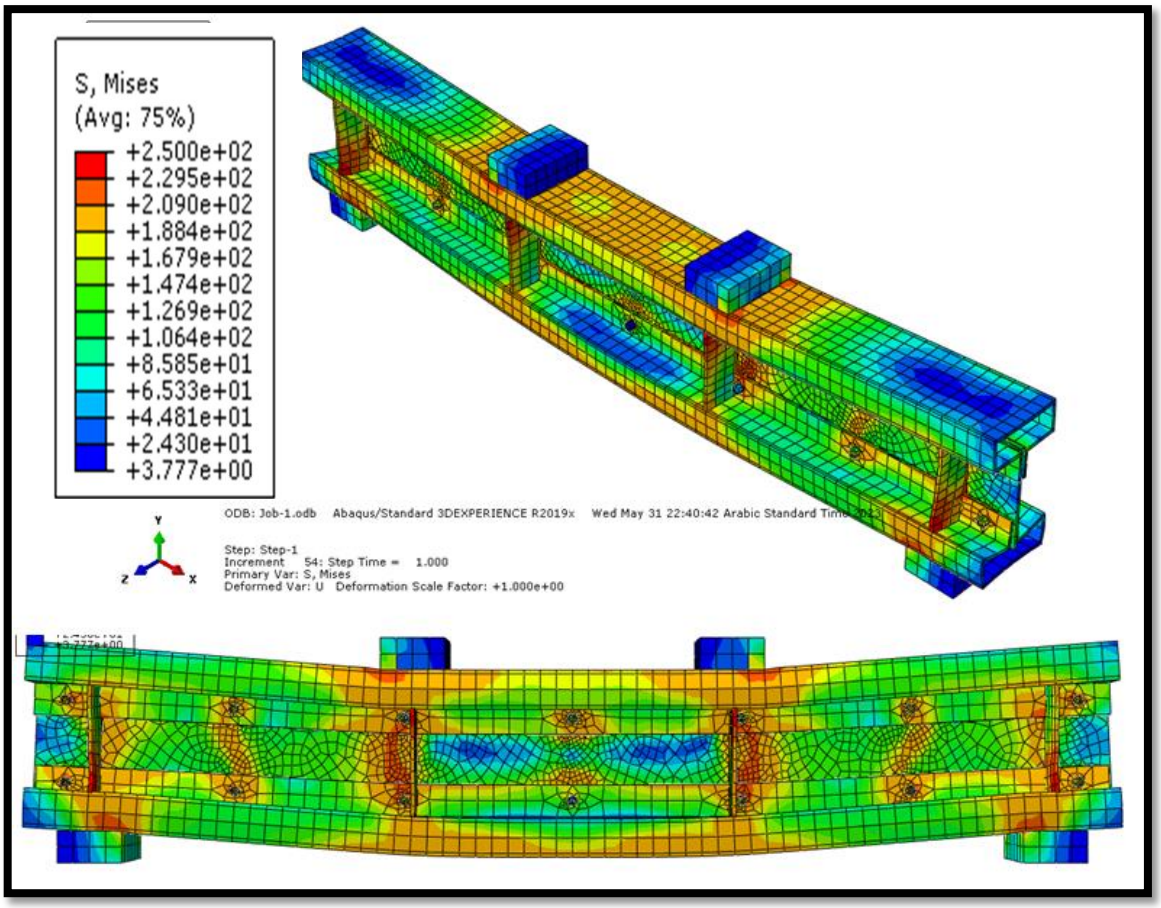

Plate (5-6): Stress Distribution at Ultimate Load for **A60T6**.

5.4.3 Effect of Strengthening Compression Flange

The compression flange of A60CFNC was strengthened only with normal concrete. In this section, strengthening the compression flange only did not have any good effect, on the contrary, the deflection increased when compared with A60 by 91% and the ultimate capacity decreased by 4.6% .

Table (5-8): The Result of Numerical Analysis of A60CFNC

Specimens	Ultimate applied load(kN)	Mid-span deflection(mm)	Failure Mode
A60CFNC	**190.3**	**51.8**	**Flexural**

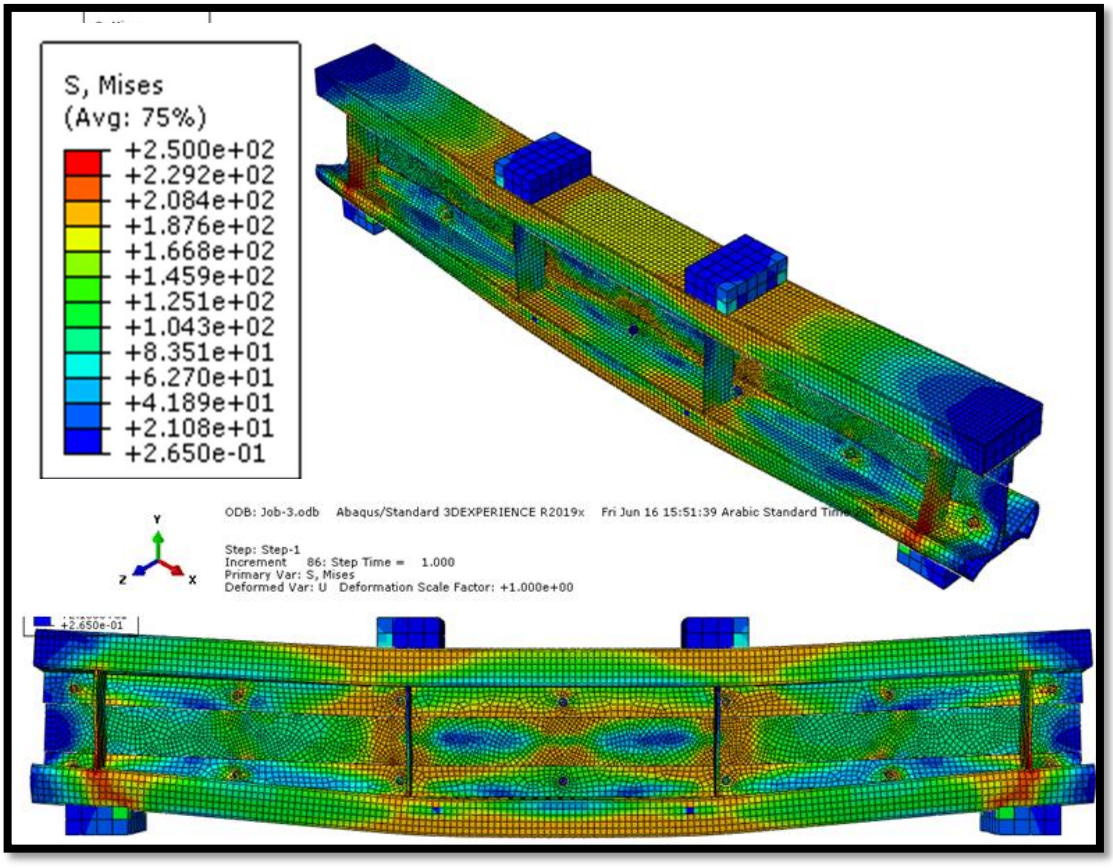

Plate(5-7): Stress Distribution at Ultimate Load for **A60CFNC**.

5.4.4 Effect of Using Different Depth of Hollow Flange

A6090 consisted of two flanges and web, the compression flange with a depth of 60mm and the tension flange with a depth of 90mm. When comparing A6090 with A60 and A90, the bearing capacity increased by 5.3% and decreased by 17.5%, respectively. The deflection decreased by 89.6% and 5.1%, respectively.

Table (5-9): The Result of Numerical Analysis of A6090

Specimens	Ultimate applied load(kN)	Mid-span deflection(mm)	Failure Mode
A6090	**168.9**	**13**	**Flexural**

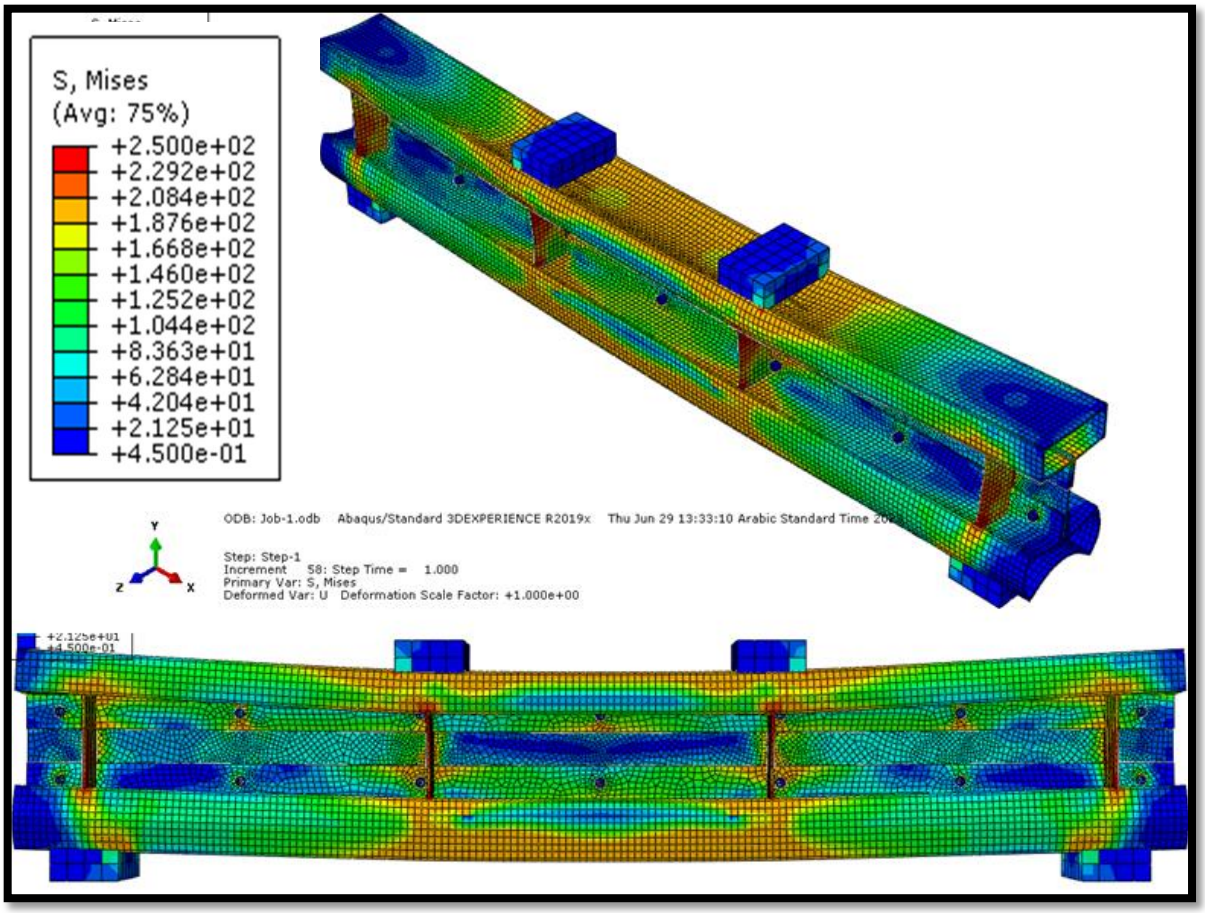

Plate (5-8): Stress Distribution at Ultimate Load for **A6090**.

5.4.5 Effect of Ultra-High Strength of Concrete

A60 strengthened the rectangular hollow flanges with ultra-high strength concrete, UHSC is a modified kind of reactive powder concrete with compressive strengths often exceeding 150MPa and improved resistance to failures occurring as a result of compression, tension, and bending. The properties of ultra-high strength concrete were taken from [51]**.** When comparing A60UT with A60NC, the bearing capacity increased by 28.6% and the deflection increased by 74.4%.

Table (5-10): The Result of Numerical Analysis of A60UH

Specimens	Ultimate applied load(kN)	Mid-span deflection(mm)	Failure Mode
A60UH	**278.6**	**18.1**	**Flexural**

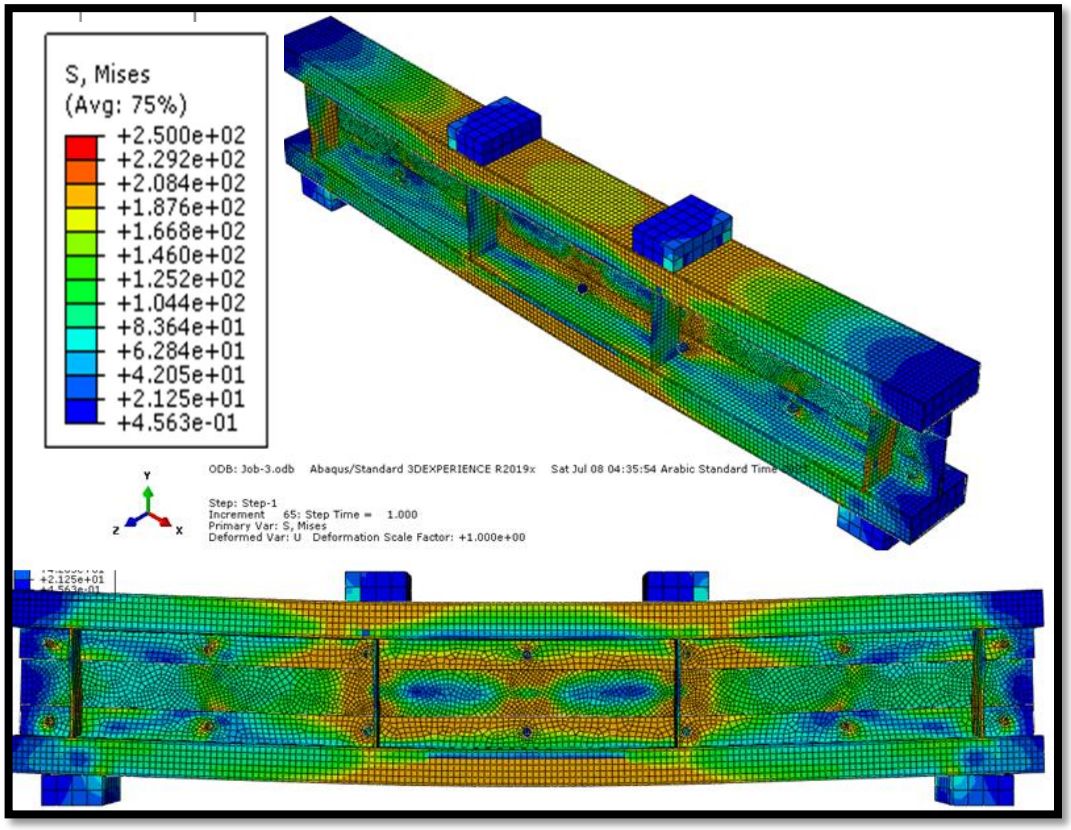

Plate (5-9): Stress Distribution at Ultimate Load for **A60UH**.

CHAPTER SIX

CONCLUSIONS AND RECOMMENDATIONS

CHAPTER SIX

CONCLUSIONS AND RECOMMENDATIONS

6.1 Introduction

Depending on obtained results from the experimental study and finite element simulation by the ABAQUS software for the rectangular hollow flange cold-formed steel beam models subjected to a four-point bending condition, the following conclusions and recommendations which can be mentioned .

6.2 Conclusions

1. For the first group, the beam with a hollow flange 30mm is the best in terms of load bearing capacity, as the higher beams were resistant and efficient. As for beams with 60mm, 90mm, and 120mm, it became evident that as the flange depth increased, the flexural behavior improved for these beams, enhancing their load-bearing capacity and reducing deflection. Therefore, when choosing a specific beam type, we prefer the beam with hollow flange 30mm due to its high load-bearing capacity compared to the other beams, however, these other beams have several advantages, including the ability to use their hollow flanges for electrical, cooling, communication, and other purposes.

2. Strengthening the hollow rectangular flanges with different strengthening materials improved the behavior of the sections, as all the strengthened sections increased the ultimate capacity by a rate ranging between (16% and 29%) and a decrease in deflection by a rate ranging between (65% and 86%) when compared with beam with flange depth 60mm.

3. The ultimate load of the tested strengthening specimens increased in direct proportion to the compressive strength of the strengthened materials, except

for the sections that were strengthened with concrete, whose components were replaced with sawdust and crushed glass.

4. After calculating the ductility of all beams, it was found that the beam with a flange depth of 60mm was the most ductile in group I. As for group II, the beams that were strengthened with normal concrete and those whose components were replaced with sawdust, fine and coarse rubber, and coarse shattered glass were the more ductile.

5. It was found that the greater the depth of the flange, the greater the stiffness of the section, and this was found in group I. As for group II, the percentage of stiffness increased for all beams with rates ranging between (294-821)% when compared with a beam with a flange depth of 60mm.

6. The use of stiffeners in load bearing areas and supports was ideal in order to prevent web buckling, as it prevented any deformation of the web.

7. Failure mode for all sections happened in steel and/or concrete section and no failure of bolts that connection between flanges and web.

8. No type of failure occurred in the welding that was used to connect the parts of the flange together, as well as that used to connect the stiffeners with the web, and this gives the ability to form different shapes that do not exist ready.

9. Replacing coarse or fine aggregates in concrete with crushed glass and iron fillings improved the properties of concrete, as the compressive strength increased by (5% and 15%), respectively, compared to normal concrete.

10. The results of the experimental tests showed that the bearing capabilities designed for the beams according to the 1996-1999 edition of AISI specifications are well expected in plastic stage but conservative in elastic stage.

11. Experimental and numerical results agree in terms of section load capabilities and associated failure modes where the difference in ultimate load range between (-1% - 16%) for group I and (-15% - -1 %) for group II,

this demonstrates the dependability of the ABAQUS 2017 finite element analysis program used in this experiment.

6.3 Recommendations

Some points are recommended for future works for hollow flange cold formed steel beams as follows :

1. Study sections with other hollow flange shapes, such as hexagonal or circular.

2. Study the effect of using shear connectors between steel beam and concrete, which will certainly improve the beams behavior.

3. Study sections larger or smaller. It is also recommended to use a different span length for future studies. As well as testing the depth-to-span length ratio and its effectiveness and impact on the design in order to establish a useful design method in the future for the hollow flange section beam.

4. Study sections of different thicknesses of the flange and web in the same section and verify the extent of this effect on the behavior of the section.

5. Study other sections with changing the type of flange connection to the web.

6. Study the effect of changing the distance between the bolts on the behavior of the sections, where it is recommended to study the same section in this research with different connecting distances and compare the results.

7. Extensive study on the properties of concrete that replaced some of its components with crushed glass and iron filings in order to confirm the behavior of concrete and the possibility of using these two materials as substitutes for coarse and fine aggregates in concrete, as this will reduce the cost because they are cheap materials.

8. A numerical study in order to find equations to represent the materials that were used as a substitute for fine and coarse aggregate in concrete.

REFERENCES

REFERENCES

1- Nadya, R.U.K.; and Usman, F.; "BOLTED CONNECTION OF COLD-FORMED STEEL SECTION - A REVIEW", ARPN Journal of Engineering and Applied Sciences, VOL. 13, NO. 17, SEPTEMBER, 2018.

2- Kumar, S. R. S. and Kumar, A.R.S., "Design of Steel Structures II", Department of Civil Engineering, Indian Institute of Technology, Madras, Chennai – 600036.

3- Somadasa, W.," Flexural Behaviour and Design of Cold formed Steel Beams with Rectangular Hollow Flanges", School of Urban Development, December, 2005.

4- Cold-formed steel-wikipedia. American Iron and steel INSTITUTE(AISI), INTERnet Guideline. https://en.wikipedia.org/wiki/coldformed-steel.

5- Mohammed, Z.M., "Effect of Top-Hat Shear Connector on the Strength of Cold-Formed Steel-Concrete Composite Beams", M.S. thesis, Univ. of Babylon, Babil, Iraq, 2021.

6- Alhadded ,W., and Halabi, Y., "Manufacturing, Applications, Analysis and Design of Cold-Formed Steel in Engineering Structures: A Review", Conference Paper august 2019. https://www.researchgate.net/publication/336715997

7- Kimcheng, K., "INVESTIGATION ON FLEXURAL BEHAVIOR OF COLD-FORMED STEEL C BACK-TO-BACK BEAMS", a thesis submitted in partial fulfillment of the requirements for the degree of master of science (engineering and technology), Sirindhorn International Institute ofTtechnology Thammasat University Academic year 2016.

8- Groover , M.P.," Fundamentals of Modern Manufacturing ,Materials ,Processes ,and Systems" ,4th edition, JOHN WILEY & SONS, INC.,2010.

9- Wei-Wen, Y., "Cold-Formed Steel Design". Curators' Professor Emeritus of Civil Engineering Director, Center for Cold-Formed Steel Structures University of Missouri-Rolla.

10- Abou-Rayan, A.M., Khalil, N.N. and Zaky, A.A., 2020. Experimental investigation on the flexural behavior of steel cold-formed I-beam with strengthened hollow tubular flanges. Thin-Walled Structures, 155, p.106971. https://doi.org/10.1016/j.tws.2020.106971.

11- Croccolo ,D., Agostinis, M. D., Fini , S., Khan, M. Y., Mele, M. and Olmi, G., " Optimization of Bolted Joints: A Literature Review", Department of Industrial Engineering, University of Bologna, 40136 Bologna, Italy, 2023, 13, 1708. https://doi.org/10.3390/met13101708.

12- Laim , L., Rodrigues, J.P.C., and Craveiro, H.D., "Flexural behaviour of beams made of cold-formed steel sigma-shaped sections at ambient and fire conditions", Thin-Walled Structures 87(2015) 53-65.

13- Awaludin, A., Rachmawati, K., M. Aryati, and Danastri, A.D., "Development of cold formed steel – timber composite for roof structures: compression members". Procedia Engineering 125 (2015) 850 – 856.

14- Wang, L., and Young, B., "Design of cold-formed steel built-up sections with web perforations subjected to bending". Thin-Walled Structures 120(2017) 458-469.

15- Jenitha , G., Gokul Nath , V. and Kumar ,N. G., "Analysis of Cold-Formed C-Beam and Built Up Beam". Indian Journal of Science and Technology, Vol 9(2), DOI: 10.17485/ijst/2016/v9i2/86350, January, 2016.

16- Roy, K., Lau , H.H., Ting, T.C.H., Chen, B., and Lim, J.B.P., "Flexural capacity of gapped built-up cold-formed steel channel sections including web stiffeners". Journal of Constructional Steel Research 172(2020) 106154.

17- Zhu, J.H., Mei-Ni, S., Zhu, X., Daniels, J., and Young, B., "Flexural behaviour of cold-formed steel oval hollow section beams". Journal of Constructional Steel Research 180(2021)106605.

18- Avery,P., Mahendran, M., and Nasir, A., "Flexural capacity of hollow flange beams". Journal of Constructional Steel Research 53 (2000) 201–223.

19- Trahair ,N., "Multiple design curves for beam lateral buckling procceding of the 5 th international colloquium on stability and ductility of steel structures ". Nagoya, Japan, 1997:33-44.

20- Dong , J., and Sause, R., " Flexural strength of tubular flange girders". Journal of Constructional Steel Research 65 (2009) 622–630.

21- Wimer, M.R., and Sause, R., "Rectangular tubular flange girders with corrugated and flat webs. 2004.

22- Kim, B.G., and Sause, R., "High performance steel girders with tubular flange ". 2005.

23- Hassanein, M.F., and Kharoob, O.F., " Flexural strength of hollow tubular flange plate girders with slender stiffened webs under mid-span concentrated loads". Thin-Walled Structures 69(2013) 18-28.

24- Keerthan , P., Hughes,D., and Mahendran, M., " Experimental studies of hollow flange channel beams subject to combined bending and shear actions". Thin-Walled Structures 77(2014) 129-140.

25- Siahaan, R., Mahendran , M., and Keerthan, P., " Section moment capacity tests of rivet fastened rectangular hollow flange channel beams". Journal of Constructional Steel Research 125(2016) 252-262.

26- Perera, N., and Mahendran, M., " Section moment capacity tests of hollow flange steel plate girders". Journal of Constructional Steel Research 148(2018) 97-111.

27- Adil, D. M., Narayanan, S., Dar,A.R., and Anbarasu, M., "Flexural strength of cold-formed steel built-up composite beams with rectangular compression flange". Steel and Composite Structures · January 2020. DOI: 10.12989/scs.2020.34.2.171.

28- Shanmugam , B., Palanisamy, M., Awoyera, P. O., Chinnasamy, S., and Subramaniam, M. " A Study on the Effect of Hollow Tubular Flange Sections on the Behavior of Cold-Formed Steel Built-Up Beams". Hindawi Advances in Civil Engineering Volume 2021, Article ID 4482887, 9 pages https://doi.org/10.1155/2021/4482887.

29- Gao, F., Zhu, H.P., Zhang, D.H., and Fang, T.S.. "Experimental investigation on flexural behavior of concrete-filled pentagonal flange beam under concentrated loading". Thin-Walled Structures 84(2014) 214-255.

30- Shao, Y., Wang , Y.," Experimental study on static behavior of I-girder with concrete-filled rectangular flange and corrugated web under concentrated load at mid-span". Engineering Structures 130(2017) 124-141.

31- Hassanein, M.F., Kharoob, O.F., and Taman, M.H., "Experimental investigation of cementitious material-filled square thinwalled steel beams". Thin-Walled Structure 114(2017) 134-143.

32- Wang, Y.M., Shao, Y.B., Chen, C., and Katwal, U., "Prediction of flexural and shear yielding strength of short span I-girders with concrete-filled tubular flanges and corrugated web - II: Numerical simulation and theoretical analysis". Thin-Walled Structures 148(2020)106593.

33- Gao,F., Yang, F., Liang, H., and Zhu, H., "Numerical study and strength model of concrete-filled high-strength tubular flange beam under mid-span load". Engineering Structures 221(2021) 111654.

34- Gao, F., Yang,F., Zhu, H. and H.Liang, " Lateral-torsional buckling behaviour of concrete-filled high-strength steel tubular flange beams under mid-span load". Journal of Constructional Steel Research, 176, 2021.

35- Sifan, M., Gatheeshgar, P., Navaratnam, S., Nagaratnam, B., Poologanathan, K., Thamboo, J. and Suntharalingam,T., "Flexural behaviour and design of hollow flange cold-formed steel beam filled with lightweight normal and lightweight high strength concrete". Journal of Building Engineering 48(2022) 103878.

36- ASTM A370-05, "Standard Test Method and definition for mechanical Testing of steel products," 2005 Annual Book of ASTM Standards, Vol.01.01, ATSM, Philadelphia,PA.,2005.

37- Iraqi specification No.5, "Portland cement", Baghdad, 1984.

38- Iraqi specification, No.45, "Aggregate from Natural Sources for concrete and construction". Baghdad, Iraq, 1984.

39- ACI Committee 211.1-95, "Standard practice for Selection proportions for Normal, Heavy weight and Mass concrete", ACI Manual of concrete practice", Part1-1995.

40- ASTM C39/C39M-05;"Standard Test Method for compressive Strength of cylindrical concrete specimens, "Annual Book of ASTM standard, American Society for testing and material, pp.1-7.

41- ASTM Designation C496-96. "Standard specification for splitting tensile strength of cylindrical concrete specimens", Annual Book of ASTM standard, American society for testing and Material, Philadelphia, Pennsylvania section, vol. 4.02, 1996, 1-4PP.

42- ASTM C78-02; "Standard Test Method for flexural strength of concrete (using simple Beam with Third-point loading). "Annual Book of ASTM Standards, American society for Testing and Materials.

43- Rafat, S., Malkit, S., Sourav, M., and Rafik , B., "Utilization of treated Sawdust in concrete as partial replacement of natural sand". Journal of Cleaner Production, 261(2020)121226.

44- Sangha, C.M., , Alani , A.M., and Walden, P.J., "Relative strength of green glass cullet concrete". Magazine of Concrete Research, 56(2004), 5, 293-297.

45- Ameer , M.H. , "Behavior of Reinforced Concrete Horizontally Curved Box Girders with Openings Under Monotonic and Repeated Loads". D.Sc. thesis, Univ. of Babylon, Babil, Iraq, 2021.

46- Muthuswamy, K.R., and Thirugnanam, G.S.,"Structural behavior of hybrid fibre reinforced concrete exterior Beam-Column joint subjected to cyclic loading". International Journal of Civil & Structural Engineering,4(3), 262-273,2014.

47- Ye, J., Hajirasouliha, I., Becque, J., and Pilakoutas,K., "Development of more efficient Cold-Formed Steel Channel Sections in bending". Thin – Walled Structures,(101), 2016, 1-13.

48- Ayoob, A.I., Najla'a, H.A., Muna, H.J., Rafea, F.H., Husam, H.H., and Nabeal, H.A., "Experimental investigation of flexural and shear behaviors of reinforced concrete beam containing fine plastic waste aggregates". Structures, 2022, 1-13.

49- Wu, Y., " Shear strengthening of single web prestressed hollow core slabs using externally bonded FRP sheets". University of Windsor, Electronic Theses and Dissertations, 2015, 5310.

50- Mansur, M.A., "Design of reinforced concrete beams with web openings". Proceedings of the 6th Asia-pacific Structural Engineering and Construction Conference(ASPEC 2006), 5-6.

51- Prabhat, R.P., Bharatkumar, B.H., & Nagesh, R.L., "Mechanical properties of ultra high performance concrete". World academy of Science, Engineering and Technology, International Journal of Civil and Environmental Engineering, 6(2012), 8.

52- https://en.wikipedia.org/wiki/.Sawdust.

53- Horisawa , S., Sunagawa , M., Tamai, Y., Matsuoka, Y., Miura , T. and Terazawa, M., " Biodegradation of nonlignocellulosic substances I1: physical and chemical properties of sawdust before and after use as artificial soil", The Japan Wood Research Society 1999.

54- Schaefer, R. J., " CHAPTER 33: MECHANICAL PROPERTIES OF RUBBER" harris-shock-and vibration-handbook-fifth-edition. https://www.globalspec.com/reference/64445/203279 .

55- Normanyo , E. and Adetunde , A., " Redesign of a Grinding Mill for the Minimisation of Iron Filings Production". European Journal of Scientific Research, ISSN 1450-216X Vol.36 No.3 (2009), pp 418-436.

56- Shelby , J. E., " Introduction to Glass Science and Technology Second Edition". New York State College of Ceramics at Alfred University School of Engineering, Alfred, NY, USA, 2005.

57- Rahman , R. A., Esa , M. and Almutairi, S.. " Main Challenges to Concrete Recycling in Practice". Sustainability, MDPI, Basel, Switzerland, 13, 11077, 2021. https://doi.org/10.3390/su131911077.

58- https://leca.asia/ar/properties/.

59- ABAQUS, C.2017 "Analysis User", Manual version.

60- Chaudhari, S.R., and Chakabarti, M.A.(2012). Modeling of concrete for nonlinear analysis using finite element code ABAQUS. International Journal of computer Applications, 44(7),14-1.

61- Daud, R.A. (2015). "Behavior of reinforced concrete slabs strengthened externally with two-way FRP sheet subjected to cyclic loads". The university of Man-chester United Kingdom.

62- Rusinowski, P. 2005. "Two-way concrete slabs with openings: experiments, finite element analysis and design".

63- Hillerborg, A., Modeer, M., and Petersson, P.E.(1976). "Analysis of crack formation and crack growth in concrete" research, (696), 773-781.

64- Lubliner, J., Oliver, J., Oller, S., and Oňate, E. (1989). "Aplastic-damage model for concrete". International Journal of solids and structures, 25(3),299-326.

65- Lee,J., and Fenves, G.L.(1998). "Plastic-damage model for cyclic loading of concrete structures". Journal of engineering mechanics, 124(8), 892-900.

66- Lundqvist, J. (2017). "Numerical analysis of concrete elements strengthened with carbon fiber reinforced polymers". (Doctoral dissertation, Luleå tekniska universtitet).

DESIGN OF TESTED BEAM SPECIMEN

Design procedure of the rectangular hollow flange cold-formed steel I-beam specimen is produced in the present appendix. some results were presented herein. The design is conducted according to the theories and the limitations of composite section of AISC.

1. Design Moment and Ultimate Load for all Specimens.

A- Elastic stage:

- $My = S \times Fy$ …… (1)
- $Py = \frac{3My}{L}$ …… (2)
- $\emptyset = 0.95$ …… (3)
- $S = \frac{I}{\acute{y}}$ …… (4)

Table(A-1): Moment of Inertia and Modulus of elastic for All Specimens.

Specimens	ý (mm)	I (mm^4)	$S_{(mm^3)}$
A30	**150**	**63213637.34**	**421420.25**
A60	**150**	**54175186.8**	**361167.91**
A90	**150**	**46788440**	**313034.05**
A120	**150**	**44130760.1**	**294205.1**

Table(A-2): Design Moment and Ultimate Load for All Specimens.

Specimens	My (KN.m)	Py (KN)	$Ø\ Py$ (KN)
A30	112.1	224.2	213
A60	96.1	192.14	182.533
A90	83.3	166.53	158.21
A120	78.3	156.52	149

B- Plastic stage:

- $Z = \frac{At}{2} \times a$ ……(5)
- $Mp = Z \times Fy$ ……(6)
- $Pu = \frac{3Mp}{L}$ ……(7)

Table(A-3): Design Moment and Ultimate Load for All Specimens.

Specimens	At (mm^2)	a (mm)	Z (mm^3)	Mp (KN.m)	Pu (KN)	$Ø\ Pu$ (KN)
A30	4552	224.16	510180	135.71	271.4	257.83
A60	4760	200.02	476047.6	126.63	253.26	240.6
A90	5000	173.96	434756	115.7	231.3	219.74
A120	4920	158.32	389476	103.6	207.2	196.84

Where:-

- My = Yield moment of steel beam(KN.m).
- S = Elastic section modulus(mm^3).
- Fy = Yield stress of steel plate (MPa).

- $\boldsymbol{Py}$= Yield load of beam(KN).
- $\boldsymbol{L}$ = Clear span of beam between the supports(m).
- $\boldsymbol{I}$ = Moment of Inertia of beam bout neutral axis(mm^4).
- Ý = The distance from the center of compression area to the top edge (mm).
- $\boldsymbol{Z}$ = Plastic section modulus(mm^3).
- $\boldsymbol{At}$ = Total area of beam(mm^2).
- $\boldsymbol{a}$ = The distance between the compression and tension areas of beam in plastic stage(mm).
- $\boldsymbol{Mp}$ = Plastic moment(KN.m).
- $\boldsymbol{Pu}$ = Ultimate load (KN).
- $\emptyset$ = Resistance factor for reducing the flexural strength or bending moment.

2. Ultimate Shear.

- **If a/h > 1**

Then :

$$\boldsymbol{Kv = 5.34 + \frac{4}{\left(\frac{a}{h}\right)2}} \qquad \ldots\ldots(8)$$

- **If h/t ≤ 0.96$\sqrt[2]{\boldsymbol{EKv/Fy}}$**

Then:

$$\boldsymbol{Vn = 0.6\ Fy\ \times h \times t} \qquad \ldots\ldots(9)$$

Table(A-4): Design Ultimate Shear for All Specimens.

Specimens	a/h	h/t	Kv	$Vn(KN)$
A30	**2.06**	**60**	**6.265**	**153.216**
A60	**2.78**	**45**	**5.86**	**114.912**
A90	**4.2**	**30**	**5.6**	**76.61**
A120	**8.3**	**15**	**5.4**	**38.31**

Where:-

- a = The clear distance between transverse stiffeners(mm).
- **h** = Depth of the flat portion of the web measured along the plane of the web(mm).
- Kv = shear buckling coefficient.
- t = Thickness of steel plate(mm).
- E = Modulus of elasticity(MPa).
- Vn = nominal shear strength of beam(KN).

3. Checking of Stiffeners.

All intermediate stiffeners should be designed to satisfy the following requirements for spacing, moment of inertia, and gross area:

3.1 Spacing a between stiffeners:

- $\mathbf{a} \leq (\frac{260}{\frac{h}{t}})^2 h$
- $\mathbf{a} \leq 3h$

Table(A-5): Checking stiffeners spacing.

Specimens	a(mm)	$(\frac{260}{\frac{h}{t}})^2$ h(mm)	$3h$(mm)
A30	**500**	**4506.7**	**720**
A60	**500**	**6008.9**	**540**
A90	**500**	**9013.33**	**360**
A120	**500**	**18026.7**	**180**

3.2 Moment of inertia I_s:

$$Is \geq 5ht^3\left(\frac{h}{a}-\frac{0.7a}{h}\right)$$

$$Is \geq \left(\frac{h}{50}\right)^4$$

Table(A-6): Checking of Moment of inertia I_s.

Specimens	I_s (mm^4)	$5ht^3\left(\frac{h}{a}-\frac{0.7a}{h}\right)$ (mm^4)	$(\frac{h}{50})^4$ (mm^4)
A30	**79488000**	**75136**	**530.8**
A60	**33534000**	**91264**	**168**
A90	**9936000**	**102784**	**33.2**
A120	**1242000**	**109696**	**2.1**

Where:-

- I_s = Moment of inertia of stiffeners(mm^4).

3.3 Gross area As of intermediate stiffeners:

$$As \geq \frac{1-Cv}{2}\left[\frac{a}{h}-\frac{(a/h)^2}{(a/h)+\sqrt{1+(a/h)^2}}\right]YDht$$

$$C_v = \begin{cases} \dfrac{1.53Ek_v}{F_y(h/t)^2}, \\ \dfrac{1.11}{h/t}\sqrt{\dfrac{Ek_v}{F_y}}, \end{cases}$$

Table(A-7): Checking of Gross area As.

Specimens	As (mm^2)	C_v	$\frac{1-Cv}{2}\left[-\frac{(a/h)^2}{(a/h)+\sqrt{1+(a/h)^2}}\right]YDht$
A30	16560	1.3	381.4
A60	12420	1.64	797
A90	8280	2.4	1743
A120	4140	5.4	4450

Where:-

- A_S = Cross-sectional area of transverse stiffeners(mm^2).
- C_v = Factor calculated as above.
- Y = Yield point of web steel/yield point of stiffener steel.
- D = 2.4 for single-plate stiffeners.

PROPERTIES OF MATERIAL

1.Cement

Table (B-1): Chemical analysis for cement.

Compound composition	Chemical composition	Percentage by weight	Limits (IQS NO.5/1984)
Lime	CaO	63.66	----
Silica	SiO2	21.86	----
Alumina	Al2O3	3.96	----
Iron oxide	Fe2O3	4.72	----
Magnesia	MgO	2.24	<5.00
Sulfate	SO_3	2.21	<2.50
Loss on ignition	L.O.I	1.20	<4.00
Insoluble residue	I.R	1.46	<1.5
Lime saturation factor	L.S.F	0.89	0.66-1.02
Main compounds (Bogue's equs.)		Percent by weight of cement	
Tricalcium silicate (C_3S)		51.00	
Dicalcium silicate (C_2S)		23.28	
Tricalcium aluminate (C_3A)		2.51	
Tetracalcium aluminoferrite (C_4AF)		14.36	

Table (B-2): Physical properties for cement.

Physical properties	Test results	Iraqi specifications limits (I.O.S.5/1984)
Setting time (Vicat s method)		
Initial setting, hr: min		≥00:45
Final setting, hr: min	4:24 5:32	≤10:00
Fineness (Blaine Method), m^2/Kg	314	≥250
Compressive strength, MPa		
3days	25.7	≥15:00
7days	29.68	≥23:00
Soundness (Autoclave) method %	0.15	≤0.8

2. Coarse Aggregate

Table (B-3): Grading of coarse aggregate.

Sieve size	Passing %	
	Coarse aggregate	Limits of Iraqi Specification No. 45/1984
14mm	100	100

Table (B-4): Physical properties of coarse aggregate.

Physical Properties	Test Results	Limits of Iraqi specification No.45/1984 for Zone (2)
Specific gravity	2.66	_
Sulfate content SO_3	0.6%	_
Absorption	0.043%	0.1%

3. Fine Aggregate

Table(B-5): Grading of fine aggregate.

Sieve size	Passing (%)	
	Fine aggregate	Limits of Iraqi specification No. 45/1984 for Zone
10 mm	100	100
4.75 mm	92	90-100
2.36 mm	81	75- 100
1.18 mm	73	55-90
600 mm	55	35 - 59
300mm	24	8 - 30
150 mm	7	0-10

Table (B-6): Physical properties of fine aggregate.

Physical properties	Test results	Limits of Iraqi specification No.45/1984 for zone (2)
Specific gravity	2.67	_
Sulfate content SO_3	0.09%	≤ 0.5
Absorption	0.76%	_

3. Sawdust

A by-product or waste product of woodworking processes such sawing, sanding, milling, planning, and routing is sawdust (also known as wood dust). Little wood chips make up its material. These tasks can be carried out with hand tools, portable power equipment, or woodworking machinery. Moreover, several creatures, birds, and insects that inhabit wood, including the woodpecker and carpenter ant, produce wood dust as a byproduct. It can

be a serious fire risk and a source of occupational dust exposure in several manufacturing businesses[52].

Plate(B-1): Sawdust.

Table(B-7): Physical and Chemical properties of Sawdust[53]

Chemical properties	Value	Physical properties	Value
Extractives	3.3	Moisture content	10.8
Lignin	29.3	Apparent specific gravity	0.14
Hollocellulose	83.8	Porosity (%)	84
Carbon (C) (%)	61.58	Water retention (%)	50
Hydrogen (H) (%)	5.32	Water drainage (mls-1)	282.0
Oxygen (O) (%)	33.04		
Nitrogen (N)	0		

4. Rubber

Rubber is a unique material that is both elastic and viscous. Rubber parts can therefore function as shock and vibration isolators and/or as dampers. Although the term *rubber* is used rather loosely, it usually refers to the compounded and vulcanized material. In the raw state it is referred to as an *elastomer*. Vulcanization forms chemical bonds between adjacent elastomer chains and subsequently imparts dimensional stability, strength, and resilience. An un vulcanized rubber lacks structural integrity and will “flow” over a period of time. Rubber has a low modulus of elasticity and is capable

of sustaining a deformation of as much as 1000 percent. After such deformation, it quickly and forcibly retracts to its original dimensions. It is resilient and yet exhibits internal damping. Rubber can be processed into a variety of shapes and can be adhered to metal inserts or mounting plates. It can be compounded to have widely varying properties. The load deflection curve can be altered by changing its shape. Rubber will not corrode and normally requires no lubrication.

Plate(B-2): Rubber.

Rubber finds a wide field of application because of the following properties:

1. It is elastic; because of this property a rubber band can be stretched to 9 or 10 times its original length and when the load is removed it regains its original length.
2. It is strong and tough. Because of this property it can be put to use even under abnormal conditions.
3. It is highly impermeable to both water and air and therefore, it can be used to retain water as in rubber bottles, hoses etc.
4. It exhibits a great resistance to abrasion, tearing and cutting over a wide range of temperature—7 to 115°C.
5. It is a bad conductor of heat.
6. It can contain liquids and gases.

7. The synthetic rubber offers great resistance to acids, petroleum products etc.
8. Its properties such as hardness, strength, abrasion, resistance etc., can be modified to the desired extent by compounding techniques.
9. When two fresh surfaces of milled rubber are pressed together, they coalesce to form a single piece. This property (known as tackiness) of rubber makes the manufacturing of composite articles such as a tire, from a separate piece very simple.
10. The plasticity of rubber makes it pliable and amenable to all manufacturing processes.
11. By vulcanizing the rubber, its mechanical properties can be considerably improved.
12. Rubber insulation and other rubber products require shaping prior to vulcanisation because the vulcanised rubber cannot be shaped by mechanical pressing once it has acquired its characteristic plasticity. By vulcanizing rubber in molds, products of rather intricate shape can be obtained.
13. The electrical insulating properties of pure rubber are inferior to those of vulcanized rubbers
14. Ordinary electrical insulating rubbers, have the following electrical characteristics under normal conditions :

- Volume resistivity- 1 x 10^{14} to 1 x 10^{15} ohm cm.
- Loss tangent- 0.01 to 0.03 at 50 Hz.
- Dielectric Constant: 2.5 to 5.[54]

5. Iron Filings

Iron filings are fine granules of iron that take a powder-like shape between them. Iron filings are considered by-products, that is, they are industrial waste from the process of filing, drilling, or scraping iron

pieces, or as a result of polishing finished products. The size of the particles or granules present in the iron powder does not exceed 0.3 mm in length and the smallest of them may reach a mundane length of a few micrometers. Due to the increased surface area of the iron exposed to the reaction in the form of a powder, the iron can easily burn in this form when exposed to fire.[55]

6. Glass

Glass is an inorganic solid, usually transparent or translucent, hard, brittle, and impermeable to natural materials. Although it has been used since ancient times, it is still very important in various uses, such as buildings, tools, household utensils, and wire communications equipment. The types of glass vary widely according to their components and physical properties. As for the most common type of glass throughout the ages, especially in our time, it is that used in the manufacture of windows and drinking utensils, which is soda-lime glass, which consists of 75% of silica, sodium oxide and calcium oxide; With or without other additives. [56].

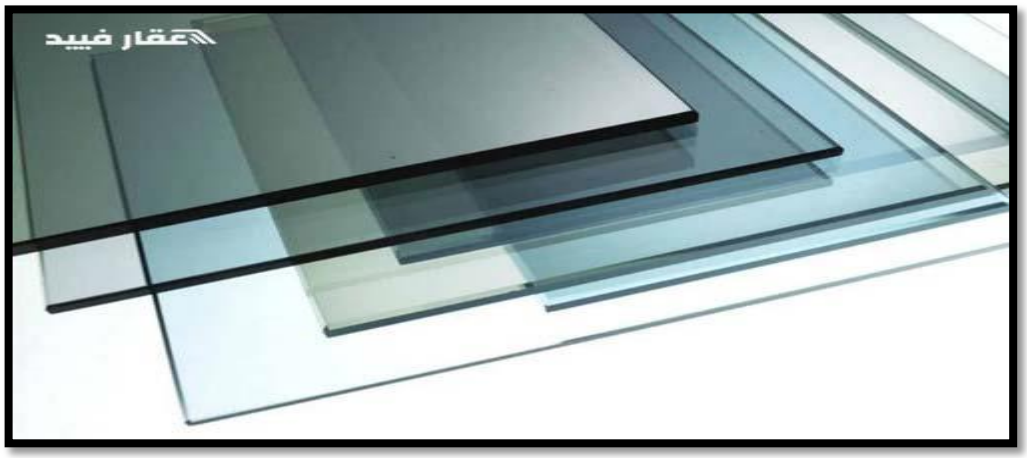

Plate(B-3): Glass,[56].

7. Recycled concrete

When demolishing or restoring structures made of concrete, recycling concrete is becoming an increasingly popular way to make use of the rubble. Recycling brings a number of benefits that make it a more attractive option in today's age of greater environmental awareness, environmental laws, and the desire to reduce construction costs.

Concrete blocks are collected from demolition sites by crusher machine. Breaking facilities only accept uncontaminated concrete, which must be free of waste, wood, paper and other such materials. Metals such as rebar are acceptable, as they can be removed using magnets and other sorting devices and then melted down for recycling elsewhere. The remaining rubble blocks are sorted by size. Large blocks may pass through the crusher again. After the fraction is made, other fine particles are filtered out by a variety of methods, including hand picking and water flotation.

On-site crushing using mobile crushers reduces construction costs and pollution when compared to transporting materials to and from a quarry. Large, mobile road machinery can crush asphalt and concrete debris at a rate of 600 tons per hour or more. These systems typically consist of an aggregate crusher, a side discharge conveyor, a screener, and a return conveyor from the sorter to the inlet of the crusher for oversize material reprocessing. Compact standalone compactors are also available that can handle up to 150 tons per hour and fit into tighter areas. The trend towards on-site recycling with smaller amounts of material is increasing with the advent of crusher attachments - those attached to various construction equipment, such as excavators. These attachments cover quantities of 100 tons per hour and less. Small blocks of concrete are used as gravel in modern construction projects. A base layer of gravel is placed as a bottom layer in the road, and a layer of concrete or pure asphalt is poured over it. The United States Federal Highway Administration may use such means to construct

new highways from old highway materials. Recycled crushed concrete can also be used as a dry aggregate for new concrete if it is free of contaminants. Concrete pavements can also be broken into place and used as a base layer for an asphalt pavement by the ramming process.

Larger blocks of crushed concrete can be used in rock paving layers, and are "a very effective and popular method of controlling erosion of raceways".

With good quality control at break facilities, well graded and aesthetically pleasing materials can be provided as an alternative to landscaping stone or mulch. Cages can be filled with crushed concrete and piled together to provide economical retaining walls. Stacks are also used to build filter walls **(**instead of fencing).[57]**.**

8. Lica (coarse aggregate)

Lica has superior properties due to its properties such as low thermal conductivity (temperature is less high at the unheated surface), low coefficient of expansion and greater stability of the granules that have been subjected to high heat during forming. Through the pyro process, the clay expands and expands like popcorn, and the lica becomes a material with porous circular granules. The cellular structure of the lica granules improves the density and the resistance ratio of this material, so the lica granules can play an important role as a raw material for the production of lightweight cement materials (concrete). A great solution for leveling everything related to heavy loads related to concrete materials in projects, in addition to its additional benefits and the improvements it can add. It has several properties and benefits such amazing light weight, Soundproof, Environmentally friendly and natural, Good thermal insulation, fire resistance and excellent stress (fracture) strength. [58].

ABAQUS SOFTWARE WITH MATERIALS MODELS AVAILABLE IN THE PROGRAM.

C.1 Introduction.

This appendix describes the constitutive relationships for the materials comprising the beams subjected to two concentrated . The constitutive model of the nonlinear behavior should be in such a form that it could be easily incorporated into a numerical analysis procedure to simulate the structural behavior. The materials used in this research are concrete and steel. The built-in material models available in ABAQUS were used in this study. These models efficiently represent the main parameters governing the response of structural concrete. Reinforcing concrete is a composite material containing a mix of several different materials, including sand, aggregate cement and steel bars. This mix of materials means concrete does not have well-defined constitutive properties like steel. The finite element model has to apply these nonlinear properties to produce results that will match the true behavior of reinforcement.

C.2 ABAQUS Software.

ABAQUS is a world-leading Finite Element Analysis (FEA) software that can do complex finite element analyses. Many major corporations in various engineering disciplines commonly use it. ABAQUS software can provide a powerful and complete solution for linear and nonlinear problems and other explicit engineering problems. The Rectangular Hollow Flange Cold-Formed Steel I-Beam can be defined accurately by its powerful graphic interface tool. ABAQUS package contains different analysis modules designed for different applications such as; ABAQUS/CAR, which is used to create

(including input all model data such as assigning material properties, loads, boundary condition, etc.) and run analysis to view the result. ABAQUS/Standard is used for nonlinear solid mechanics to provide accurate stress solutions in low-speed dynamics and static analysis. ABAQUS/ Explicit for transient dynamic problems. Finally, ABAQUS/CFD is the other main product used for fluid mechanics. However, the user must be careful when interpreting the output. In finite element software, it is easier to interpret the result than prove their validity. Consequently, it has to be used with carefulness. **[ABAQUS manual. (2017)][58].**

C.3 Description of Available Elements in ABAQUS.

An element library in ABAQUS is available to provide a powerful tool for different applications to solve various engineering problems. Every type of these elements is divided into various categories according to five characteristics, including; its degree of freedom, its formulation, its number of nodes, its integration points and finally, its family. Each element is given a name that distinguishes each of these five characteristics. Figure (C-1) shows the element families available in the **ABAQUS** library that is most commonly used. Geometry type is the main difference between their element families. Translational degrees of freedom is most important in stress/displacement simulation, and it is the fundamental variable calculated in the analysis.

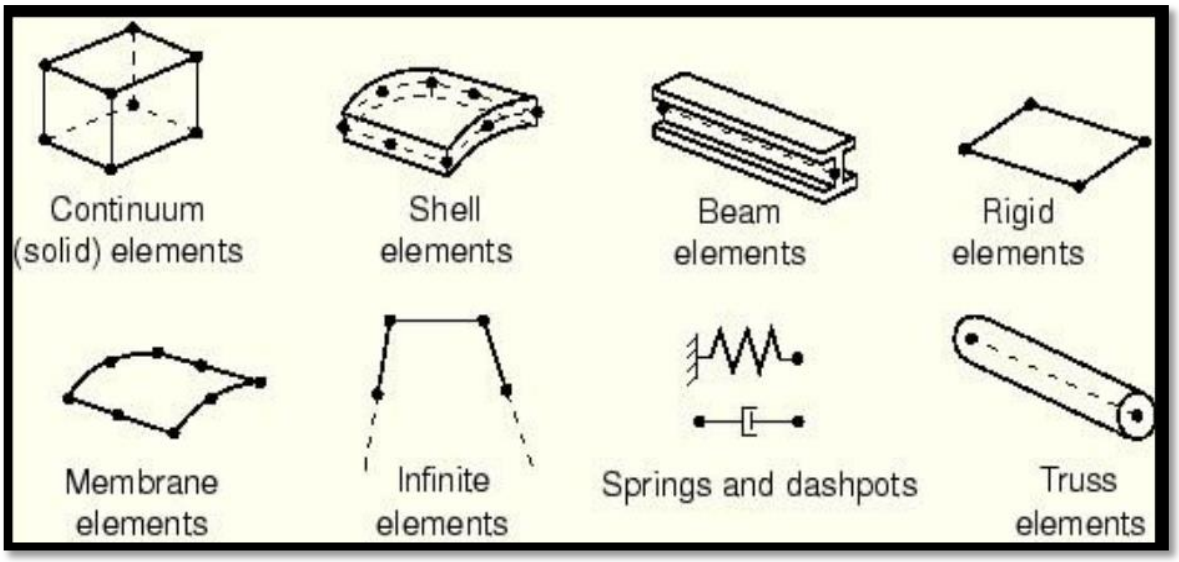

Figure (C-1): Element families available in the ABAQUS library that is commonly used [58].

Any degree of freedom, such as displacement, will be calculated at the nodes. By interpolating from the nodal displacements, displacement can be obtained at any other point in the elements. Usually, the order of interpolation determines it depends on the number of nodes in the used element. A wide variety of elements are available in ABAQUS that can be used, and it is important to select the proper element which is suitable for the problem. Because the steel does not provide a very high bending stiffness, truss elements are used and modeled as an embedded element. Their contact with the concrete is assumed to be perfectly bonded. The can be modeled by modifying the behavior of concrete. This, however, is not studied in the present work. An 8-node linear brick (C3D8R) element is used for modeling steel sections and concrete parts. The element tends to be not stiff enough in bending and stresses; strains are most accurate in the integration points. The integration point of the C3D8R element is located in the middle of the element. Therefore, small elements are required to capture a stress concentration at the boundary of a structure. On the other hand, a linear 3D two-node truss element with three degrees of freedom at each node (T3D2)

is used for the embedded reinforcement bars. Figure (C-2) shows the 8-node brick element with the integration point.

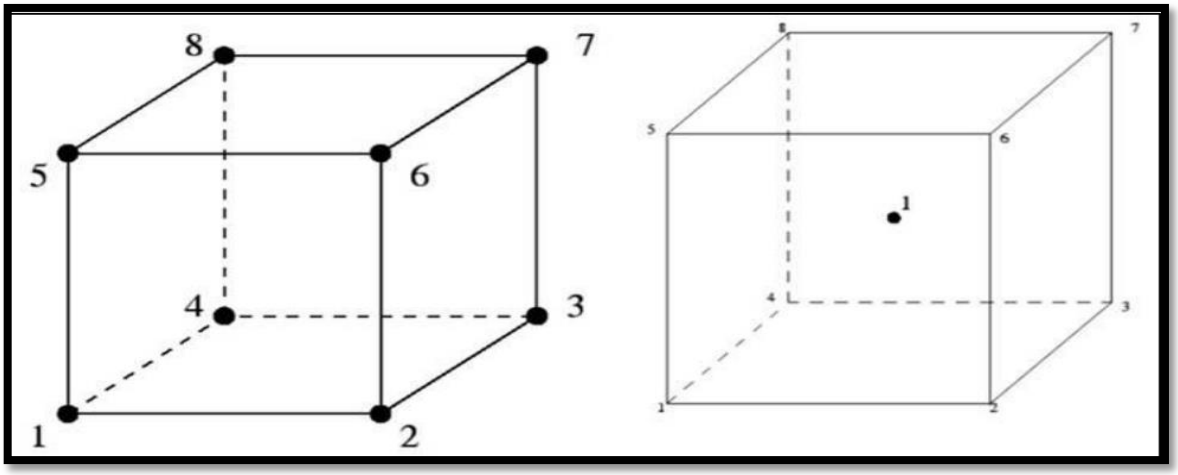

Figure (C-2): 8-node brick element with the integration point.

In practice, two lines of nodes must be created from two different materials Figure (C-3). These lines must be as close as possible, which makes contact between the closer front nodes. This precaution ensures good convergence of the iterative process. The friction coefficient between components was assumed to be 0.4. This value was obtained after several trials to find the number that reduces the difference as minimum as possible between the experimental and numerical results under monotonous loading.

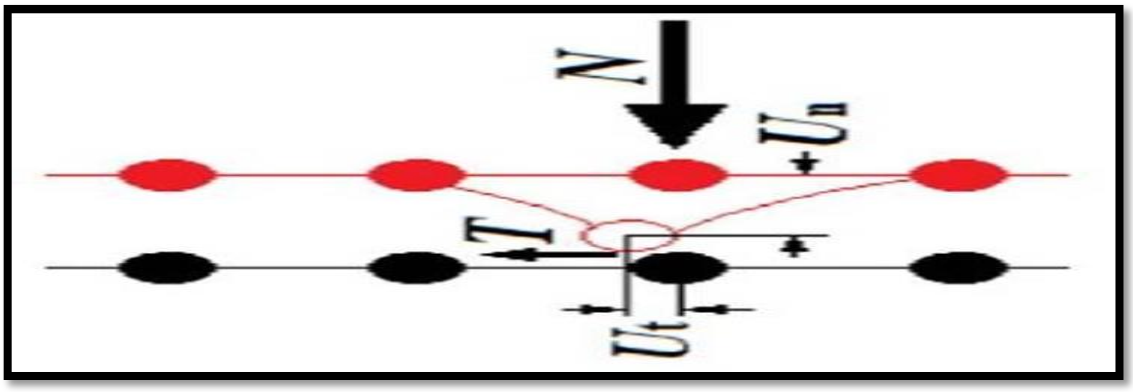

Figure (C-3): Contact variables.

For instance, the 8-node brick element, which has one node only at the corners, as shown in Figure (C-4) called a linear element because these elements use linear interpolation for interpreting the result. It is also called

the first-order element. 20-node brick element, which has nodes on the mid-side of each edge beside the corner nodes, use quadratics interpolation and is called a quadratic element or second-order element.

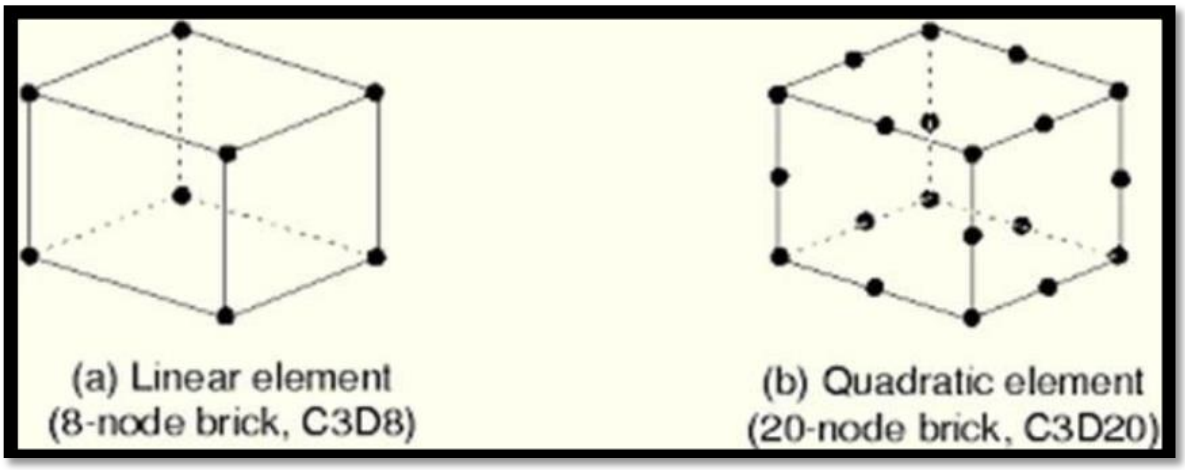

Figure (C-4): Linear and quadratic brick elements[58].

Element formulation provided by ABAQUS refers to the mathematical theory used to define the behavior of elements, such as Lagrangian formulation, which is the most common formulation used in stress/displacement analysis in ABAQUS. Another standard formulation is Eulerian, which is mainly used for fluid simulation.

ABAQUS has another alternative formulation in addition to the standard formulation, such as a hybrid formulation, mainly used for incompressible material or inextensible behavior. There are several numerical techniques in ABAQUS to integrate different quantities over the volume of the element. Gaussian quadrature is used to evaluate the material response for the most element at each integration point in the element. First-order (linear) elements will be used in this work despite the fact that they provide less accuracy than second-order elements because they require less computational time, and they appear to be steadier when used with concrete damage plasticity. For instance, the 20-node brick element with a reduced integration scheme has eight integration points only (2x2x2), but when the user 20-node brick element with full integration (3x3x3) has 27 integration points. Therefore,

element assembly takes 3.5 additional time for fully integrated elements. For most continuum elements, reduced or full integration points can be used. Reduce integration will be used in this research as a choice to lower the order of integration in order to form the stiffness matrix of element property. First-order elements with a reduced integration scheme have been chosen to reduce the running time, **[58].**

C.4 Material Model for Steel.

Compare d to concrete, steel is a much simpler material to represent. Its strain-stress behavior can be assumed identical in Tension and in compression. A typical uniaxial stress-strain curve for a steel specimen loaded monotonically in Tension is shown in Figure (C-5).

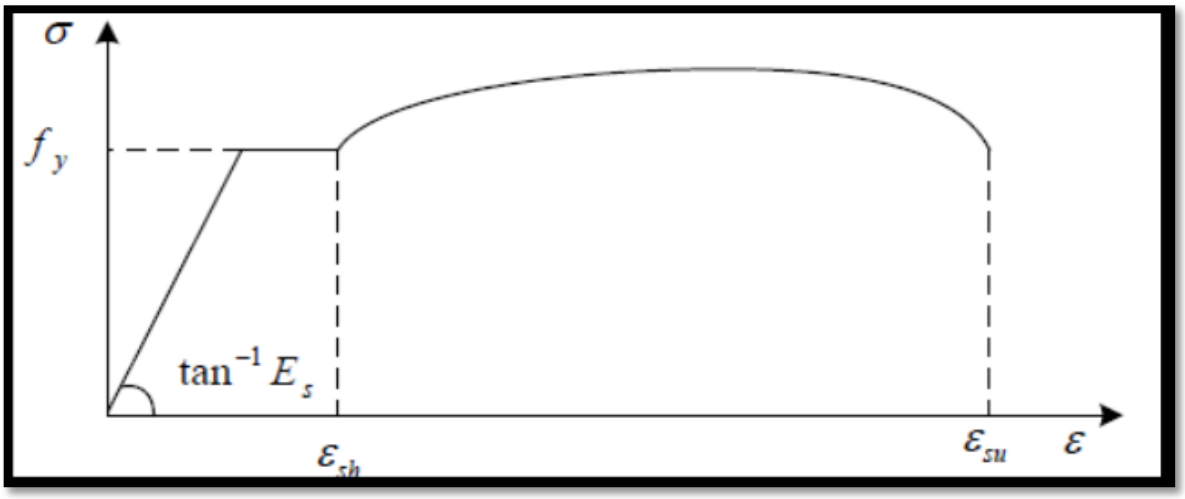

Figure (C-5): Typical stress-strain curve for steel.

Figure (C.6) exhibits an initial linear elastic portion, $\sigma_S = E_S \varepsilon_S$, a yield plateau at, $\sigma_S = f_y$ Beyond which the strain increases with little or no change in stress and a strain-hardening range until rupture occurs at the tensile strength, $\sigma_S = f_{su}$.Various steel grades are usually defined in terms of yield strength f_y. The extension of the yield plateau depends on the steel grade; its length generally decreases with increasing strength. In the present work, since the behavior of the cold-formed steel is not studied after the

yielding of the plate, a perfect plastic idealization of the stress-strain response of steel is sufficient for this study Figure (C-6). Therefore, only young's modulus **ES** , whose nominal value is taken as 200000MPa, and the yielding stress, whose nominal value is equal to 266.7MPa,need to be inputted into ABAQUS.

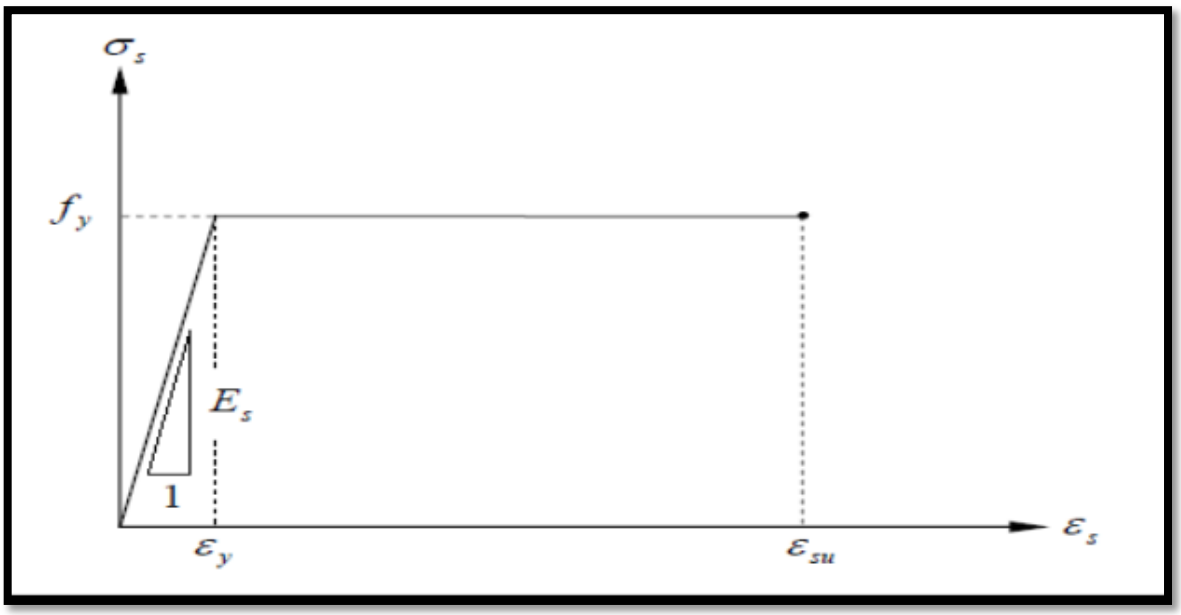

Figure (C-6): Perfect-plastic idealization of steel .

C.5 Material Model for Concrete.

ABAQUS software provides the capability of simulating the damage using either of the three crack models for concrete elements: (1)Smeared crack concrete model, (2) Brittle crack concrete model, and (3) Concrete damaged plasticity model. The smeared crack concrete model presents a general ability for modeling concrete in different structures, including beams, trusses, shells and solids. Individual macro cracks are not tracked during the analysis in this model. Constitutive calculations are attributed to an integration point translated into a deterioration of the current stiffness and strength at that integration point. Three cracks only can occur at any integration point (one in a uniaxial stress case, two in a plane stress case). The crack affects the constitutive calculations because of the oriented

damaged elasticity concepts. These concepts are carried out to describe the reversible part of the response of the material after failure cracking [59] However, it is difficult to make the model suitable in 3D applications because of the convergence problems, which may be caused by the nonexistence of cyclic/unloading response or the damage inthe elastic stiffness resulting from plastic straining [60].

Moreover, the damaged plasticity model is essentially used in structures subjected to dynamic or cyclic loading because of the capability to anticipate the behavior of the test up to failure [61] For a reason mentioned above, the damage plasticity model has been used to analyze the mechanical device segments. Out of the three concrete crack models, the concrete damaged plasticity model is selected in the present study .This technique can represent complete inelastic concrete behaviors in Tension and compression, including damage characteristics. Further, this is the only model which can be used both in **ABAQUS/Standard** and **ABAQUS/Explicit** and thus enable the transfer of results between the two. Therefore, developing a proper damage simulation model using the concrete damaged plasticity model will be useful for analyzing reinforced concrete structures under any loading combinations, including both static and dynamic loading **[58]**.

The concrete damaged plasticity model assumes that the two main failure mechanisms in concrete are tensile cracking and compressive crushing. In this model, the uniaxial tensile and compressive behavior are characterized by damaged plasticity. The model considers the degradation of the elastic stiffness induced by plastic straining in both Tension and compression. Two variables control the evolution of the failure surface($\boldsymbol{\varepsilon_t^{pl}}$ and $\boldsymbol{\varepsilon_c^{pl}}$), which are referred to as tensile and compressive equivalent plastic strains, respectively. In this study, the Poisson coefficient (ν) of 0.15 was used for concrete, and

the concrete density of 24 KN/m3was used in the computation of the dead load.

C.5.1 Tension Behavior.

The tensile behavior of concrete is a key factor in service ability considerations such as the assessment of crack spacing and crack width, concrete and reinforcement stresses and deformations. The stress-strain response of a concrete member in uniaxial Tension, Figure (C-7), is initially almost linear elastic. Near the peak load, the response softens due to micro-cracking, and a crack forms as the tensile strength is reached. However, the tensile stress does not instantly drop to zero; instead, the carrying capacity decreases with increasing deformation, i.e., a strain softening or quasi-brittle behavior can be observed. Under uniaxial Tension, the stress-strain response follows a linear elastic relationship until the value of the failure stress,($\boldsymbol{\sigma_{t0}}$),is reached. The post-failure behavior is modeled with the "tension stiffening" option available in ABAQUS, which allows the user to define the strain-softening behavior for cracked concrete.

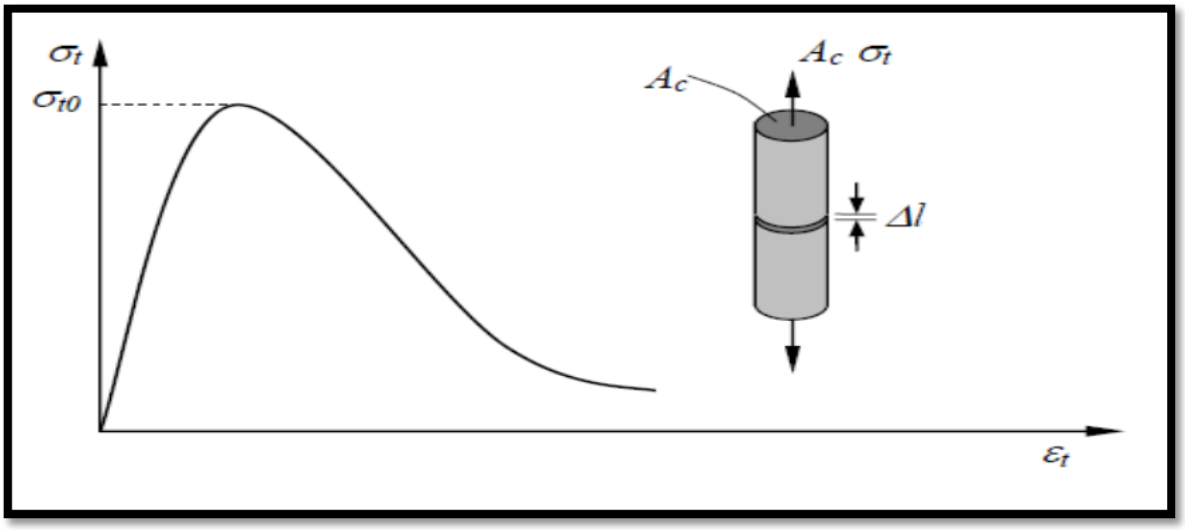

Figure (C-7): Stress-strain response of concrete to uniaxial loading in Tension.

C.5.1.1 Tension Stiffening.

The Tension stiffening effect is considered owing to the fact that the cracked concrete will initially carry some tensile stresses in the direction normal to the crack due to concrete and steel reinforcement interaction. This can be performed by assuming a gradual release of the concrete stress component normal to the cracked plane. Interface behavior between rebar and concrete is modeled by implementing Tension stiffening in the concrete modeling to simulate load transfer across the cracks through the rebar. Tension stiffening also allows the modeling strain- softening behavior for cracked concrete. Thus, it is necessary to define Tension stiffening in the CDP model. ABAQUS allows us to specify Tension Stiffening by post-failure stress-strain relation or by applying a fracture energy-cracking criterion [58] shown in Figure (C.8). There is a mesh sensitivity problem when cracking failure is not distributed evenly. This phenomenon exists when there is no reinforcement in significant regions of the model. To overcome this un reasonable mesh sensitivity problem, fracture energy approach can be used instead of the post-failure stress-strain relation [62].

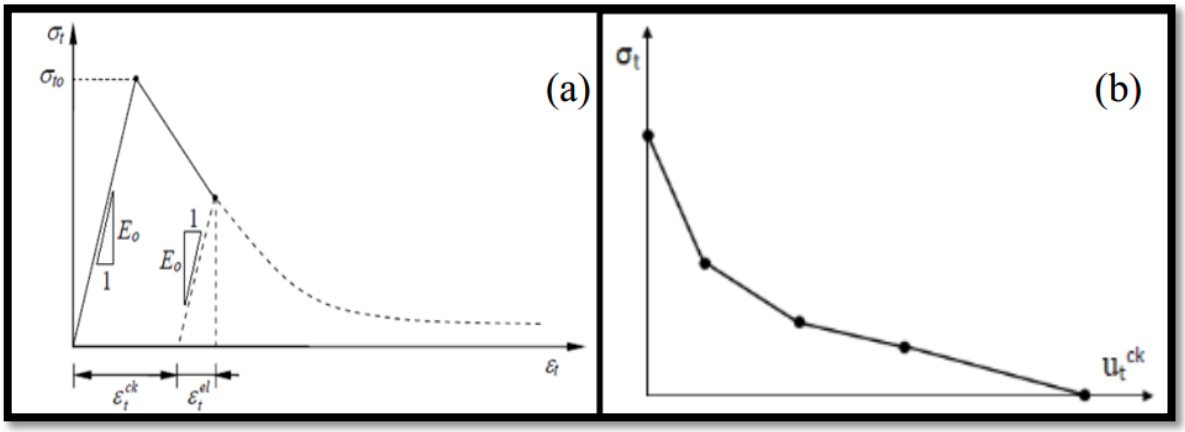

Figure (C-8): Post-failure tensile behavior: (a) stress-strain approach; (b) fracture energy approach [58] .

Tension stiffening models based on strength criteria have been represented by three curves, which are linear, bilinear and exponential curves in the current analysis. The linear one was obtained.

C.5.1.2 Tension Stiffening Relationship.

To simulate the complete tensile behaviors of reinforced concrete in ABAQUS, a post-failure stress-strain relationship for concrete subjected to tension Figure (C-9) is used, which accounts for tension stiffening, strain-softening, and reinforcement (RF)interaction with concrete. To develop this model, the user should input young's modulus (E_0), stress (σ_t), cracking strain (ε_t^{ck}) values and the damage parameter values (d_t) for the relevant grade of concrete. The cracking strain ($\boldsymbol{\varepsilon_t^{ck}}$) should be calculated from the total strain using equation (C-1) below**:**

$$\varepsilon_t^{ck} = \varepsilon_t - \varepsilon_t^{el} \qquad \text{……C.1}$$

Where: = $\varepsilon_t^{el} = \sigma_t / E_C$ the Elastic strain corresponding to the undamaged material, ε_t=total tensile strain.

$$\sigma_t = f_t\,(\varepsilon_{cr}/\,\varepsilon_t)^{0.4} \qquad \varepsilon_t > \varepsilon_{cr} \qquad \text{…… C.2}$$

ABAQUS checks the accuracy of the damage curve using the plastic strain values($\boldsymbol{\varepsilon_t^{pl}}$) calculated as in equation (C.3) below. Negative and/or decreasing tensile plastic strain values are indicative of incorrect damage curves, which may lead to generating error massage before the analysis is, performed [58].

$$\varepsilon_t^{pl} = \varepsilon_t^{ck} - \frac{d_t}{(1-d_t)}\,\frac{\sigma_t}{E_0} \qquad \text{…….C.3}$$

The reasonable starting point for a typical reinforced concrete structure modeled with a detailed mesh is to assume that the strain softening after failure reduces the stress linearly to zero at a total strain of about 10 times the strain at failure.

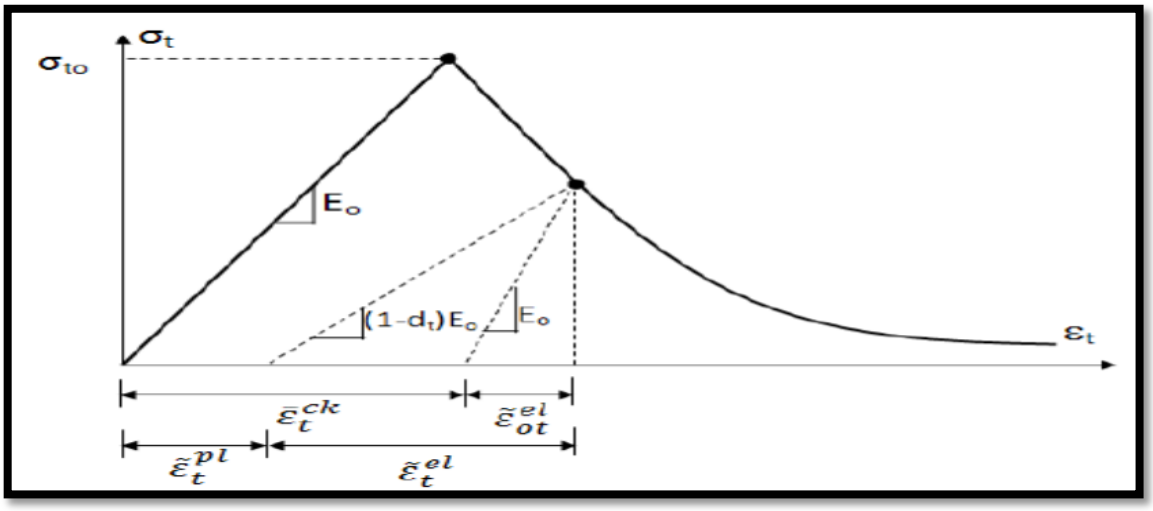

Figure (C-9): Behavior of concrete under axial tension strength [58].

C.5.2 Compression Behavior.

Figure (C-10) shows a typical stress-strain relationship subjected to uniaxial compression. This stress-strain curve is linearly elastic, up to 30% of the maximum compressive strength. Above this point, the tie curve increases gradually up to about70-90% of the maximum compressive strength. Eventually, it reaches the pick value, which is the maximum compressive strength (σ_{cu}). Immediately after the pick value, this stress-strain curve descends. This part of the curve is termed as softening. After the curve descends, crushing failure occurs at an ultimate strain (ε_{cu}).

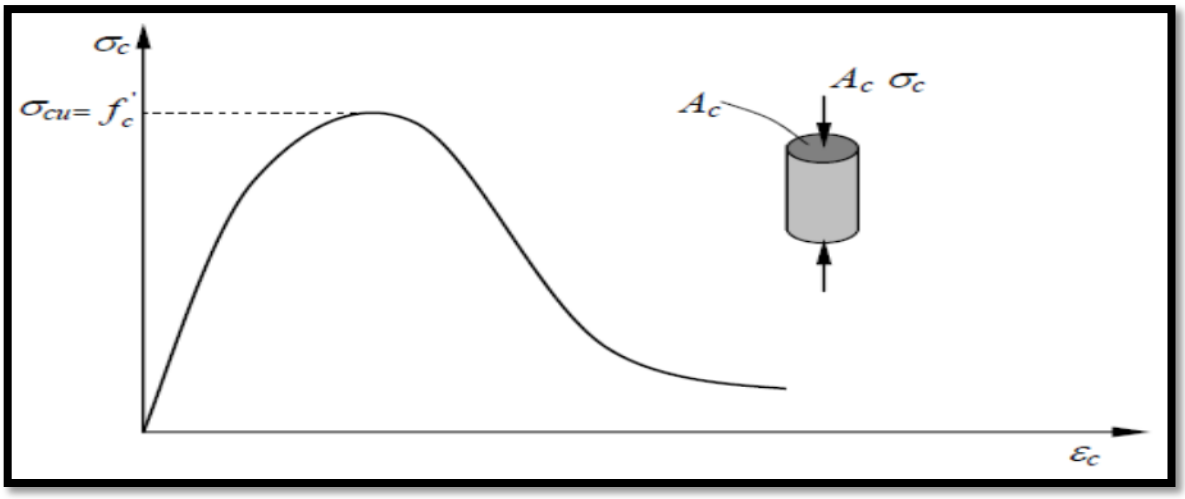

Figure (C-10): Compressive stress-strain curve of concrete.

C.5.2.1 Compressive Stress-Strain Relationship.

The finite element analysis described in this work was conducted based on the uniaxial compressive concrete model of (BSI (2004)) Euro code 2 Design of concrete structures, and it is described by the expression:

For

$$0<|\varepsilon_{c1}| < |\varepsilon_{cu1}| \qquad \frac{\sigma_c}{f_{cm}} = \frac{k_n - n^2}{1+(k-2)n} \qquad \text{.....C.4}$$

$$n = \frac{\varepsilon_c}{\varepsilon_{c1}} \qquad \text{.....C.5}$$

$$k = 1.05E_{cm} \times \left|\frac{\varepsilon_{c1}}{f_{cm}}\right| \qquad \text{.....C.6}$$

Where; ($\boldsymbol{\varepsilon_{cu1}}$)is the nominal ultimate strain 0.0035; ε_{c1} the strain at peak stress (as given in Table B-1); and ($f_{\mathbf{cm}}$)is mean compressive strength.

Table (C-1): Strength and deformation characteristics for concrete (BSI (2004).

Strength classes for concrete															Analytical relation/ Explanation
f_{ck} (MPa)	12	16	20	25	30	35	40	45	50	55	60	70	80	90	
$f_{ck,cube}$ (MPa)	15	20	25	30	37	45	50	55	60	67	75	85	95	105	
f_{cm} (MPa)	20	24	28	33	38	43	48	53	58	63	68	78	88	98	$f_{cm} = f_{ck} + 8\ (MPa)$
f_{ctm} (MPa)	1,6	1,9	2,2	2,6	2,9	3,2	3,5	3,8	4,1	4,2	4,4	4,6	4,8	5,0	$f_{ctm} = 0{,}3 \times f_{ck}^{(2/3)} \leq \frac{C50}{60}$ $f_{ctm} = 2{,}12.\ln\left(1 + \left(\frac{f_{cm}}{10}\right)\right) > \frac{C50}{60}$
$f_{ctk,0,05}$ (MPa)	1,1	1,3	1,5	1,8	2,0	2,2	2,5	2,7	2,9	3,0	3,1	3,2	3,4	3,5	$f_{ctk,0,05} = 0{,}7 \times f_{ctm}$ 5% $fractile$
$f_{ctk,0,95}$ (MPa)	2,0	2,5	2,9	3,3	3,8	4,2	4,6	4,9	5,3	5,5	5,7	6,0	6,3	6,6	$f_{ctk,0,95} = 1{,}3 \times f_{ctm}$ 95% $fractile$
E_{cm} (GPa)	27	29	30	31	33	34	35	36	37	38	39	41	42	44	$E_{cm} = 22\,[\frac{f_{cm}}{10}]^{0.3}$
$\varepsilon_{c1}(\%0)$	1,8	1,9	2,0	2,1	2,2	2,25	2,3	2,4	2,45	2,5	2,6	2,7	2,8	2,8	$\varepsilon_{c1}\ (\%0) = 0{,}7\ f_{cm}^{0.31} < 2{,}8$ $for\ f_{ck} \geq 50\ MPa$
$\varepsilon_{cu1}(\%0)$	3,5									3,2	3,0	2,8	2,8	2,8	$\varepsilon_{cu1}(\%0) = 2{,}8 + 27\,[\frac{98 - f_{cm}}{100}]^4$

To define the stress-strain relation of concrete, the user needs to enter the stresses (σc), inelastic strains ($\boldsymbol{\varepsilon_c^{in}}$) corresponds to stress values and damage properties(d_c) with inelastic strains in tabular format. Therefore, total strain values should be converted to the inelastic strains using equation (C.7):

$$\boldsymbol{\varepsilon_c^{in} = \varepsilon_c - \varepsilon_c^{el}} \qquad \textbf{……C.7}$$

Where: $\boldsymbol{\varepsilon_c^{el}} = \sigma_c/E_c$ the elastic strain corresponding to undamaged material (ε_t) total strain, the elastic modulus (E_c) is calculated using the following equation:

$$E_c = 4700\sqrt{fc'}\ \text{MPa} \qquad \textbf{…….C.8}$$

Further, corrective measures should be taken to ensure that the plastic strain values($\boldsymbol{\varepsilon_c^{pl}}$) calculated using equation (C.9) are neither negative nor decreasing with increased stresses [58].

$$\varepsilon_c^{pl} = \varepsilon_c^{in} - \frac{d_c}{(1-d_c)} \frac{\sigma_c}{E_0} \qquad \text{.....C.9}$$

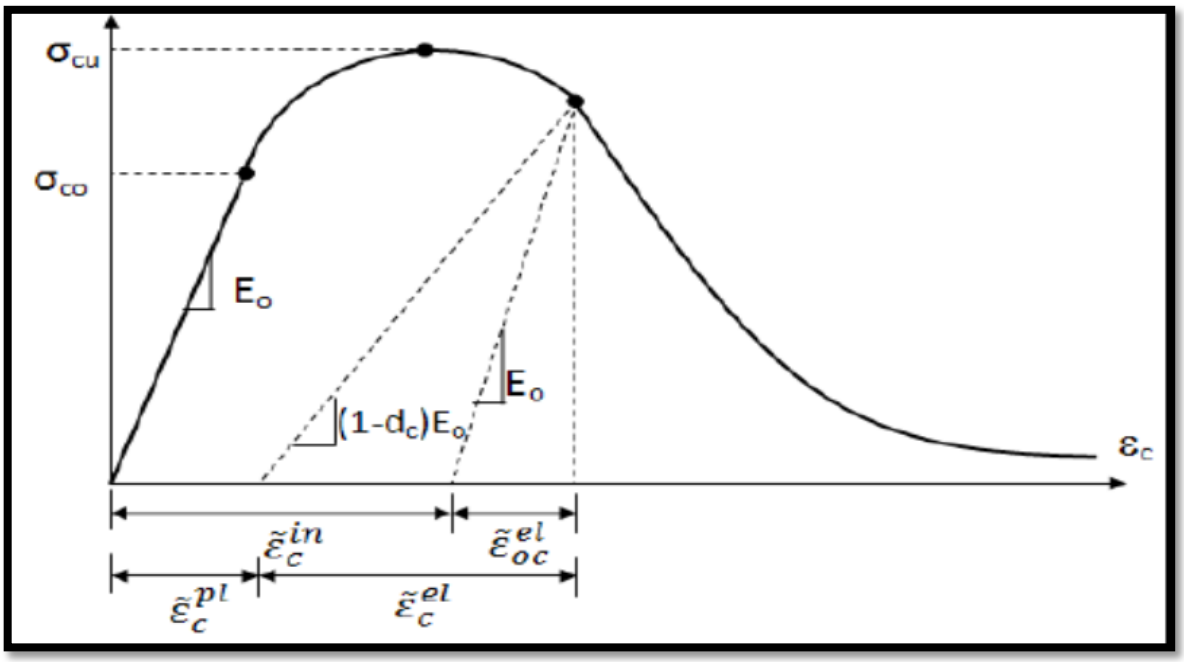

Figure (C-11): Behavior of concrete under axial compressive strength [58].

C.5.3 Concrete Plasticity Parameters

The yield function is one of the main parameters defining the concrete-damaged plasticity model of ABAQUS. The yield surface uses two stress invariants of the effective stress tensor, the hydrostatic pressure stress.

$$\bar{p} = -\frac{1}{3} trace(\bar{\sigma}) \qquad \text{.....C.10}$$

Where the effective stress tensor is defined as:

$$\bar{\sigma} = \mathrm{D}: (\varepsilon - \varepsilon^{pl}) \qquad \text{.....C.11}$$

and the Huber-Mises equivalent effective stress.

$$\bar{q} = \sqrt{\frac{3}{2}(\bar{s} : \bar{s})} \qquad \text{.....C.12}$$

Where; $\bar{S}$ is the effective stress deviator, defined as $\bar{S} = \sigma + \bar{p}\,\bar{l}$

The Drucker-Prager flow potential yield surface proposed by [63] with modifications proposed by [64] can be solved by defining five parameters. To find the exact value of these parameters, many tests would have to be conducted for different materials used in the experimental model; the proposed numerical parameters investigations or default parameters in ABAQUS have been used. The five parameters that need to be defined are:

• Ψ is the dilation angle which represents the ratio of the volume change to shear strain, determined in the plane $\bar{p} - \bar{q}$ at high confining pressure and σ_1 σ_2 are maximum and minimum principal stresses in a tri-axial test. Most of the published research takes the dilation angle for concrete between "12° to 37°" [65] .

• ∈ Is a parameter referred to as flow potential eccentricity that defines as the eccentricity tends to zero the flow potential G tends to a straight line (0.1 the default eccentricity value is used).

• $\epsilon_{b0}/\epsilon_{c0}$ is the ratio of initial equi-axial compressive strength to initial uniaxial compressive strength (the default value is used in analysis 1.16), as shown in Figure (C.12).

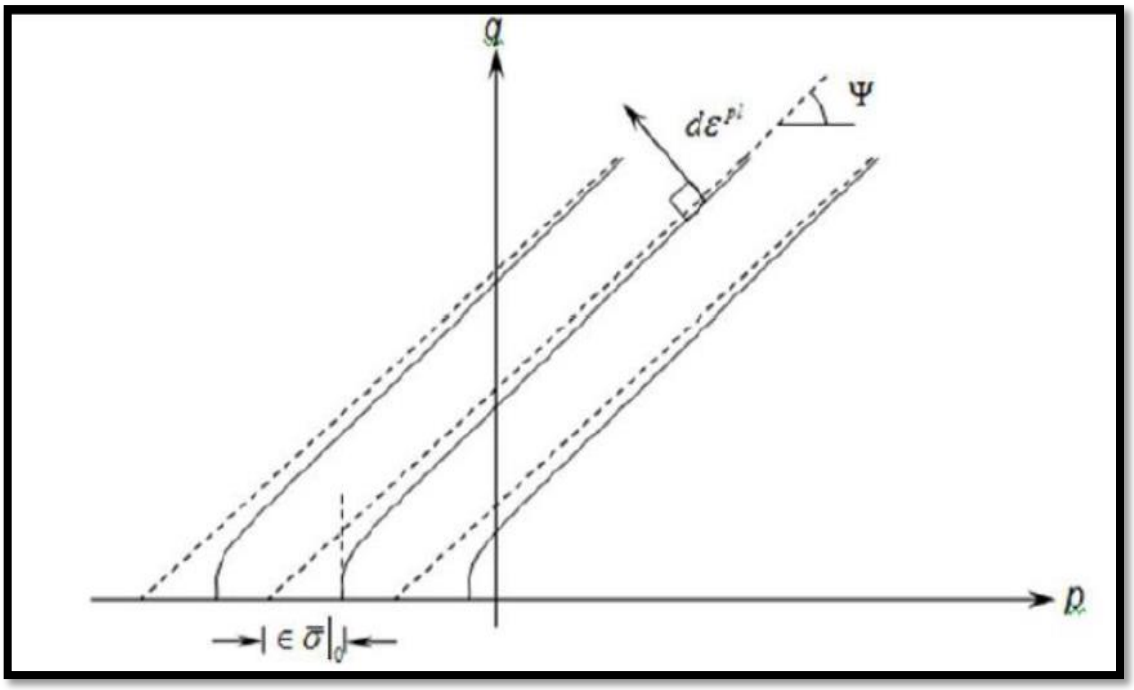

Figure (C-12): Flow potentials in $\bar{p}$ -$\bar{q}$ plane [58].

• **μ** is the viscosity parameter which represents the relaxation time of the viscoplastic system and usually helps improve the rate of convergence of the slab model in the softening region; the viscosity parameter is assumed to be zero because the slab model did not cause the severe convergence difficulty (**μ** = 0.0001 used in the current analysis).

• $\mathbf{K_c}$ Is the ratio of the second stress invariant on the tensile meridian (T.M.) to that on the compressive meridian (C.M.), and it represents the yield surface in the deviatoric plane, as shown in Figure (C.13), and it should satisfy the condition $0.5 < \mathbf{K_c} \leq 1.0$.

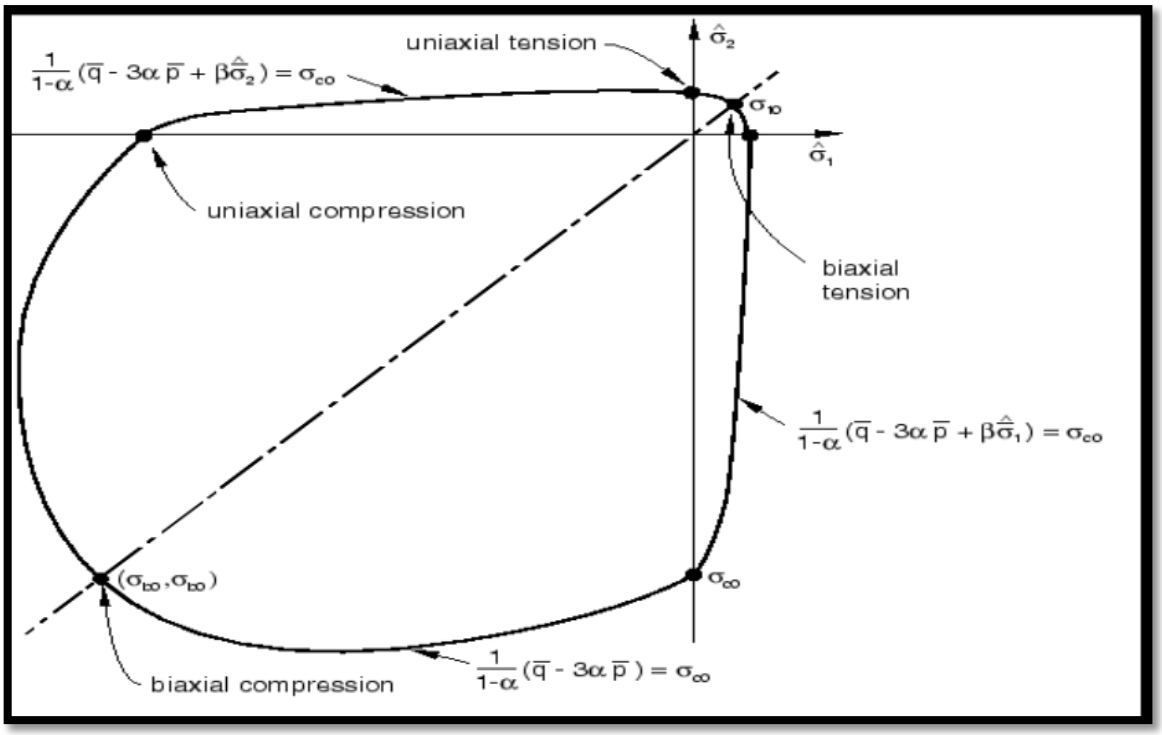

Figure (C-13): Yield surface in plane stress [58].

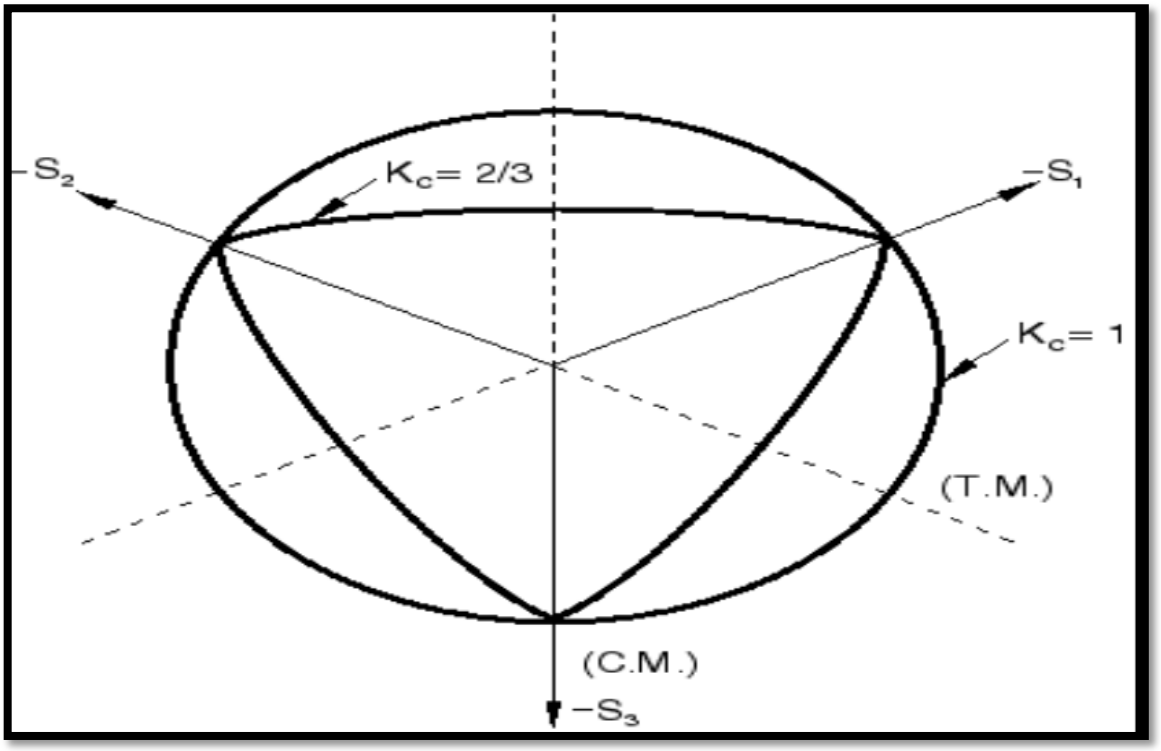

Figure (C-14): Yield surfaces in the deviatoric plane, corresponding to different values of $\mathbf{K_c}$ [58] .

الخلاصة

الحديد المشكل على البارد هو الشائع لمنتجات الفولاذ المشكلة بدرجة حرارة قريبة من درجة حرارة الغرفة بعملية (bending, press-brake, operation machine press) من صفائح الفولاذ او الواح شريطية او اشرطة مسطحة. ويكون ذات أسماك مختلفة تتراوح ما بين (٠.٢٥ – ١٢)ملم. وله العديد من الاستخدامات في الجسور والابراج وفي صناعة البناء والى جانب هذه الاستخدامات يستخدم في السيارات والسكك الحديدية والطائرات والسفن والآلات الزراعية والمعدات الكهربائية وما الى ذلك.

هنا في هذه الدراسة تم عمليا وعدديا دراسة سلوك الانحناء لاثني عشر عتب (I) من الحديد المشكل على البارد ذو شفاه مجوفة مستطيلة بدون تقوية ومع تقوية وتم ذلك على مجموعتين.

في كلا المجموعتين كان الطول الصافي للعتب الواحد بين المساند (١٥٠٠ ملم) وعمق العتب (٣٠٠ ملم) وعرض العتب (١٥٠ ملم) وكان الربط بين الشفاه والشبكة بواسطة براغي ذات قطر(١٠ ملم) والمسافة بين كل برغيين مساوية الى (الطول الصافي للعتب/٦).

كان العامل المتحكم في المجموعة الاولى عمق الشفاه حيث تم عمل اربعة اعتاب بأعماق شفاه (٣٠، ٦٠، ٩٠ و ١٢٠)ملم وبعد فحصها واكمال نتائجها وجد ان العتب ذو عمق شفاه(٦٠ ملم) هو الاقل تحملا للأحمال وهو الذي تم اختياره لعمل ثمانية اعتاب للمجموعة الثانية. وكان العامل المتحكم في المجموعة الثانية هو نوع المواد التي استخدمت لتقوية الشفاه المجوفة المستطيلة حيث استخدم نوعين من الخرسانة وهما الخرسانة العادية و الخرسانة الخفيفة الوزن لتقوية عتبين وكذلك استخدم نفس خلطة الخرسانة العادية لكن استبدل الركام الناعم والخشن بنسب معينة بمواد بديلة وهي (الخرسانة المعاد استخدامها، نشارة الخشب، المطاط الناعم والخشن، برادة الحديد والزجاج المكسر تكسير خشن) لتقوية الشفاه المجوفة لستة اعتاب اخرى وكان العتب ذو عمق شفة (٦٠ ملم) من المجموعة الاولى هو العتب الذي قورنت معه نتائج اعتاب المجموعتين.

وبعد اكمال كافة الفحوصات لأعتاب المجموعتين وفحوصات الشد والانضغاط للخرسانة وحساب النتائج وجد في المجموعة الاولى ان كلما ازداد عمق الشفة عن ٦٠ملم تحسن سلوك الانحناء حيث تزداد قابلية التحمل للأحمال ويقل التشوه والهطول للمقاطع حيث ازدادت قابلية التحمل عند مقارنة النتائج مع عتب ذو عمق شفة(٦٠ ملم) بنسب تتراوح بين(١١% الى ١٥%).

اما بالنسبة لأعتاب المجموعة الثانية فعند مقارنتها مع العتب ذو شفة (٦٠ملم) وجد زيادة بقابلية التحمل تتراوح بين (١٦% - ٢٩%) ونقصان في الهطول يتراوح بين (٦٥% - ٨٦%) ، وكذلك لوحظ ان زيادة قابلية التحمل للأعتاب تتناسب طرديا مع مقاومة الانضغاط للخرسانة التي استخدمت لتقوية كل عتب.

وفي الجانب النظري تضمن استعمال التحليل اللاخطي بواسطة طريقة العناصر المحددة وتم تحليل النماذج العددية ببرنامج (ABAQUS/standard/explicit 2017) وتمت مقارنة ومعايرة نتائج البرنامج مع نتائج الجانب العملي من حيث مخططات الحمل و الهطول وتوزيع الاجهادات وشكل الفشل وبعد هذه المقارنة وجد ان الفرق في قابلية التحمل بين النظري والعملي يتراوح بين(-١.١% الى ١٥.٤%) ووجد توافق جيد بين العملي والنظري.

جمهورية العراق
وزارة التعليم العالي و البحث العلمي
جامعة بابل
كلية الهندسة
قسم الهندسة المدنية

سلوك الانثناء للعتبات الفولاذية المشكلة على البارد ذات الشفاه المجوفة

رسالـة

مقدمة الى كليَّةِ الهندسة / جامعةِ بابل وهي جزء مِنْ متطلبات نيل درجة الماجستير في الهندسة المدنيةِ/ (هندسة الإنشاءات)

من قبل

علياء صلاح فلاح مشعل

بكالوريوس علوم في الهندسة المدنية (٢٠٠٩) م

أشراف

أ. م . د : نجلاء حميد عباس الشريف

أب
2023

صفر
١٤٤٥